Removal of Interference Inherent in the Lens Radar System

by

DAVID J. KIRCHNER

Thesis submitted to the Faculty of the

Virginia Polytechnic Institute and State University

in partial fulfillment of the requirements for the degree of

Master of Science

in

Electrical Engineering

APPROVED:

Dr. G. S. Brown, Chairman

Dr. T. Pratt

Dr. W. L. Stutzman

6/6/88

Blacksburg, Virginia

Removal of Interference Inherent in the Lens Radar System

by

DAVID J. KIRCHNER

Dr. G. S. Brown, Chairman

Electrical Engineering

(ABSTRACT)

The NASA GSFC/Wallops Flight Facility focused radar system employed a large (43 cm diameter) dielectric focusing lens such that the water surface (target) was illuminated by a small radar spot (~1.25 cm diameter). With this small spot size, surface profiles and probability density functions could be generated. The system suffered an interference problem which made reliable data collection impossible. Study showed that the system had to be operated bistatically in order to reduce the effects of interference found to be caused by signal leaking directly from the transmitter to the receiver. Since the system was operated in a confined space (the wind-wavetank), multipath was found to generate interference signals. The multipath interference was reduced via strategic placement of radio frequency absorber. A comparison was made between experimental results with the original system and the final bistatic system to demonstrate the effect of the reduction in interference. A model was also derived for the direct leakage interference and used to explain experimental results.

Acknowledgements

I wish to thank Professor Gary Brown for his support and guidance. I also wish to thank the following people at NASA Wallops Island: for many helpful discussions, for help in digitizing and storing experimental data, and especially for his invaluable aid in helping to set-up and run countless experiments. Thanks also to all my friends for helping me keep my piece of mind.

Table of Contents

List of Illustrations

Nomenclature

A	area of lens aperture
A_h	area of horn 1
d	horn to lens distance
F_1, F_2	foci of the lens
f_1	frequency of the lower sideband
f_2	frequency of the higher sideband
G	gain of the lens aperture
$G_h(0°)$	horn gain along the boresight
HFT	high frequency terms
I	in-phase output signal
k	wavenumber of the carrier
k_1	wavenumber of the lower sideband
k_2	wavenumber of the higher sideband
L	diameter of the lens aperture
m_ζ	error
P_r	target reflected power
P_l	coupler leakage power
P_{LN}	lens reflected power
P_a	power illuminating the lens aperture
P_{in}	transmitter power
P_{rec}	power received by the lens aperture
P_{reco}	return power without interference
$(P_{rec})_{sum}$	return power histogram with interference
$(P_{reco})_{sum}$	return power histogram without interference

Q	quadrature phase output signal
Q_D	quadrature phase signal
R	distance from lens aperture to target
R′	distance from the horn to the target
r_i	instantaneous range referenced to the mean range
r	range to the metal plate
t	time
V_D	voltage out of the detector
$V_{F1, VF2}$	voltages at the detector due to the sideband signals
V_F	signal voltage after the low pass filter
V_P	measure of backscattered power
V_l	leakage voltage
V_r	target reflected voltage
V_1, V_2	target reflected voltages
V_4, V_5	lens reflected voltages
V_7, V_8	leakage voltages
V_{LN}	lens reflected voltage

Greek Symbols

α	a pathlength internal to the radar
α_c	coupler isolation
β	constant phase change
γ	a pathlength internal to the radar
Γ_{LN}	reflection coefficient of the lens
Γ_t	reflection coefficient into port 1 of the coupler
Γ_r	reflection coefficient into the detector
δ_{az}	azimuth resolution length
δ_r	range resolution length

Δk	difference in the sideband wavenumbers, k_2-k_1
$\Delta\omega$	difference in the sideband frequencies, ω_2-ω_1
ζ	water height
η	horn efficiency
λ	wavelength
π	pi, 3.1416
σ	radar cross section
σ°	radar cross section per unit area
ψ	grazing angle
ψ_1, ψ_2	constant phase changes
ω	frequency
ω_1	frequency of the lower sideband
ω_2	frequency of the higher sideband
ω_3	carrier frequency

Chapter 1

SYSTEM DESCRIPTION AND PROBLEM

1.1 ORIGINAL DESIGN AS INSTALLED

1.1.1 Introduction

The lens radar system was designed primarily as a research device for studying electromagnetic bias (EM bias). A better understanding of EM bias is necessary in order to make high precision measurements (within 3 cm or less) of mean sea level (MSL) with radar altimeters. EM bias is the difference between electromagnetic mean sea level (measured by an altimeter) and geometric mean sea level (true MSL). The troughs of ocean waves seem to reflect radar signals more

strongly than the wave crests, and because of this nonuniform reflection the altimeter measured MSL is lower than true MSL.

It is hoped that by using the lens radar system to study water wave scattering in a controlled experimental environment (the wind-wavetank) conclusions can drawn about the characteristics of EM bias. For example it may be possible to relate EM bias to certain wave conditions (i.e. kurtosis, skewness, etc.)[4]. With a better understanding of EM bias, more precise altimeters can be built; and high precision altimeters are needed for future space systems (i.e. TOPEX, Eos, etc.).

The lens radar system was designed by L. S. Miller [1] to study random surface scattering. It was installed at NASA Wallops Flight Facility in 1983, and a detailed description of the system design can be found in reference 1. This section summarizes the lens radar system design and includes all changes made to the system design, given in reference 1, prior to installation. Figure 1 summarizes the main characteristics of the lens radar system. A 43 centimeter diameter dielectric focusing lens was used so that only a small spot was illuminated ($\simeq$ 1.25 cm diameter). By using a Δk modulation technique the range could be resolved on the millimeter level. A double sideband suppressed carrier signal was transmitted and the range to the target was found by comparing the phase of the reflected signal to the phase of the 480 MHz reference signal. In-phase and quadrature signals, and backscattered signal strength were measured. These quantities were digitized and processed to generate surface profiles, and probability density functions.

36 GHz WAVE PROFILING RADAR

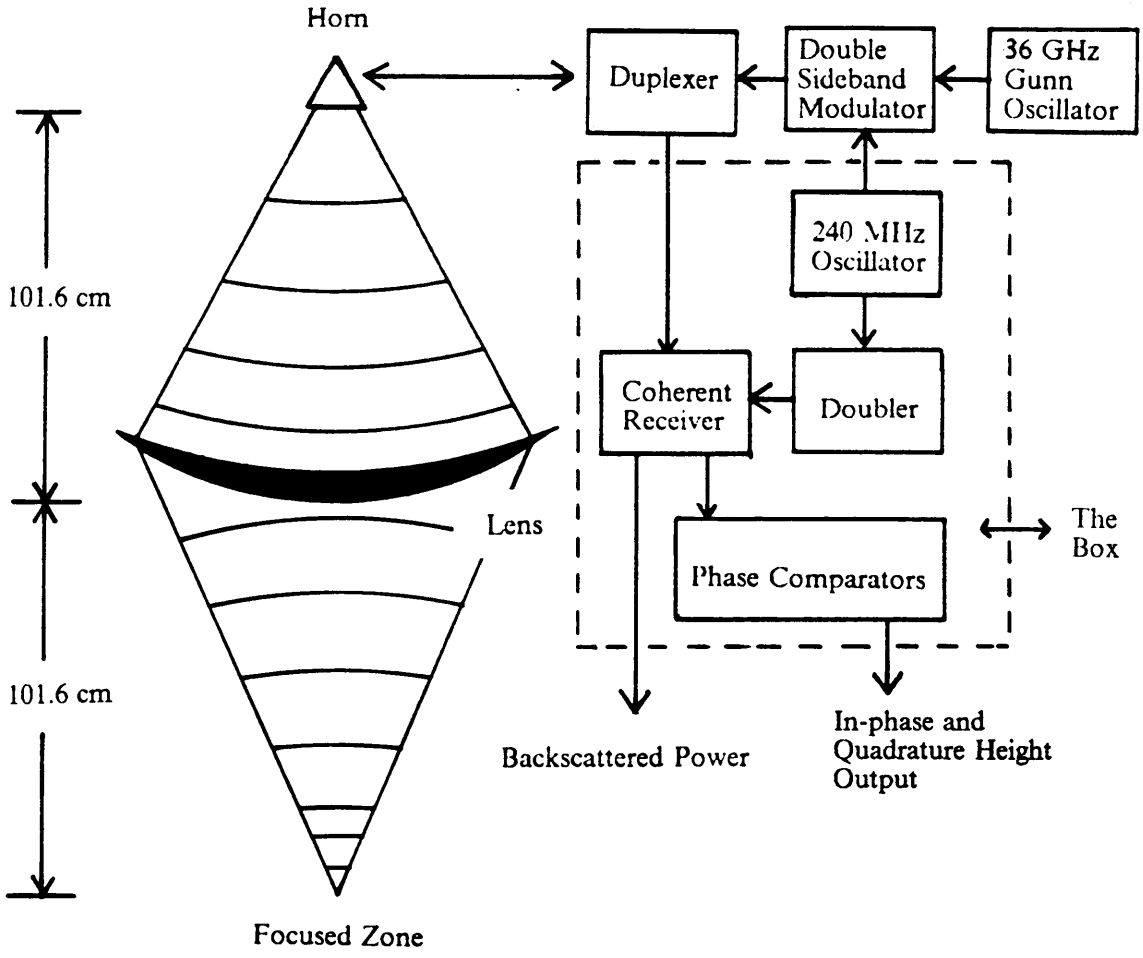

OPERATION SPECIFICATIONS

Operating wavelength	8.3 mm
Response time	10^{-6} sec
Sideband separation	480 MHz
Spot size	~1.25 cm
Unambiguous range interval	0.1563 m

Figure 1. Radar System Characteristics [1]

1.1.2 System Description

The overall system block diagram is shown in Figure 2. The 36.24 GHz Gunn diode carrier signal was suppressed and the sideband signals, at 35.76 GHz and 36.24 GHz, were generated by use of a 240 MHz oscillator and a double sideband modulator. These sideband signals were fed, via a directional coupler, into the horn (15 dB gain, 30° beamwidth). The return signal was passed into a tunnel diode detector which converted the return signal to video via a square law operation. Figure 3 shows the configuration of the microwave components.

After detection the signal was passed into the Box. The Box (outlined in Figure 1) contained all the necessary components for the extraction of the in-phase, quadrature phase, and backscattered power information. First, the return signal was amplified. Also the 240 MHz reference signal (used to generate the sidebands) was doubled to form the 480 MHz reference signal used to extract the phase information. To extract the phase information, a double conversion process was used rather than processing the signal at the 480 MHz level in order to maintain a high degree of accuracy over a large dynamic range. Mixing a 450 MHz source with both the return signal and the reference signal converted these signals to 30 MHz.

The mixer and preamplifier portions of the receiver had to be carefully shielded, because of the high level reference signal (~0 dBm) versus the low level backscattered signal (~-80 dBm). This additional isolation was achieved by using a two-stage 450 MHz coaxial cavity filter. Following the down conversion, the signal was passed through an intermediate frequency (IF) amplifier. To provide a constant input level into the phase comparators, the signal was then limited. To compensate for the ~10 dB loss introduced by the limiter, the signal was amplified again. The

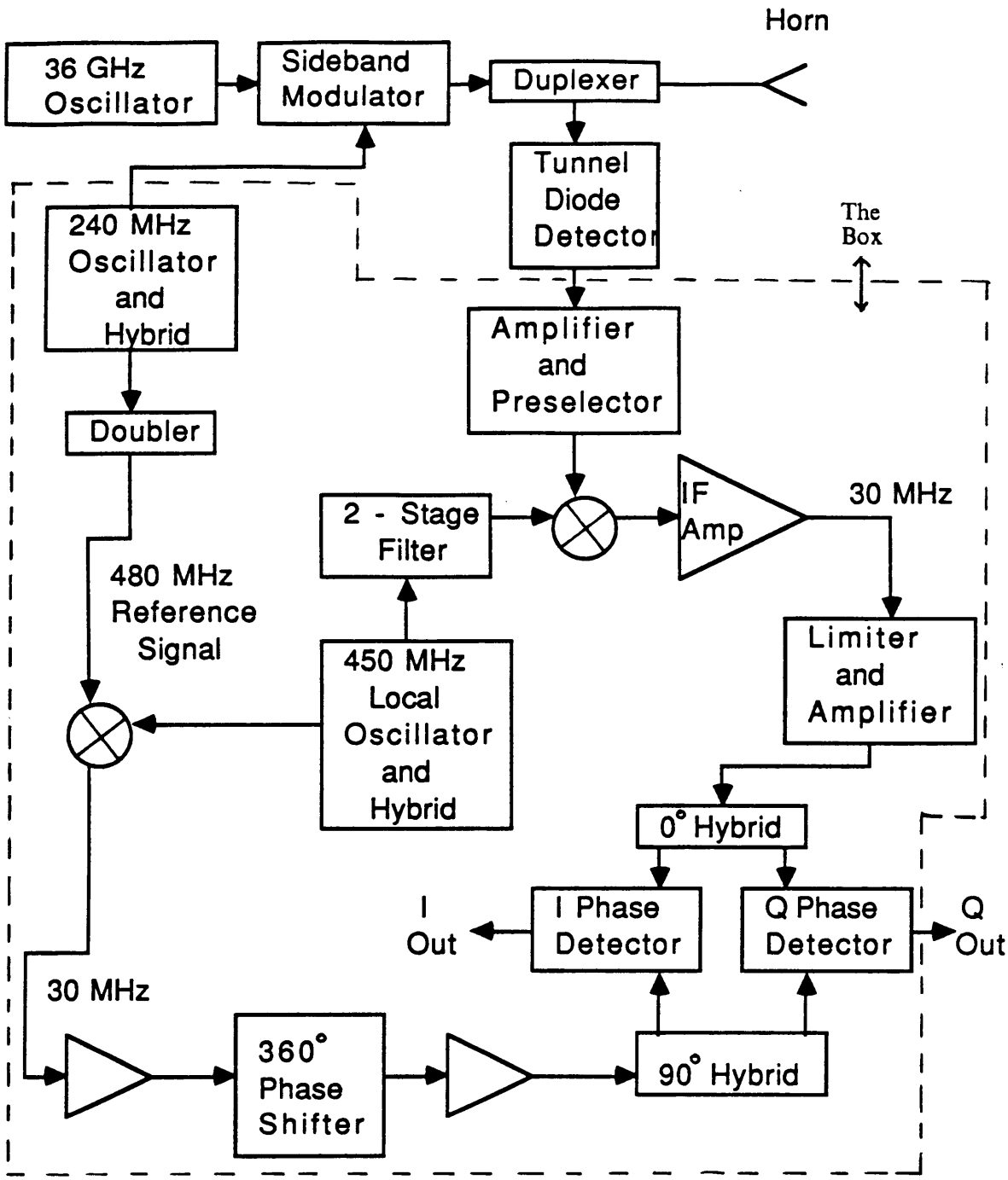

Figure 2. System Block Diagram [1]

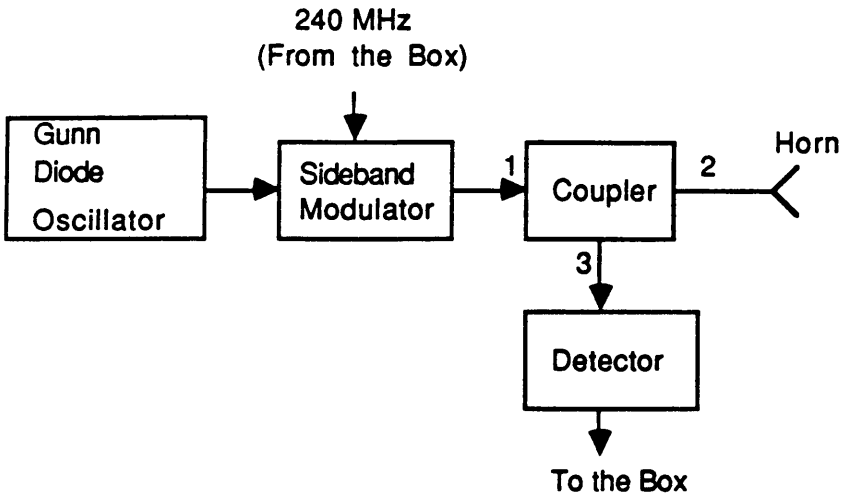

Figure 3. Radar Diagram

reference signal was also amplified to the level necessary to drive the phase comparators.

An all pass, phase shift network was included in the reference channel so that "zero" phase shift could be set to correspond to the mean target range. Hot-carrier ring diode circuits, and in-phase and quadrature hybrid junctions were used to perform the phase detection operations.

1.1.3 Range Measurement

The range measurement concept is outlined in Figure 4. The sideband signals had frequencies f_1 and f_2. The transmitted signal was received after being scattered from the surface. The voltage out of the detector (assuming a square law operation) was V_D, where V_{F1} and V_{F2} were due to the sideband return signals. After detection, the high frequency terms were filtered out with a low pass filter. This filtering left V_F. With the reference frequency, f_2-f_1, a phase detector was used to extract the range information, and the output of the phase detector was

$$V_o = 2r_i\Delta k = \frac{4\pi r_i}{\lambda} \tag{1.1}$$

where λ was the wavelength of the 480 MHz difference frequency, r_i was the instantaneous range, and Δk was the difference in the sideband wavenumbers, (k_2-k_1).

The actual output from the Box (instead of $2r_i\Delta k$) was the in-phase (I) and quadrature (Q) information.

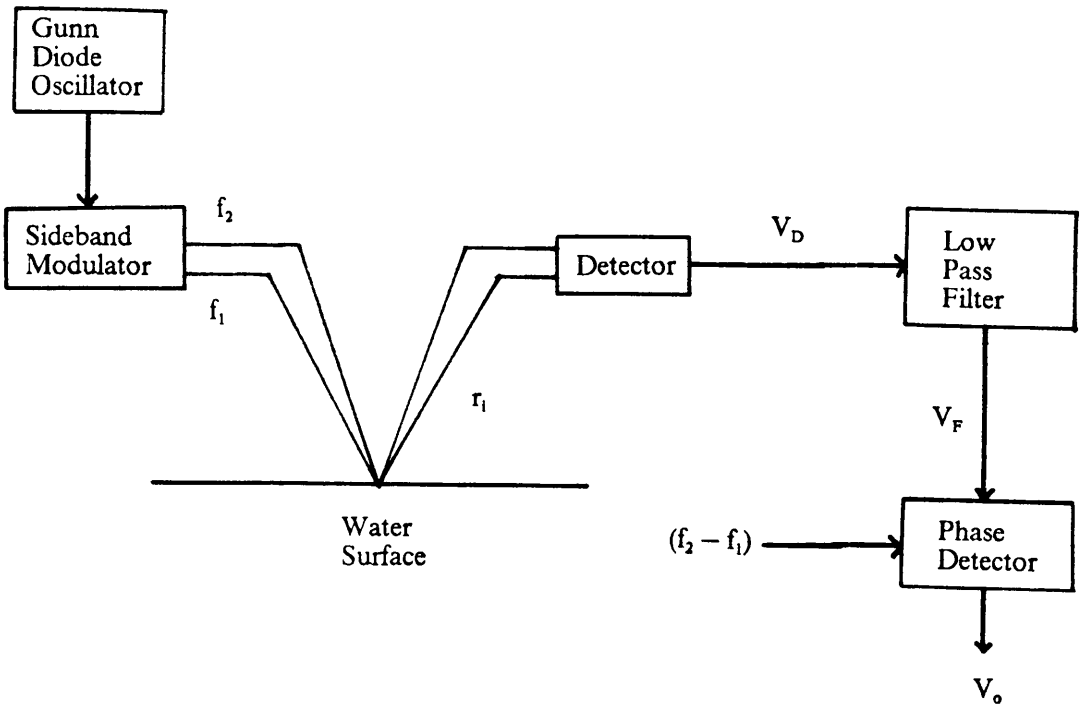

$$V_{F1} = \sin[\omega_1 t + \phi_1(t)], \quad \phi_1(t) = 2k_1 r_i$$
$$V_{F2} = \sin[\omega_2 t + \phi_2(t)], \quad \phi_2(t) = 2k_2 r_i$$

$$V_D = (V_{F1} + V_{F2})^2$$
$$= 1 + \cos[\Delta\omega t + 2r_i\Delta k] - \frac{1}{2}\cos[2\omega_1 t + 2\phi_1(t)] - \frac{1}{2}\cos[2\omega_2 t + 2\phi_2(t)]$$
$$- \cos[(\omega_1 + \omega_2)t + \phi_1(t) + \phi_2(t)]$$

$$V_F = 1 + \cos[\ \Delta\omega t + 2r_i\Delta k]$$

$$V_o = 2r_i\Delta k$$

Figure 4. Range Measurement Concept

$$\begin{aligned} I &= \cos(2r_i\Delta k) \\ Q &= \sin(2r_i\Delta k) \end{aligned} \tag{1.2}$$

From either of these outputs (I or Q), the range r_i could be calculated because Δk was known.

When using the I and Q information to calculate the range to the water, care had to be taken to insure that there was no range ambiguity. For there to be no ambiguity, there had to be a one to one correspondence between the phase information and the range. For one period of the sinusoid:

$$\begin{aligned} &0 \leq 2r_i\Delta k \leq 2\pi \\ &\text{or} \\ &r_i \leq \frac{\pi}{\Delta k} = \frac{\lambda}{2} \end{aligned} \tag{1.3}$$

Limiting the phase change to one period, limited the unambiguous range interval to be less than $\lambda/2$ or 31.25 centimeters.

A more useful choice for an unambiguous range interval, was the half period of the sinusoid which fell between $-\pi/2$ and $\pi/2$. With this restriction, there was only one phase value for each range value. Therefore as long as the range was not allowed to fall outside of this interval, there would be no second solution that would have to be eliminated, and only one phase channel (I or Q) would be required in order to solve for the range. For the 480 MHz difference frequency of the system, this corresponded to a range interval of 15.63 centimeters.

1.1.4 Power Measurement

The Box also output a voltage which was related to the backscattered power level. The relationship between this voltage and the backscattered power was nonlinear, and this nonlinearity increased the resolution of the receiver. In order for the voltage output to be useful it was necessary to generate a calibration curve which related the backscattered power to the output voltage. This calibration was done and it was found that a 6.75 dB change in power level corresponded to a 1 volt change in the Box output voltage.

1.1.5 Lens Design

The geometry used to design the lens, which was made of Rexolite 1422, is shown in Figure 5. It was assumed that path lengths between the foci, F_1 and F_2, were equal over all values of ϕ. The feed horn was located at F_1 and the rough surface (target) at F_2. A quarter-wave impedance matching coating was used to remove reflections from the back of the lens.

1.2 PROBLEM DESCRIPTION

The basic problem was that lens radar system did not produce the profiling measurements for which it was originally designed and installed. It was suspected that the measurements were being contaminated by unwanted reflections. Because

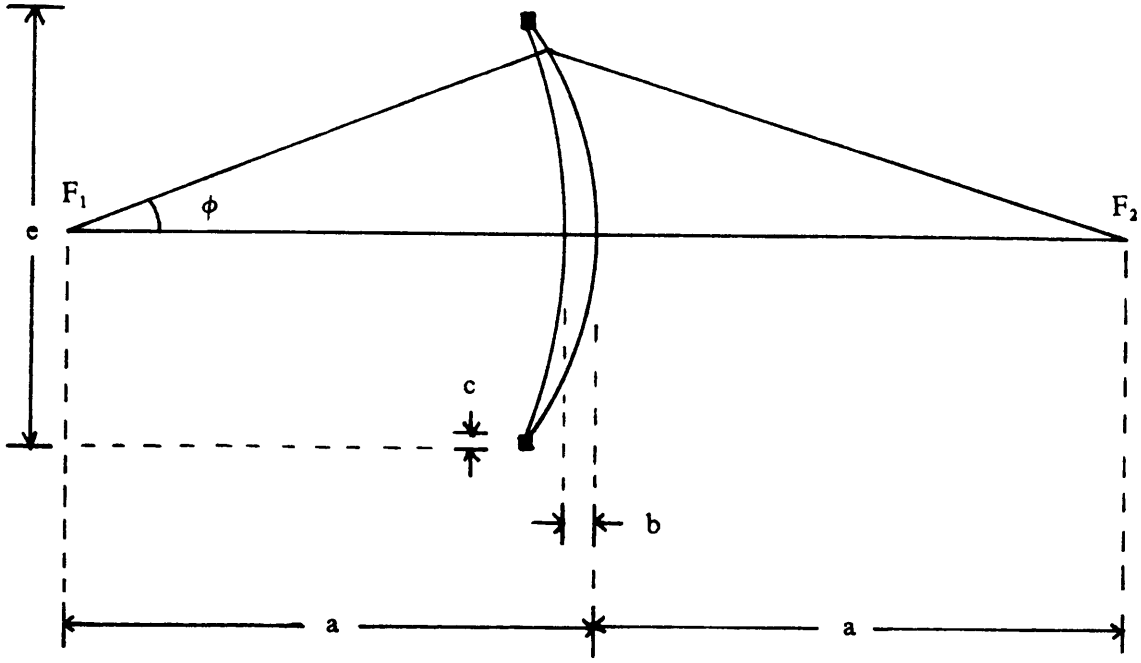

a = 101.6 cm
b = 7.85 cm
c = 0.95 cm
e = 43.58 cm

Figure 5. Focusing Lens

of this interference, the lens radar system could not be used to study electromagnetic bias (EM bias) since the desired level of wave height measurement accuracy could not be achieved.

The easiest way to see the effects of the interference was to study the backscattered power and phase when slowly increasing the range to the target. Since the water surface in the wavetank was the target, slowly draining water from the tank would gradually increase the range. If the data were interference free, the return power would change a small amount due to the $1/R^2$ (R = range) effect and defocusing effects, but because the range of interest was small (± 3.5 cm) the return power should remain fairly constant. The phase would be expected to smoothly change through one cycle (360 degrees) every 31.25 centimeter change in range. When water was drained out of the tank the actual behavior of the phase and power was quite different from the above described ideal case.

In order to understand the curves generated when a drain test was run, it is necessary to understand what was being plotted. The plotted voltages were related to the water height and backscattered power, and were what would be digitized and processed to obtain surface profiles and probability density functions if a typical experiment were being run. To get these voltages the return signal was passed into a square law detector and the output voltage of this detector was fed into the Box. The Box (described earlier) contained the circuitry necessary to convert the output from the detector into voltage levels which corresponded to the in-phase (I) and quadrature phases (Q), and the backscattered power. These voltage levels were what was plotted when a drain test was run.

The water height could be found from either the in-phase or the quadrature voltage (the relationship for finding the water height from the quadrature channel is given in section 5.2.3). The voltage out of the Box corresponding to the backscattered

power (V_p) was negative, and the more negative it was the greater the backscattered power. Also, V_p was not linearly related to the backscattered power, but the relationship was known (each 1 volt change corresponded to a 6.75 dB change in power), so that a relative power level could be calculated.

What actually resulted, when a drain test was performed, was that both the power and phase of the reflected returns were sinusoidal. The power went through one complete cycle approximately every 4 millimeter drop in water level while the mean return power remained fairly constant. The phase went through one complete cycle every 31.25 centimeter drop in water level as expected, but there was also a more rapid oscillation taking place. The faster oscillation, riding on the expected phase change, went through one complete cycle about every 4 millimeter drop in water level. The radar operated at approximately an 8 millimeter wavelength, and so a 4 millimeter drop in water level corresponded to a two-way range change of one wavelength.

The level of the interference could be described by measuring the voltage difference between a peak and an adjacent trough of an interference cycle. With the radar set-up in its original configuration, the magnitude of the interference in the phase was as large as 0.6 volt. This level of interference was quite large, as the voltage change for one cycle of phase (31.25 cm change in water level) was approximately 1.8 volts. This high level of interference destroyed the ability to resolve range accurately from the phase information. The oscillation in the power return was about 0.3 volt peak to trough. This corresponded to about a 2 dB change in power. Figure 6 shows the interference described above. In this drain test, the change in water level was about 2.5 centimeters. If there was no interference present, the power would have remained constant and the phase would have

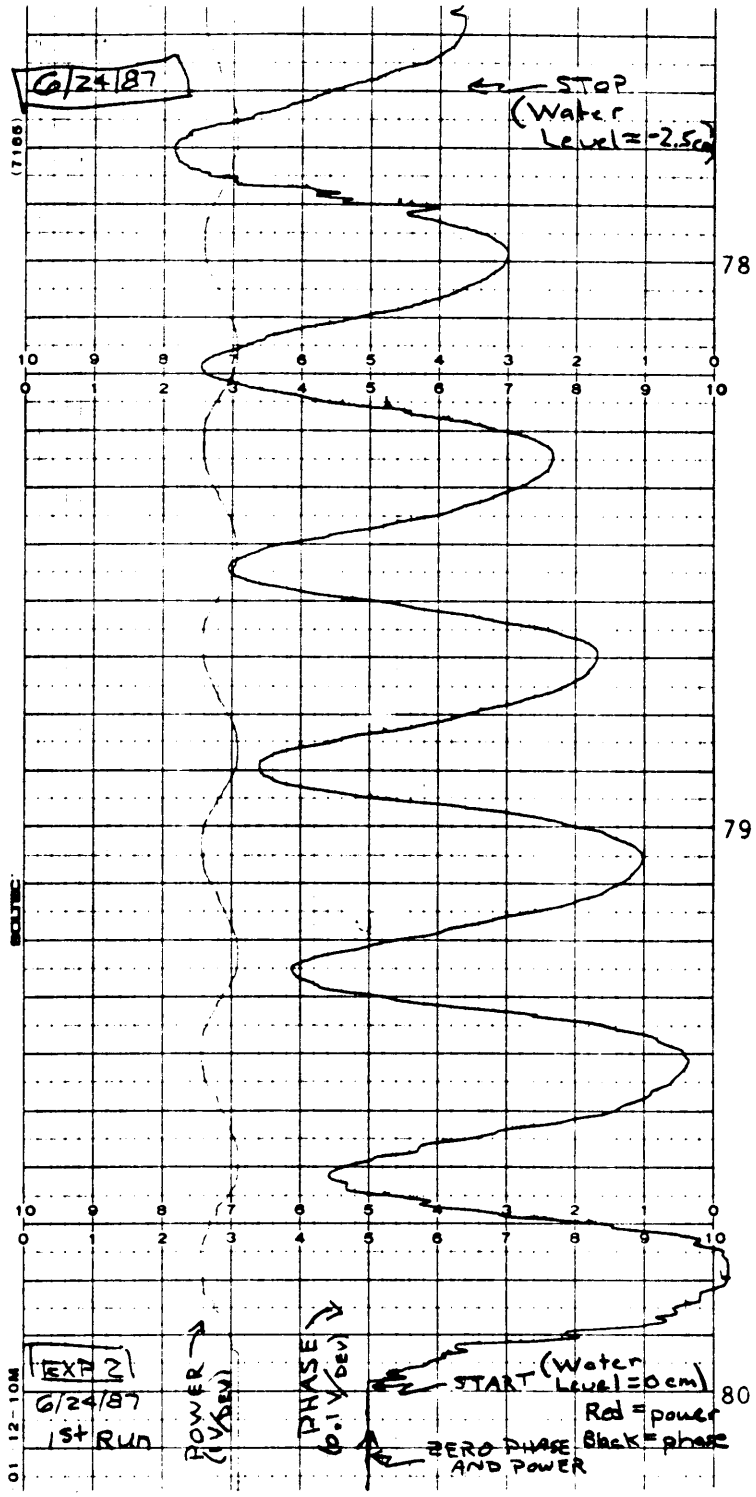

Figure 6. Monostatic Drain Test (power and phase outputs from the Box): ≃2.5 cm drop in water level

gradually changed from 0 to about 0.43 volt. Obviously much reduction in the interference was required in order to make possible the collection of useful data.

1.3 WAVETANK DESCRIPTION

The NASA Wallops Flight Facility wind-wavetank is 18.29 meters long, 1.22 meters high, and 0.91 meter wide. The mean water level is typically 0.76 meter, but this level can be changed by adding or draining water. Wind can be generated in one direction through the wavetank by a suction fan through a closed loop recirculation air system. The wind speed can be varied from 0 meters/second to over 20 meters/second. Sinusoidal or random waves can be generated at frequencies from 0 to 10 Hz by a hydraulic servo-controlled paddle [2]. The paddle can be set up at either end of the wavetank. A sloped beach (see Figure 7) was placed at the end of the wavetank, opposite to the paddle, to damp out the waves in order to remove the possibility of reflected waves.

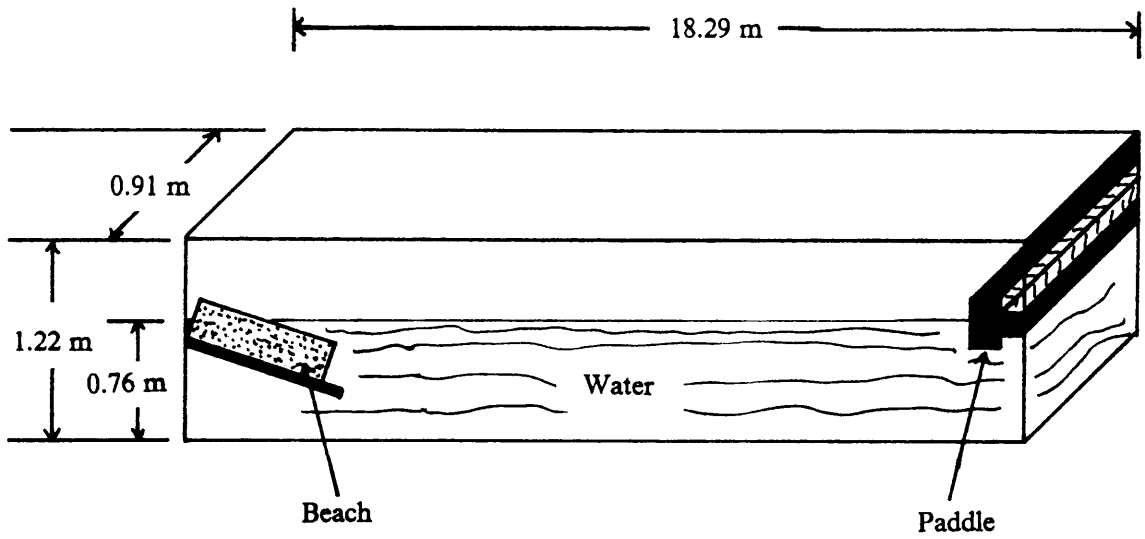

Figure 7. Wavetank Dimensions

Chapter 2

EXPERIMENTAL WORK

The most immediate goal in this project was to use available equipment to solve the interference problem by the end of a ten week summer employment period at NASA Wallops Flight Facility. Because of this time constraint, removal of the interference took precedence over the other goals which were;

-Identification of the cause of the interference

-Recommendations concerning the system's usefulness

for the study of EM bias

The problem was approached by checking the performance of the system's components, and operating the system with different components, and in different configurations (including bistatic), while noting any effects on the return power and phase.

2.1 EXPERIMENTS PERFORMED OUTSIDE OF THE WAVETANK

2.1.1 Bench Set-up Description

To more conveniently study the interference, the radar was first set up on a long bench outside of the wavetank (see Figure 8). A metal plate was used to simulate the flat water target. The plate was held by a clamp which was connected to a vernier. This arrangement made it possible to smoothly move the plate closer or farther from the transmitter by turning the vernier's crank. The wooden support was added to keep the plate from vibrating as it was moved.

The same lens horn configuration was used as in the wavetank set-up. The only changes in the system were that it was assembled on its side outside of the wavetank and the water was no longer the target.

With this set-up the same cyclic interference pattern was present when the range was smoothly changed. As the interference was still present independent of the wavetank, it is clear that even if the wavetank caused some interference, it was not the only source of interference.

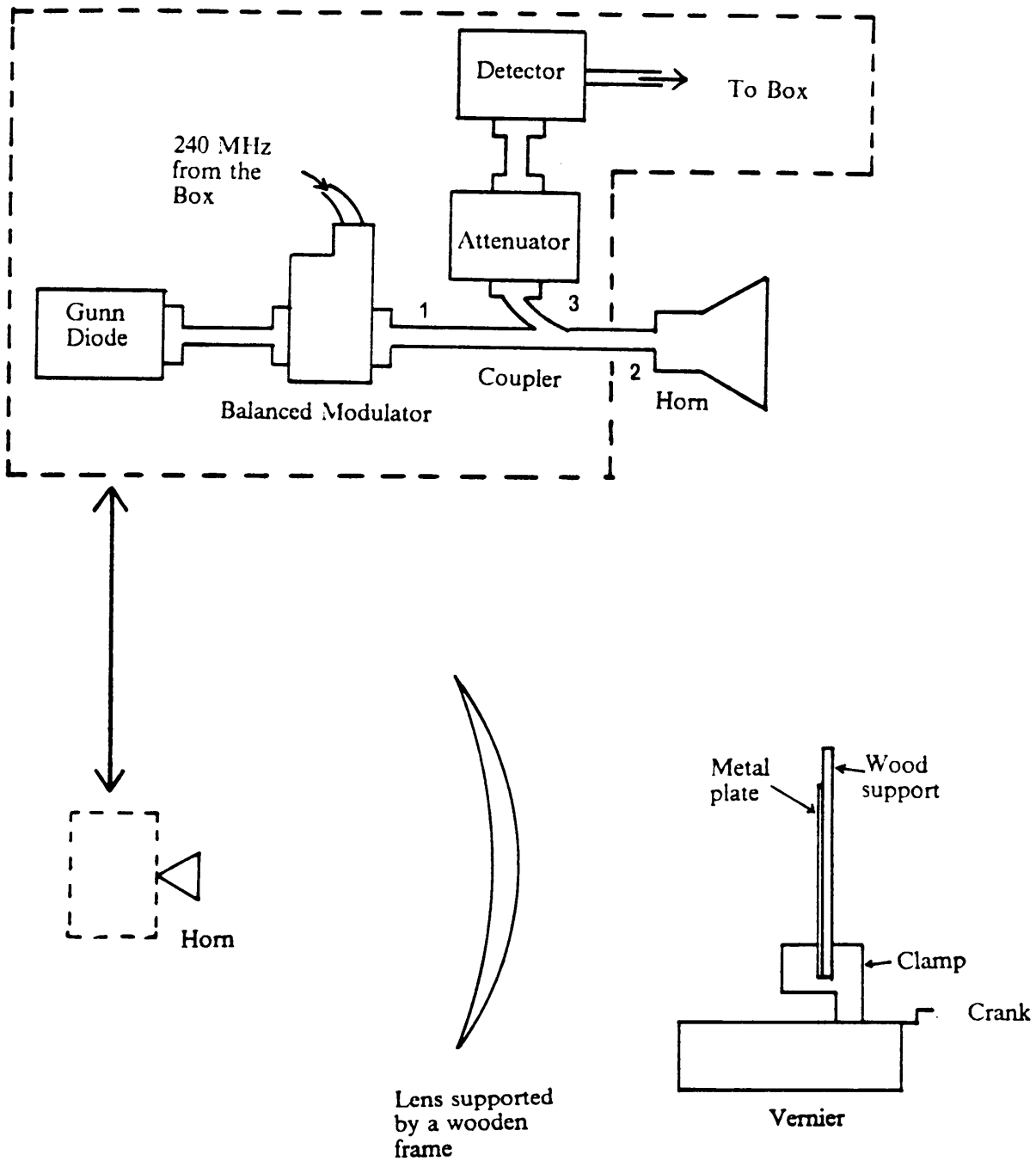

Figure 8. Bench Set-up

2.1.2 Use of Different Horns

Three different horns were available for use at 36 GHz. They will be referred to as horn 1, horn 2, and horn 3. Unless otherwise noted, horn 1 was the horn used. Horn 1 was a standard gain 36 GHz horn, with 15 dB gain and 30 degree beamwidth. Originally horn 2 had the same specifications as horn 1, but it was modified for some previous non-related task. Part of horn 2 was machined off in order to increase the beamwidth. Horns 1 and 2 had the following aperture dimensions.

Horn 1 : 2.30 cm by 1.67 cm (29/32 inch by 21/32 inch)

Horn 2 : 1.98 cm by 1.43 cm (25/32 inch by 18/32 inch)

Horn 3 was a scalar lens horn. It had greater gain than horn 1 and only a 3 degree beamwidth. The interference was present no matter which horn was used. Because the interference was present with the narrow beam horn (horn 3), the possibility of wide angle interference was eliminated.

2.1.3 Removal of Focusing Lens

As part of the original set-up, the back of the lens was covered with an impedance matching material to remove lens reflections which could be refocused back into the horn and cause interference problems. The matching material used was a soft wood (birch or poplar). The interference problem was present at the original installation of the radar system. Therefore, either the impedance matching

did not successfully remove all lens reflections or the interference was caused by some other problem (or the interference was caused by a combination of lens reflections and some other problem).

Even if the impedance matching originally removed all the lens reflections, it was possible that it did so only temporarily. This appearance of reflections could be the case if the characteristics of the wood coating changed over time (due to water absorption, warping, etc...). Although this introduction of reflections was possible, it did not seem likely, because there was no noted change in the interference characteristics over time. If lens reflections were present, possible solutions included redoing the impedance matching or operating the radar system bistatically so that the receive horn was no longer in a position that it could receive lens reflections.

To test the hypothesis that interference was being caused by something other than lens reflections, the focusing lens was removed from the system. Without the lens focusing, the signal strength was greatly reduced and the radar was unable to see the metal plate at the typical mean range (2 meters). Calculations in Appendix A support this result.

To overcome the problem of low signal strength, the target was moved to a much closer range (~.75 meters). The target was then close enough to be seen by the radar, and as it was smoothly moved in range the same interference pattern, as seen with the lens in the system, could be seen to be present (although the plate reflected signal was too weak to drive the phase comparators, so no range information was present). This result did not disprove that lens reflections could be a factor, but it did prove that something other than lens reflections introduced interference.

2.1.4 Coupler Isolation Check

One possible explanation for the interference was that the transmitted signal was leaking into the detector directly. With this leakage, the detector would see both the transmitted and target reflected signals, instead of just the target reflected signal. The combination of these two signals could result in the interference pattern noted. One possible leakage path for the transmitted signal was through the coupler. The 3 dB coupler was supposed to introduce 30 dB of isolation between the transmitter and receiver; that is, any transmitted signal leaking directly into the detector would be attenuated by 30 dB.

Using a power meter, the coupler was checked to see if it introduced the expected 30 dB of isolation between the transmitter and the detector. How this test was carried out is shown in Figure 9. In (A) 22 milliwatts of transmitted power was measured at the output port of the detector. The transmitted power leaking directly into the detector (see (B)) was found to be 0.021 milliwatt. Therefore, the 3 dB coupler did provide the expected 30 dB of isolation between the transmitter and the detector. If it turned out that 30 dB of isolation was not sufficient, the only readily available way to increase the isolation would be to physically separate the transmit and receive portions of the radar (bistatic operation), because the only other duplexers available were circulators which had an isolation of only 25 dB.

2.1.5 Gunn Diode Oscillator Leakage Check

The Gunn diode oscillator was checked for signal leakage, because it is not unusual for a Gunn oscillator to leak signal in directions other than into the

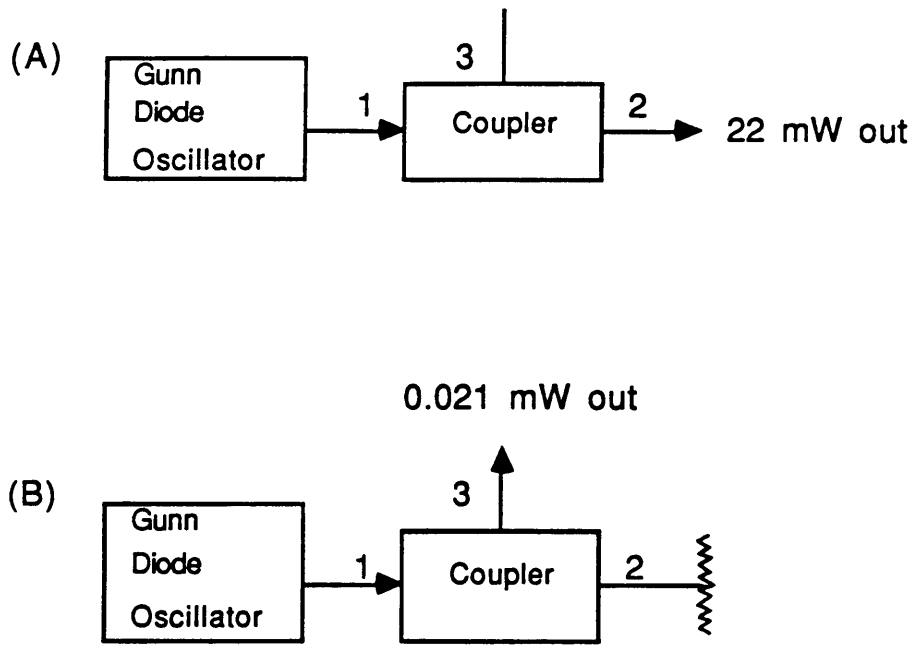

Figure 9. 3 dB Coupler

waveguide to which it is connected. This leakage could be seen when a power meter was held near the Gunn oscillator. On the remote chance that this signal leakage was influencing another part of the transmitter or being received by the horn, and thereby causing the the interference, radio frequency (RF) absorber was placed around the Gunn diode oscillator to shield the rest of the components from the leakage. RF absorber was also placed around the rest of the microwave components of the system and between the Gunn oscillator and the horn. As this absorber placement did not have any effect on the interference, it seemed unlikely that any interference was caused by Gunn diode oscillator leakage.

2.1.6 Different Horn Configurations

Other experiments run in the wavetank implied that the interference would not be present if the system were operated bistatically [3]. To confirm and further study this possibility, separate horns were used for transmission and reception. Figure 10 shows some of the transmit and receive configurations tested. Horn 1 was used for transmission and horn 3 for reception. It was necessary to use horn 3 (scalar lens horn) for reception, because it had a higher gain than horn 2. This higher gain was needed in order to detect the return signal, which was no longer being focused by the lens.

In set-up (A), the receive horn was attached to the front of the lens. This configuration physically separated the transmit and receive portions of the radar. It also removed the possibility of the receiver receiving reflections from the back of the lens. With this arrangement, the interference was still present. The only conclusion that could be drawn from this set-up was that the interference was caused by

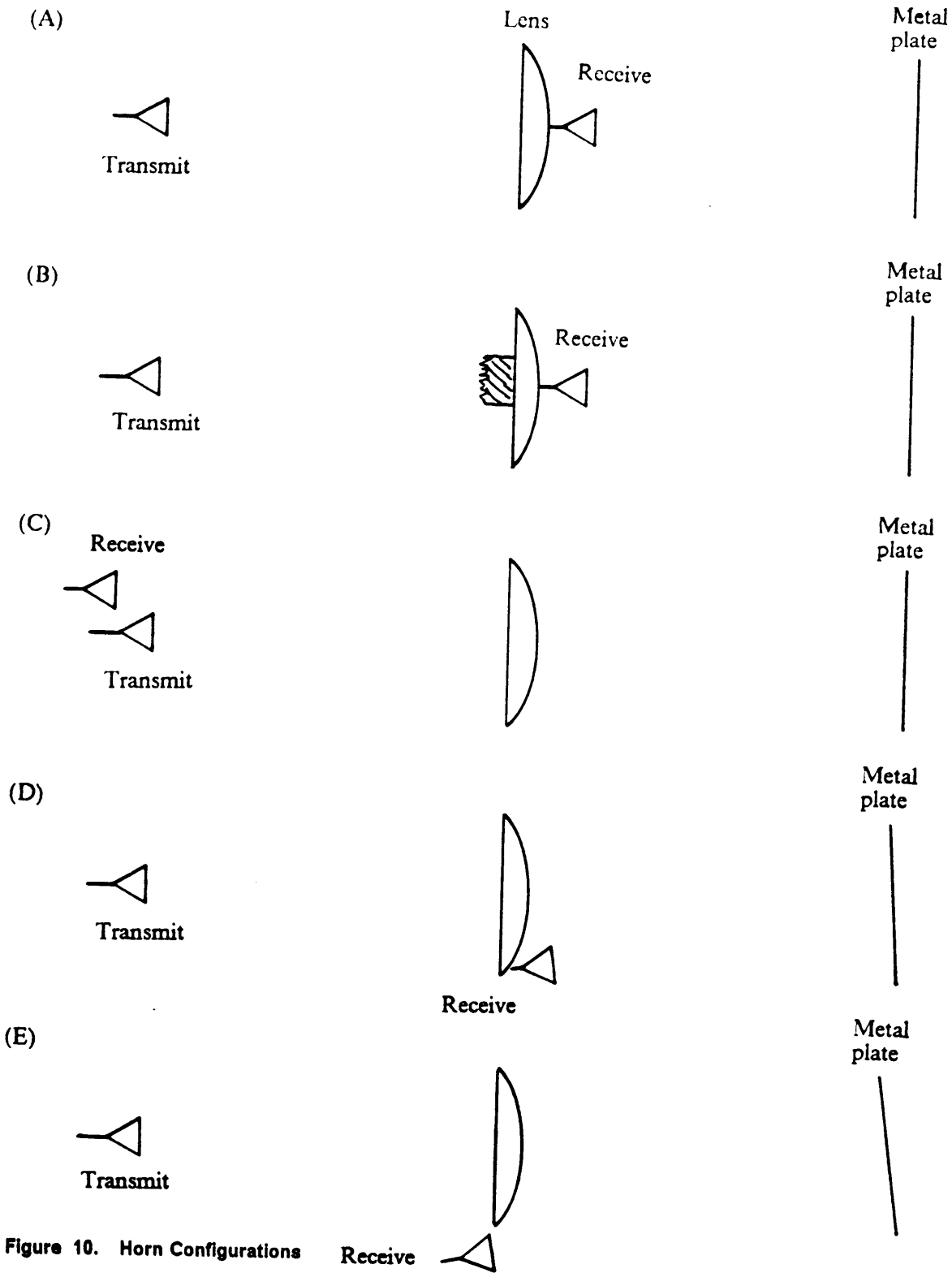

Figure 10. Horn Configurations

something other than lens reflections. This conclusion was in agreement with section 2.1.3 in which the interference was seen to be present even when the lens was removed from the system.

There may have been a problem with set-up (A), because the transmitter was radiating the back of the receive horn. In (B), RF absorber was placed on the back of the lens in an attempt to shield the receive horn from the transmitter. Even with the absorber, the interference was present. Nothing new could be concluded from this set-up, because it could not be proven that the receiver was not being influenced by the transmitter.

Set-up (C) completely removed the receive horn from the region directly illuminated by the transmitter. Also, with the receiving horn placed behind and slightly above the transmitting horn, it may have gained some benefit of the lens focusing of the return signal. The interference was found to be present with this set-up, but it was difficult to draw any useful conclusions because the close proximity of the horns could have caused antenna coupling. Also, from section 2.1.5 it was apparent that the receive horn could have seen leakage from the Gunn diode oscillator.

The set-ups shown in (D) and (E) were similar to other wavetank experiments (unrelated to the lens radar system) which did not seem to be troubled by interference [3]. In (D), the receive horn was placed adjacent to the focusing lens and the target was angled so that the receive horn was illuminated. As before, the target was moved through a range interval, and as in (A), (B), and (C) the interference was seen to be present.

Although the interference was present, its level was much reduced. This configuration was the first to cause a reduction in the interference. The oscillations riding on the expected signal were much smaller in magnitude than in any of the

other set-ups. To clearly see the difference, see Figures 11 and 12. Figure 11 shows the return power and phase for the monostatic set-up on the bench, and Figure 12 shows the return power and phase for set-up (D).

In (D), with the receive horn so close to the lens it was possible that it was being partially illuminated by the transmitter, and this illumination caused the interference. Another possible cause of the interference was that the transmitted signal was somehow corrupted by the plate reflected signal. In (D) it was possible that some of the target (plate) reflected signal was incident on the lens and was focused back into the transmitting horn. This signal would be received and propagate back through the waveguide to the sideband modulator and the Gunn diode, because these components were in no way isolated from the plate reflected signal. It seemed unlikely that this reflected signal could somehow alter the transmitter signals being generated in the Gunn diode and the modulator, but this possibility was further investigated (section 2.1.9).

In (E), the receive horn was moved further from the lens to reduce the possibility that it was being illuminated directly by the transmitter, and the target was angled further to compensate for this change in receive horn position. As can be seen in Figure 13, the interference was not present with this set-up. The target could be moved in range and there were no small oscillations (interference) riding on the expected return signal. Further experimentation showed how the horns would have to be arranged to insure that there was no interference. Figure 14 shows the necessary set-up. The angle ε had to be greater than 14 degrees or interference was present.

In the horn configuration experiments there were two common factors related to the interference. The more unlikely factor was that the interference was only present when the plate reflected signal was incident on the transmitter. If this

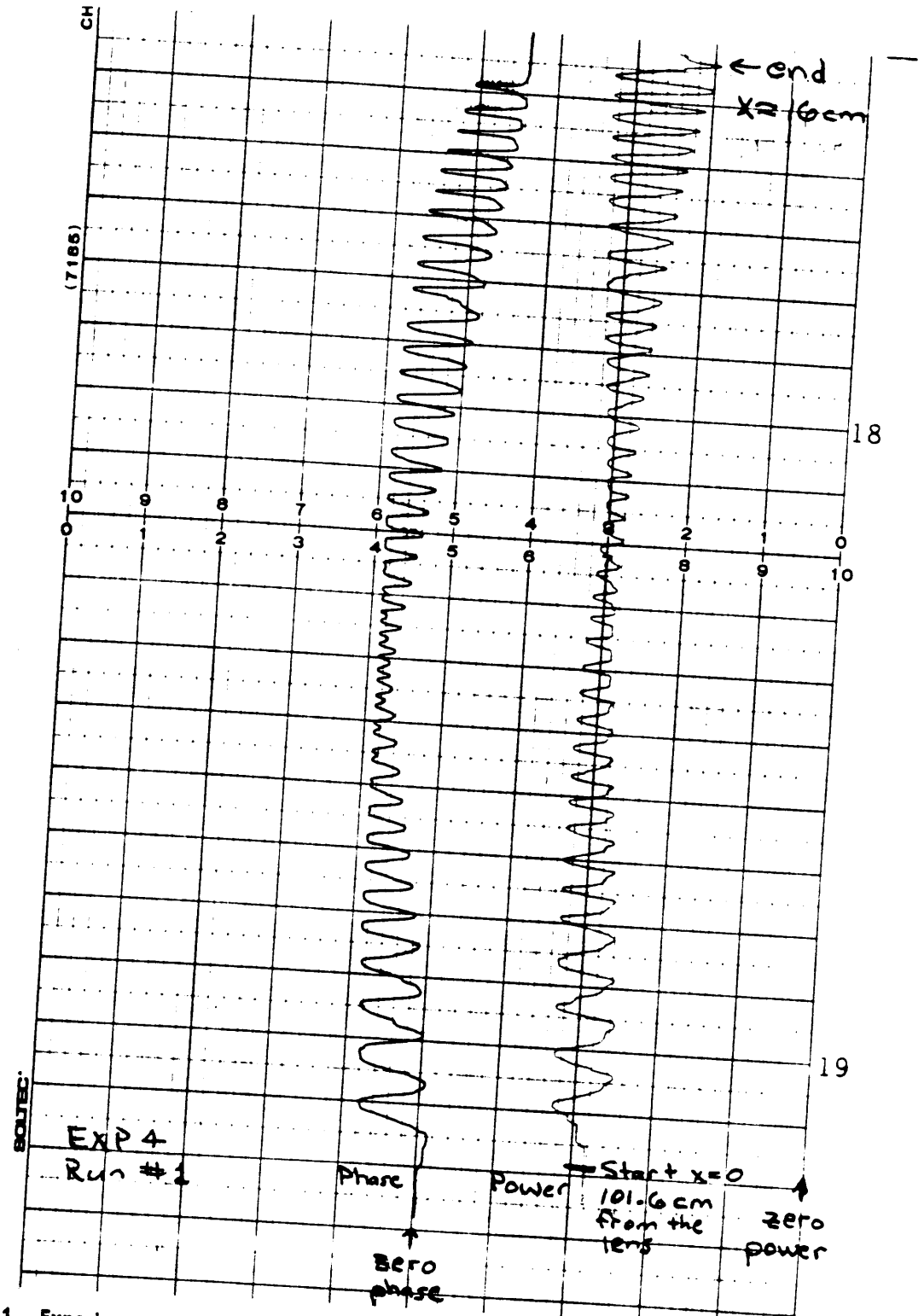

Figure 11. Experiment 4 (power and phase outputs from the Box): Run # 1

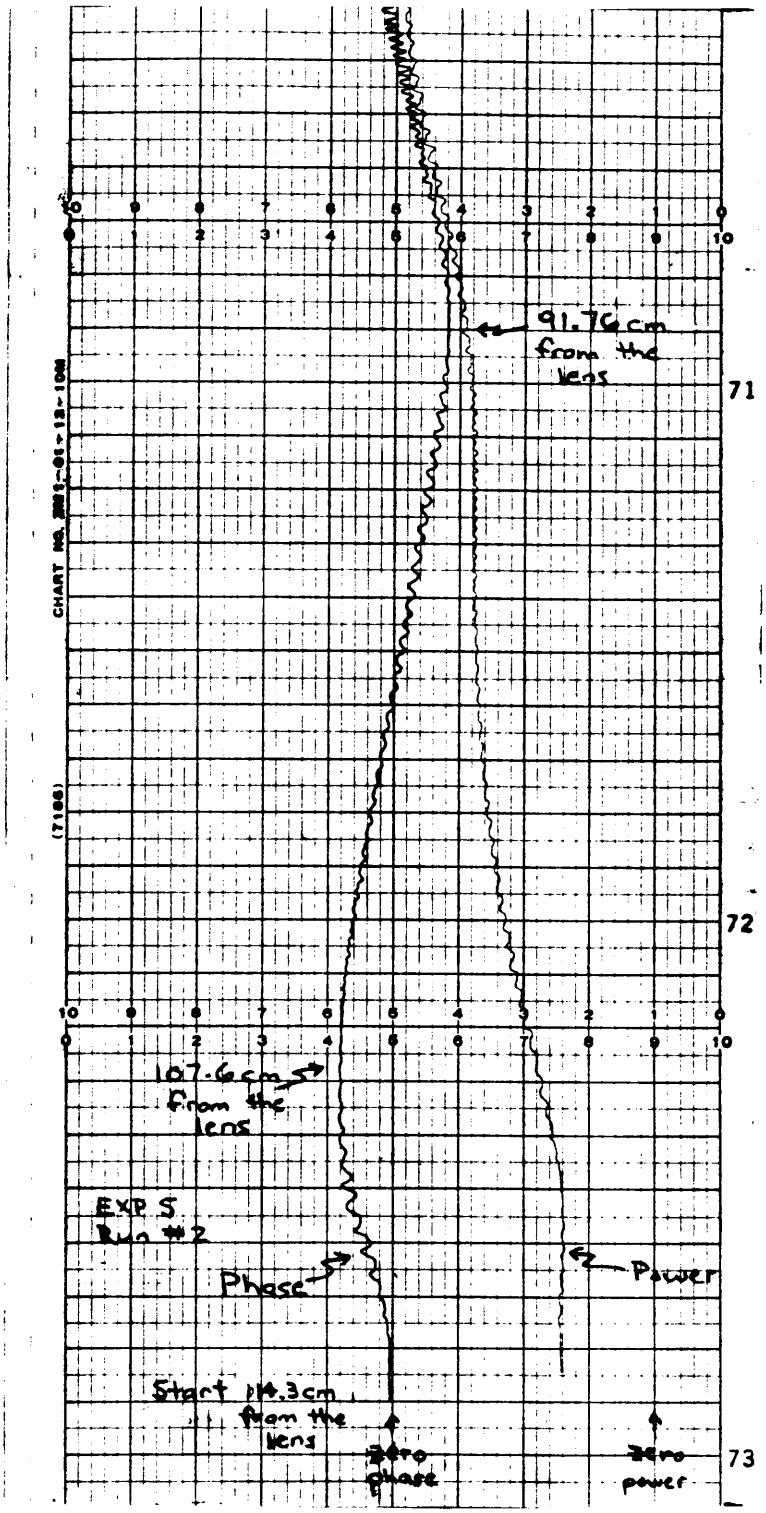

Figure 12. Experiment 5 (power and phase outputs from the Box): Run # 2

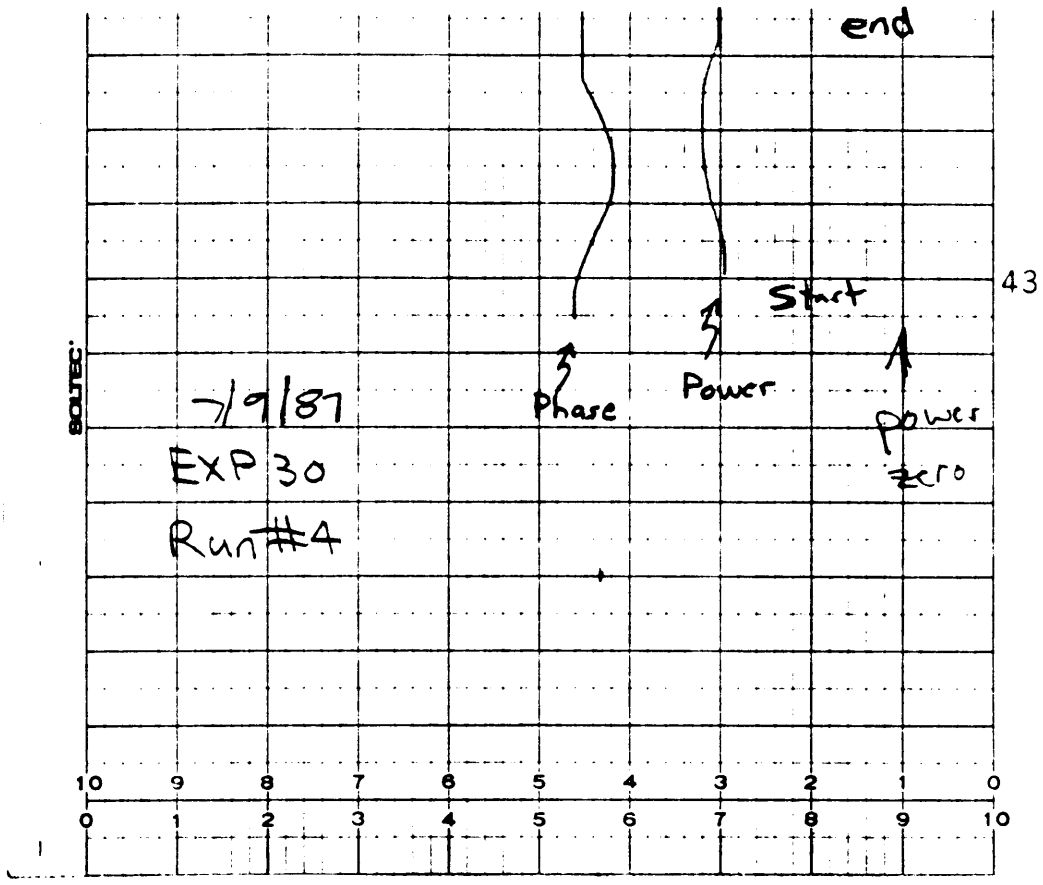

Figure 13. Experiment 30 (power and phase outputs from the Box): Run # 4

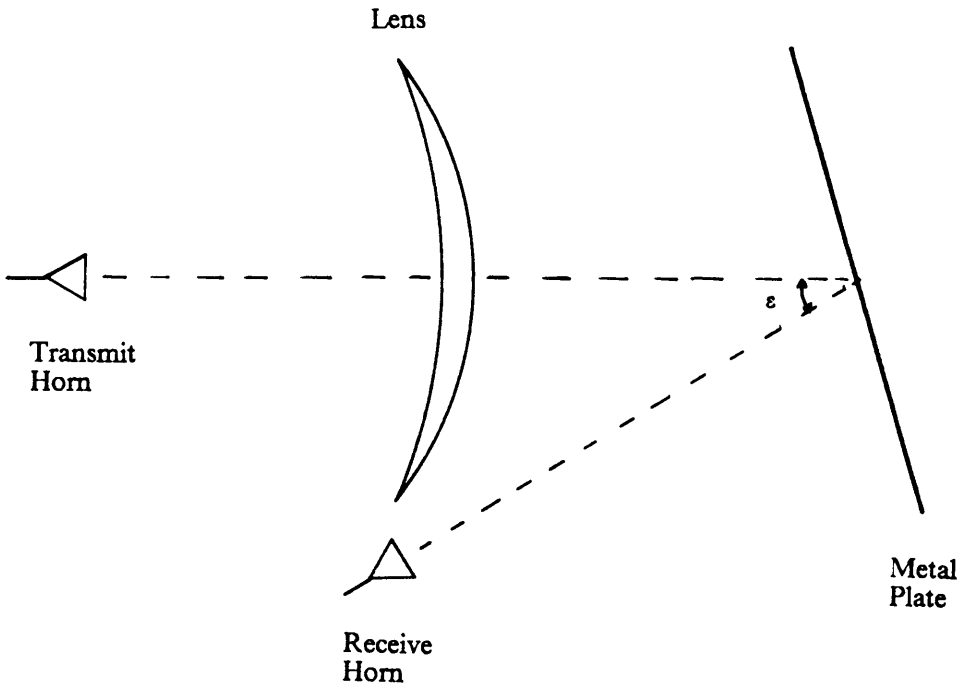

Figure 14. Interference-free Configuration

signal was the cause of the interference then somehow the plate reflected signal was corrupting the the formation of the transmitted signal. The possibilities were limited as to where the transmitted signal could be corrupted (i.e. in the Gunn diode or the sideband modulator).

The other common factor was that the receive horn was being influenced directly by the the transmitter. This implied a lack of enough isolation between the transmitter and the receiver. Either because of direct illumination, or as in the monostatic case, the 30 dB isolation of the coupler was insufficient.

2.1.7 Removal of the Lens and Horn

With the horn and lens removed, an open piece of waveguide was used to transmit and receive, and the metal plate (target) had to be moved to within 12 to 50 centimeters to be seen by the radar because the system no longer had the directivity it did with the horn and lens. Both the transmitted signal and the received signal were observed as the plate was varied in range.

To observe the transmitted and received signals, the attenuator and detector were connected to the 3 dB coupler. Figure 8 shows how the coupler was oriented when the return signal was studied. To study the transmitted signal, the orientation of the coupler was reversed. The idea that the return signal might be leaking into the modulator and or Gunn diode oscillator and influencing the transmitted signal prompted this study.

Examination of the return signal showed that the radar obviously saw the metal plate, because the interference appeared when the plate was moved in range, but moving the plate in range did not introduce the expected phase changes in the

return signal. This result implied that the return signal was weaker than the interference signal and too weak to even drive the phase comparators (Appendix B, section B.1, shows that this would be the case if the interference was caused by inadequate coupler isolation.).

When the signal formed by the Gunn diode and modulator was studied, it was expected that there would be no range information, because no range change took place (the distance between the Gunn diode and modulator, and the detector remained constant). With this set-up, as the plate was moved in range, no interference was seen in the studied signal. This result supported the conclusion that the plate reflected signal was not corrupting the transmitted signal. Because the interference was not seen with this set-up, if coupler leakage was a problem, the return signal that leaked through the coupler must have been too weak to introduce any interference (weaker than the system noise). This possibility was confirmed with calculations given in Appendix B (section B.2).

2.1.8 Reversal of the Coupler

With the focusing lens in place, the 3 dB coupler was reversed so that the signal formed by the Gunn diode and modulator could be studied. With this set-up, when the plate was moved in range, a very small interference signal was detected. As expected (as in the previous section) no range information was present. Calculations in Appendix C show that the plate reflected signal that leaked through the coupler could be the cause of this interference.

2.1.9 Use of a Spectrum Analyzer

With the spectrum analyzer it was possible to examine the carrier and sideband frequencies at different points in the system and see how they were influenced by changes to the system. First, the spectrum analyzer was used to study the effect of the Gunn diode oscillator and modulator being exposed to the target reflected (return) signal. When the attenuator/mixer/spectrum analyzer (A/M/S) was hooked up to either (A) or (B) (see Figure 15), and the plate was swung through an angle such that the transmitting horn went from not being illuminated, to being illuminated, to not being illuminated by the return signal, the 36 GHz carrier moved in frequency. The carrier moved up and down in frequency around the expected value of 36 GHz. When the plate was moved in the same manner and the spectrum analyzer was used to study the sideband signals, it was seen that they were not affected.

It seemed that some signal was getting back into the Gunn diode oscillator and interfering with the generated 36 GHz carrier frequency. To isolate the Gunn diode from the return signal a circulator was placed between the Gunn diode and the modulator (see Figure 16). With the circulator in the system, when the (A/M/S) was connected at either (A) or (B), and the plate was swung through the same angle as before, the 36 GHz carrier remained unaffected. Isolating the Gunn diode, with the circulator, removed the shift in carrier frequency, but it did not remove the interference. As the plate was moved through a range interval the interference was still present. Therefore, although this lack of isolation of the Gunn diode obviously had some effect, it was not the cause of the interference.

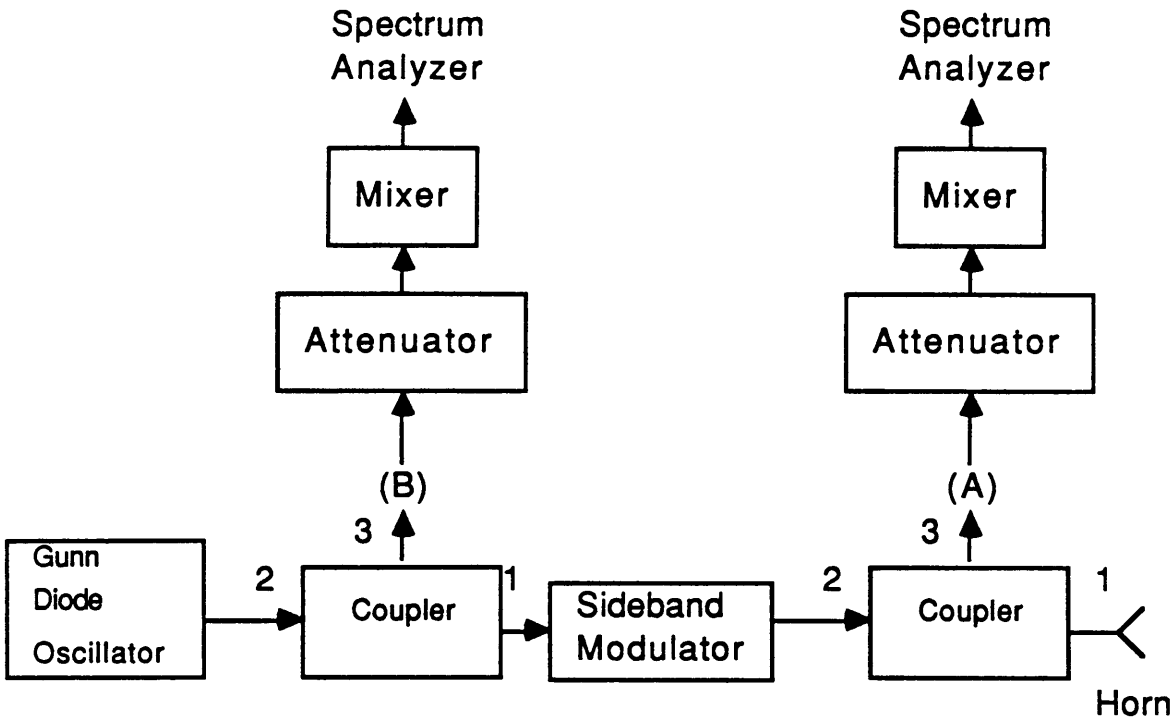

Figure 15. Spectrum Analyzer Experiments: Set-up # 1

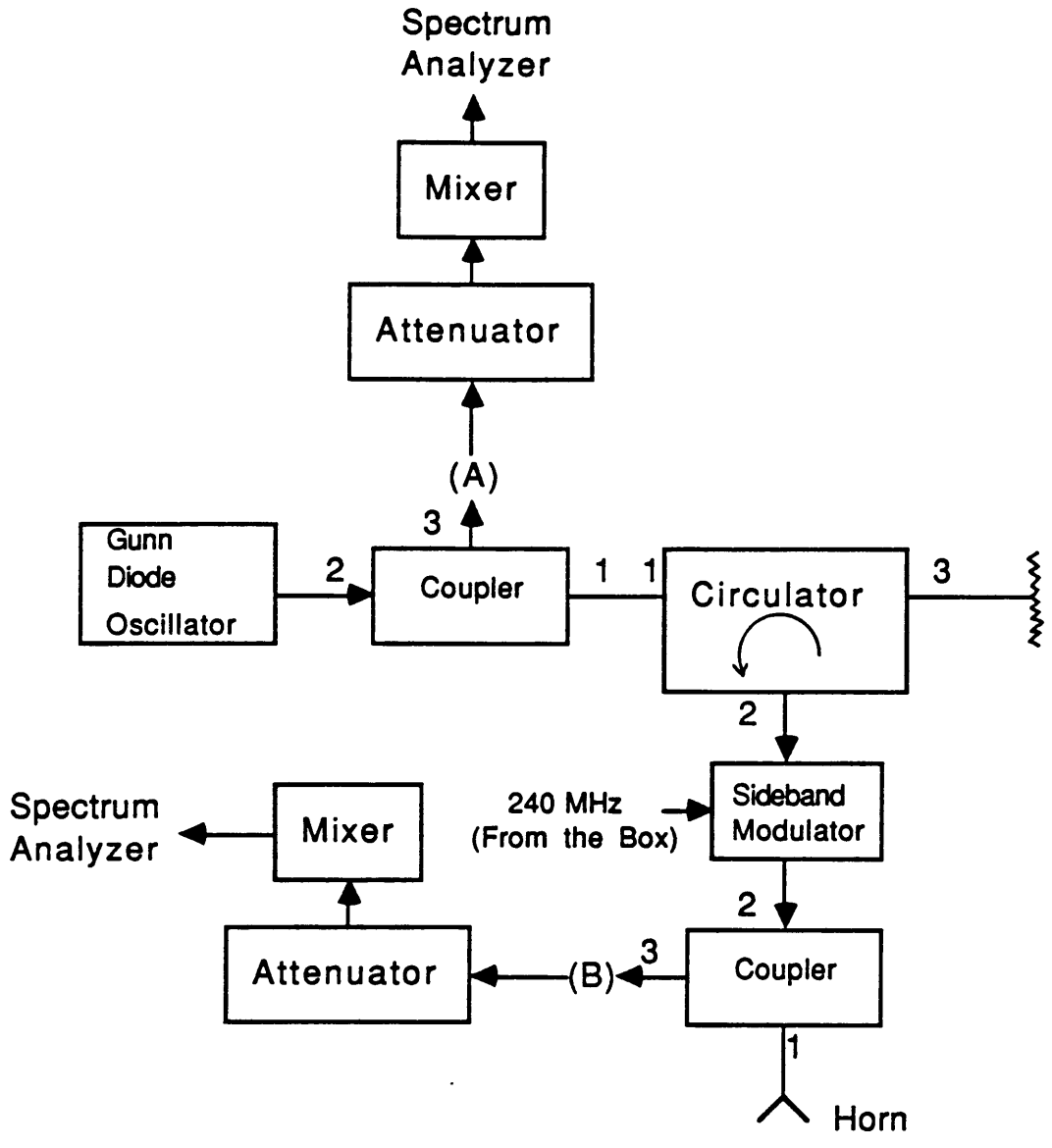

Figure 16. Spectrum Analyzer Experiments: Set-up # 2

The above discussed results support the idea that the interference was not caused by the return signal getting into the the Gunn diode or the modulator. In the above set-ups, the modulator was not isolated from the return signal. To confirm that isolating the modulator would not have any effect, a circulator was placed between the modulator and the horn (see Figure 17). As expected, with this configuration, the interference was still present.

Next the spectrum analyzer was used to study the return signal (see Figure 18) between the horn and the modulator. When looking closely at one of the sidebands, as the range to the plate was smoothly changed, the effect of the interference could be seen as follows. When the plate was moved in range, the amplitude of the sidebands cycled at the rate that corresponded to the interference (one cycle about every 4 mm range change).

When the orientation of the coupler was reversed from what is shown in Figure 18 so that the signal formed by the Gunn Oscillator and modulator could be studied, the same cyclic change in the amplitude of the sidebands could be seen as was seen in the return signal. This result was in agreement with the experiments discussed in the previous section.

2.1.10 Summary and Conclusions

Some conclusions could be drawn from the experiments made external to the wavetank. Something was causing a strong regular cyclic interference that depended on the target range and the system operating frequency. The characteristics of the interference, as seen with the radar system set up inside or outside of the wavetank, were the same. This consistency implied that even if any

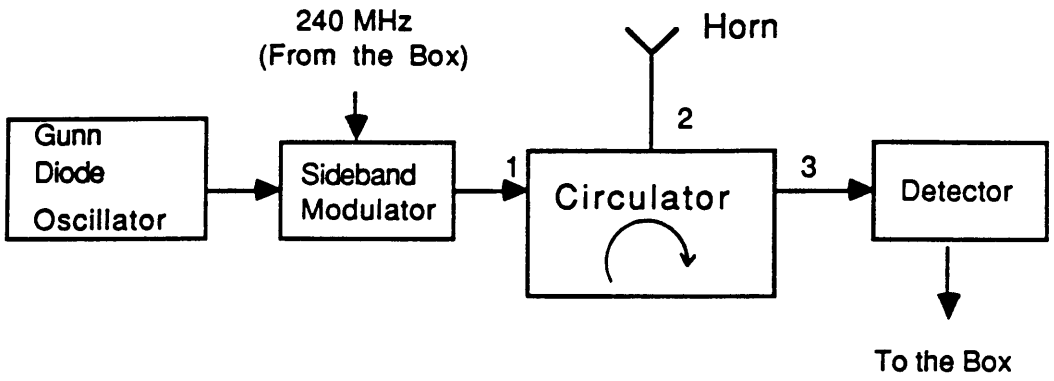

Circulator : 25 dB from 2 to 1
25 dB from 3 to 2
∞ isolation between 1 and 3

Figure 17. Spectrum Analyzer Experiments: Set-up # 3

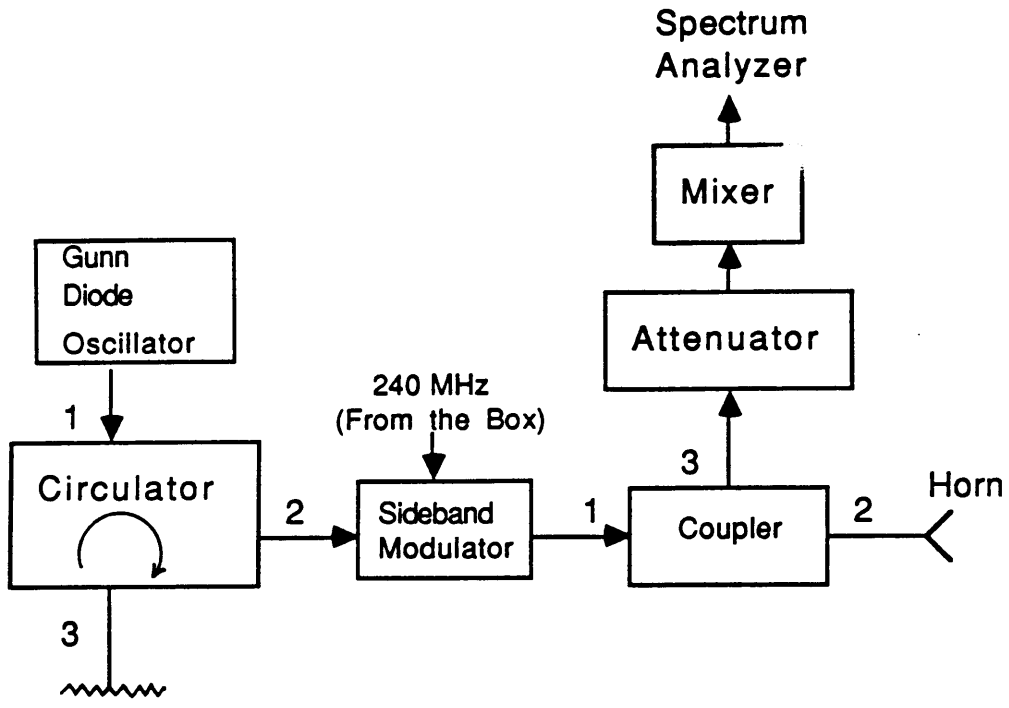

Figure 18. Spectrum Analyzer Experiments: Set-up # 4

interference was caused by the wavetank, it was not the dominant source of the interference. The interference was not caused by any of the components of the Box, because, as shown in section 2.1.6, it was possible to obtain an interference free result while using the Box.

Lens reflections were not considered to be the source of interference because the lens could be completely removed from the system (section 2.1.3) and interference was still present (also the back of the lens was coated with an impedance matching material to remove lens reflections). Section 2.1.9 argued against the interference being caused in the Gunn diode or the modulator. The interference was therefore taking place somewhere between where the signal entered the coupler and where it reached the detector. The only media between these points was the coupler, the horn, the lens, air, and the target.

There was no way for the air to cause the interference and a target (metal or water) could also not introduce the interference. Interference was present even when the lens was removed. Reciprocity says that the horn has the same transmit and receive characteristics, so the only way the horn could introduce interference was if part of the transmitted signal was reflected directly into the detector by an impedance mismatch at the horn. Not only are horns designed to minimize an impedance mismatch, but changing horns in the radar system had no effect on the the interference. Also, interference was present even when there was no possibility of reflections from the horn reaching the detector (section 2.1.6). The experiments showed a great deal of support for the idea that the interference had to do with the isolation between the transmitter and the receiver.

2.2 DISCUSSION OF THE NEED FOR BISTATIC OPERATION

It was obvious from the experiments presented in section 2.1, and the constraint that the system could only contain parts that were already available, that the only way to remove the interference problem was by operating the radar system bistatically as shown in Figure 10 (E). By using this configuration, all the possible causes of the interference discussed in sections 2.1.2 through 2.1.9 were removed. Lens reflections, horn mismatch, and lack of adequate coupler isolation all are no longer influencing factors. Lens or horn reflections could no longer reach the detector, and physically separating the transmit and receive horns introduces a higher isolation than the coupler could provide.

2.3 PROPOSED WAVETANK RADAR SYSTEM CONFIGURATION

The experiments showed the need for bistatic operation to insure the gathering of non-corrupted data. The original lens radar system was designed to study EM bias in the laboratory, so that conclusions could be drawn to better understand altimeter data. With this goal in mind, the system shown in Figure 19 was proposed to to minimize the effects of the interference. As can be seen in the figure, the lens was used to focus only the transmitted signal. By focusing the transmitted

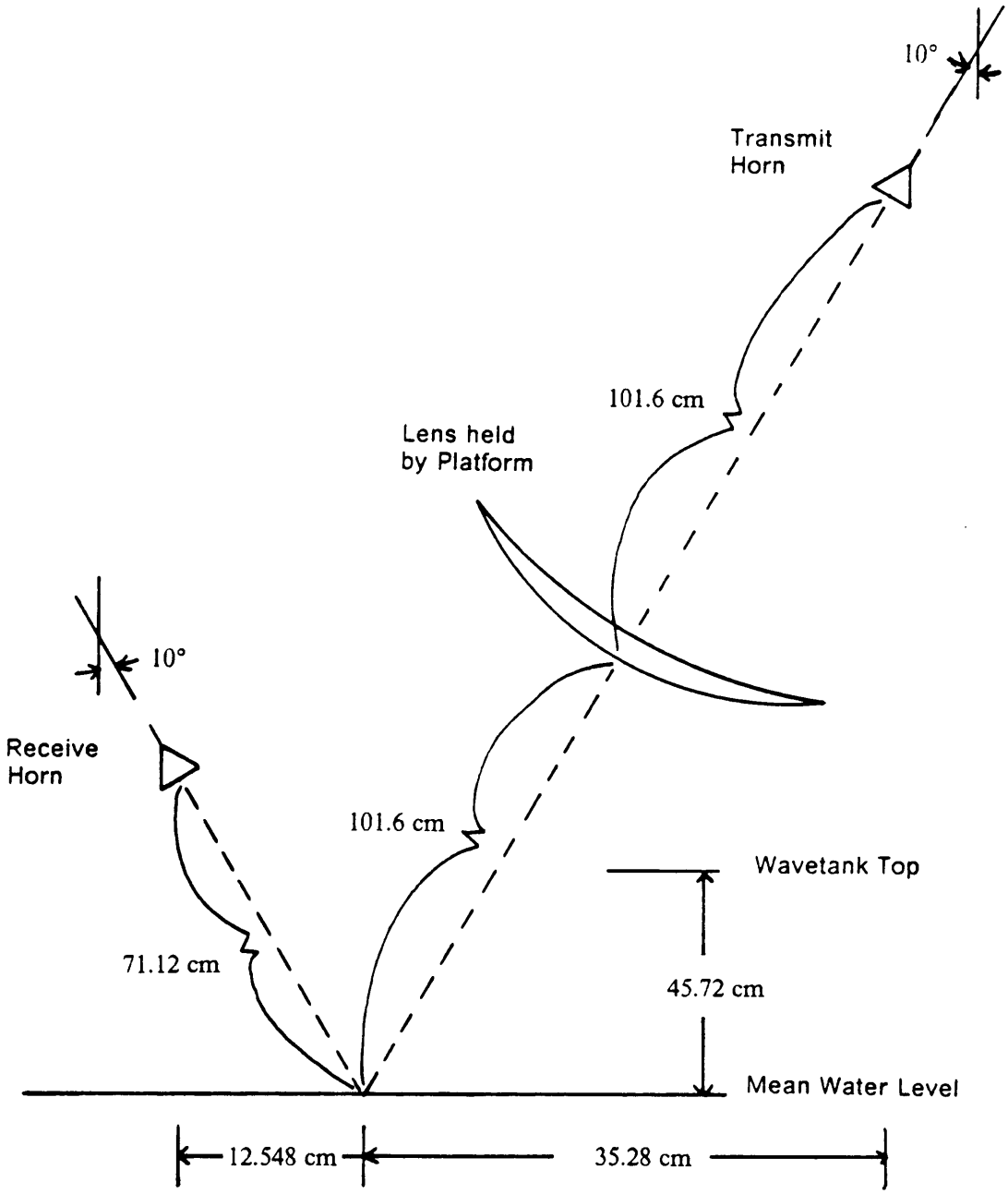

Figure 19. Bistatic Radar Set-up

signal, there was still the small spot size illuminating the water surface (as in the original design), and with this small spot the phase measurements could still be used to profile the wave height. Because the return signal was not focused by the lens, there was a considerable loss in signal strength reaching the receive horn.

An important aspect of this bistatic set-up was that both the transmit and receive horns were at the same angle off nadir and their boresights intercept at the mean water level. With this configuration the scattering facets are the zero slope facets, and zero slope facet scattering is what is important to study, because satellite altimeters primarily see scatter from zero slope facets.

There was also a change in the operating frequency for the bistatic wavetank set-up. With the reduced signal strength due to the return signal no longer being focused, the 36 GHz system did not yield a strong enough received signal level for reliable data collection. The return signal was near the noise level of the receiver and was often too weak to drive the phase comparators. In order to maintain a strong enough signal into the Box, to insure reliable data collection, a Traveling-Wave-Tube Amplifier (TWTA) had to be used to amplify the signal. There was no TWTA available for use at 36 GHz, but there was one for 13.5 GHz. Therefore, the system as shown in Figure 19 was installed in the wavetank with a operating frequency of 13.5 GHz (13.5 GHz is a frequency used by some operational altimeters).

2.4 EXPERIMENTS PERFORMED IN THE WAVETANK

2.4.1 Test of New Wavetank Radar System

The radar system as proposed in the previous section was installed in the wavetank. On the bench, this bistatic configuration (discussed in section 2.1.6) resulted in an interference free signal. With the system now in the wavetank, a drain test was run and interference was found to be present, but at a much lower level than in the monostatic case. In the range of interest, when the water level was within 3 centimeters of the mean water level, the interference in the power was less than 0.14 volt peak to trough (~0.9 dB power variation). The interference was smallest when the spot size was most focused (at the typical wavetank operating water level) and became larger as the spot defocused.

It is reasonable that the more focused the spot the less interference would be present. Both the small spot (maximum focusing) and the somewhat larger spot (slightly defocused) are going to be illuminated with the same amount of energy; which will be reflected towards the receive horn. The reflected signals undergo spreading loss and the larger the spot the more spread out the energy is when it is reflected. This spreading leads to less energy reaching the receive horn the larger the spot. Also, the more spread out the reflected signal is the more chance there is for multipath reflections to take place.

The quadrature output from the Box for this bistatic drain test is shown in Figure 20. The plot shows the phase output from when the water level is at 10

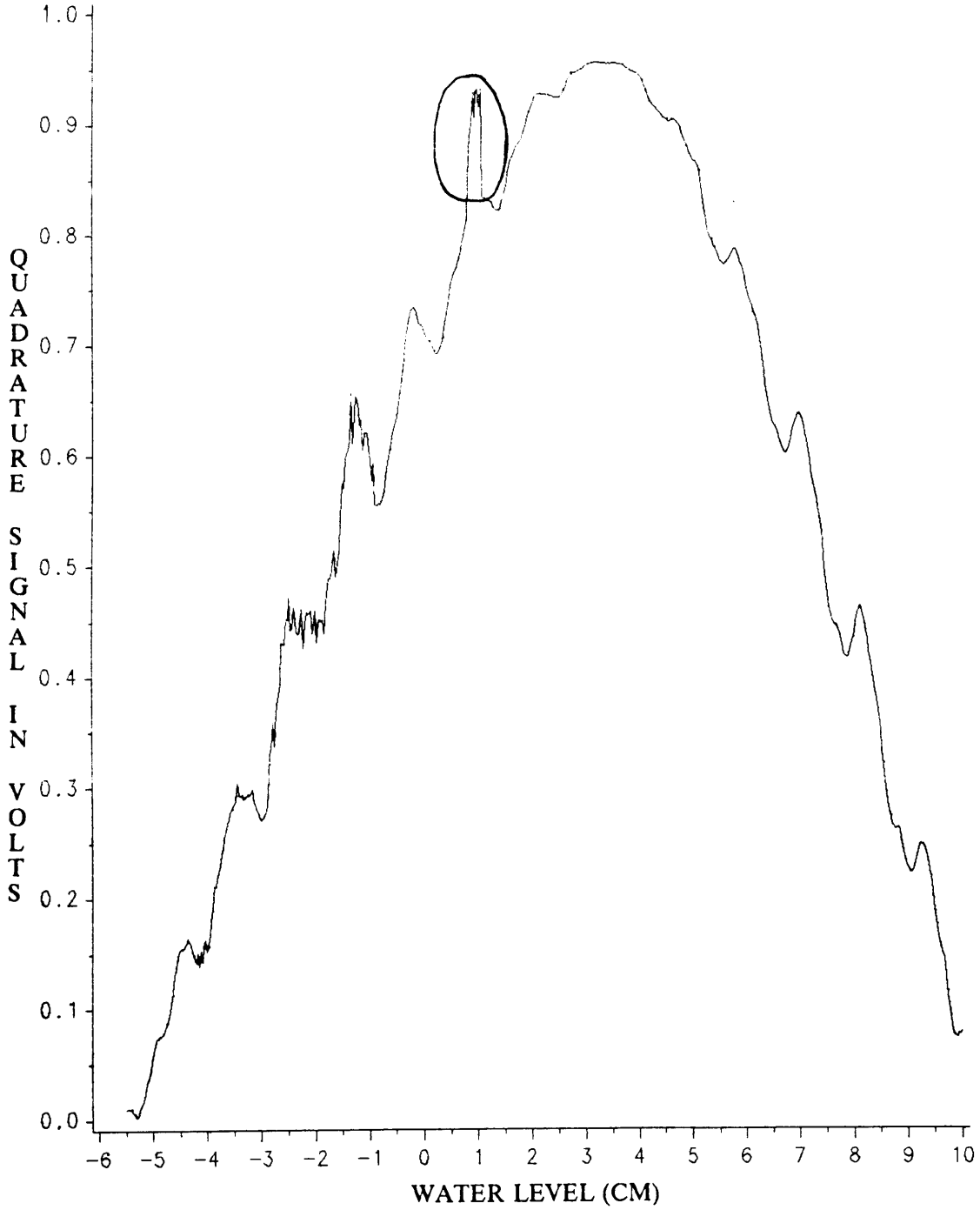

Figure 20. Quadrature output from the Box during Drain Test DRN: Bistatic radar configuration (the circled deviation corresponds to about a 1.6 cm error in the water height calculation)

centimeters above typical wavetank water level until the water level reaches 5.5 centimeters below typical wavetank water level (drain rate $\simeq$ 1.0877 cm/min). As can be seen in the plot, the phase went through about half a cycle and the largest point of interference (circled on the figure) was when the signal deviated about 0.12 volt from the expected return. This deviation corresponded to about a 1.6 centimeter error in the water height calculation. Comparing this Figure to the phase plot in Figure 6, which showed swings of 0.6 volt, illustrated the effect the bistatic system had on reducing the interference.

Since it was possible to attain an interference-free result with a set-up outside of the wavetank, it seemed likely that the tank or platform was somehow introducing the residual interference. Perhaps some form of cavity effect or multipath was taking place. Even though the interference was now less than half of what it was in the original system set-up, it was necessary to further reduce the level of interference because of the high level of accuracy necessary for EM bias measurements.

2.4.2 Description of the Interference

The interference that remained was very similar in form to the interference in the original monostatic system. It was like a sinusoidal signal riding on top of the expected signal return signal. The sinusoid was not as "clean" as in the original system; it varied in amplitude and at times it looked like more than one sinusoid adding together to form the interference. Even with these less "clean" sections, one sinusoid typically dominated and its oscillations corresponded to the operating frequency of the radar (13.5 GHz, wavelength $\simeq$ 2.2 cm). The interference went

through one cycle about every one centimeter drop in water level, and the maximum interference peak to trough was about 0.14 volt in the return power (~0.9 dB power variation).

2.4.3 Description of the Secondary Target

It was suggested that perhaps the change in (cavity) size of the wavetank, when a drain test was run, was introducing the interference because as a drain test was run the cavity size changed as the water level dropped [3]. This seemed an unlikely cause, but it was tested by introducing a secondary target that could be manually moved up or down to simulate the change in water level. Introduction of a secondary target was also used to test if multipath was a problem, by showing if the radar responded to both the target and the water when the spot size was only big enough to illuminate the target.

The secondary target consisted of a sheet of metal foil placed on the end of a flat styrofoam arm. Figure 21 shows the target's position in the wavetank. The styrofoam arm was transparent to the radar signal and the foil was a good reflector. A vernier was used to smoothly move the arm up or down a known distance.

2.4.4 Calm Water and Raising the Secondary Target

With still, calm water (typical wavetank water level), the secondary target was maneuvered to be just above water level and illuminated by the radar spot. The secondary target was then smoothly raised. The radar obviously saw the secondary

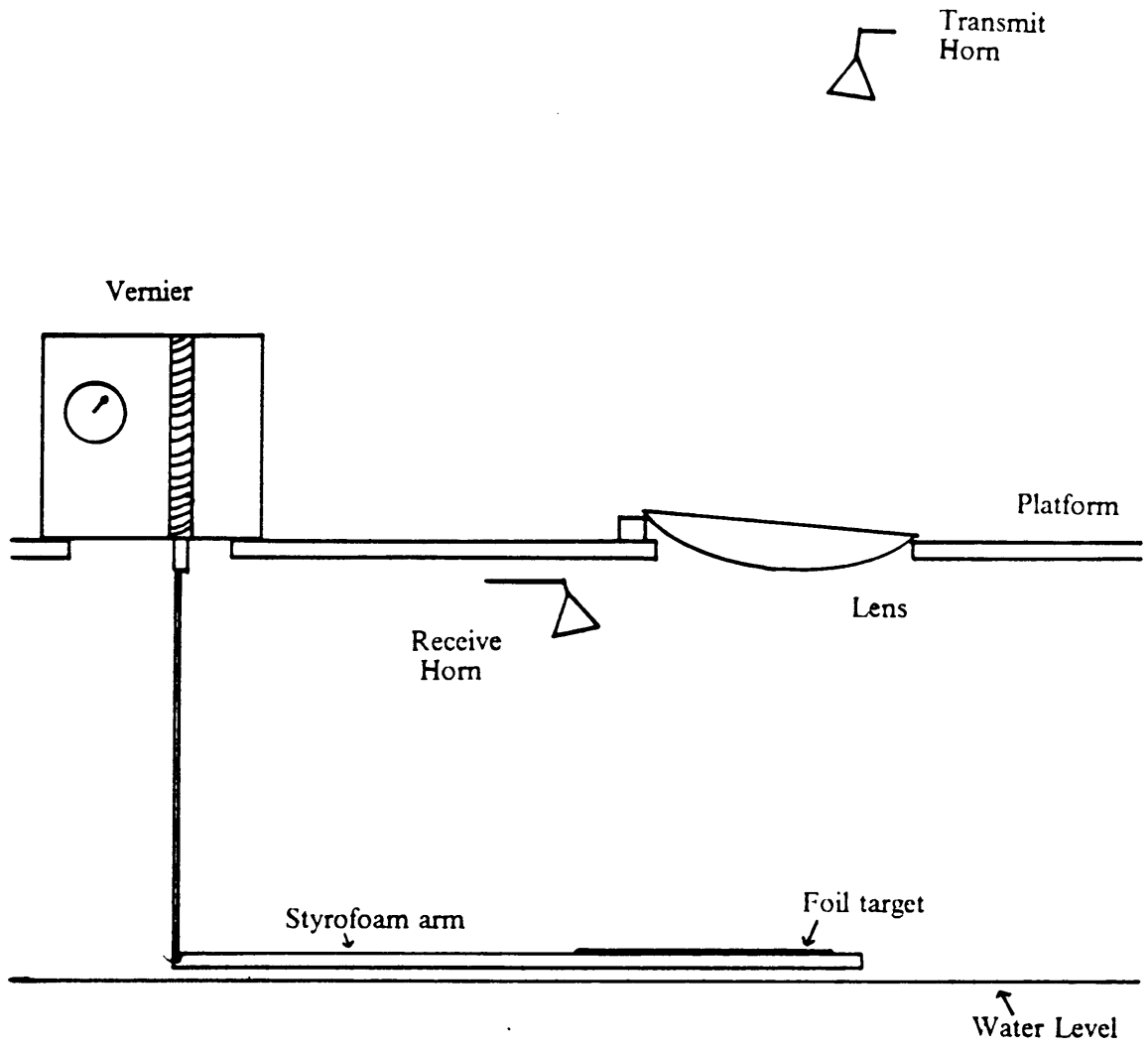

Figure 21. Secondary Target

target, because the phase changed in relation to the height change of the secondary target, but interference was also present. This experiment showed that it was not necessary for the cavity size to change in order to have the interference present.

2.4.5 Stationary Secondary Target and Draining the Tank

Next, the secondary target was held stationary, just above the initial water level, and the water level was lowered. The water was drained 9 centimeters at about a rate of 1 centimeter every 55 seconds. The return power and phase oscillated around a mean value. They went through one cycle about every 1 centimeter drop in the water level. It seemed that the radar saw the secondary target at a constant range (no large phase change) and that the lowering water level introduced the interference. This implied that the radar was getting returns from both the secondary target and the water.

2.4.6 Stationary Secondary Target and Roughening the Water Surface

The secondary target was held stationary above the water and a 0.5 volt 2 Hz paddlewave was used to roughen the water surface. The wave generated was about 6 millimeters peak to trough. What was seen by the radar was that the return power and phase oscillated around a mean value at a frequency of 2 Hz. This result confirms that the radar was seeing both the secondary target and the water.

2.4.7 Varying the Secondary Target and Roughening the Water Surface

To further confirm that the radar was seeing both the secondary target and the water, both were moved simultaneously; 2.0 Hz paddlewaves were generated and the secondary target was moved in range. The phase went through a gradual change which corresponded to the range change of the secondary target, but riding on top of this gradual change were smaller magnitude oscillations at a frequency of 2 Hz. The power had the small magnitude oscillations at 2 Hz, but it also cycled once every 1 centimeter change (interference) in the secondary target height. The above and the three previously discussed experiments clearly showed that the radar was seeing both the secondary target and the water. For both to be seen by the radar, there must have been multipath taking place (most likely inside of the wavetank).

2.4.8 Effects of RF Absorber on Multipath

To see if the interference, which seemed to be caused by multipath, could be reduced by using RF absorber, identical tests were run with and without absorber. In both tests, the water was held at a constant level and the secondary target was moved through the same range interval, while the return power was recorded. Without any absorber, the interference varied from about 1.57 volts to about 0.031 volt peak to trough. With absorber suspended across the wavetank, between the secondary target and the water, the interference varied from about 0.045 volt to about 0.028 volt peak to trough. This large reduction in the level of the interference implied that the RF absorber removed much of the multipath interference.

The above described experiment supported the idea that the in-tank interference was caused by multipath. Not only did the RF absorber greatly reduce the level of the interference, but it also made the interference maintain a more constant level. Without the absorber, the interference varied from about 0.031 volt to about 1.57 volts peak to trough, whereas with the absorber the interference variation in the interference level was was only about 0.017 volt. This result was reasonable; the more weak interference signals (multipath) that reach the receiver, the more signal variation could take place in the interference as these signals add constructively and destructively.

2.4.9 Absorber Windows on Top of the Wavetank

Because the available RF absorber was bulky, heavy, and not waterproof, it was difficult to use inside of the wavetank where most of the multipath reflections were probably taking place. Another reason for not putting much absorber inside the wavetank was it would disrupt the air flow when wind is generated in the wavetank.

Using geometrical arguments, it could be said that the signal of interest traveled as a bundle of rays along the boresight of the transmitting antenna. This bundle was reflected from the water and traveled in a straight line to the receiving horn. Because this was the signal path of interest, transmit and receive windows were built with RF absorber on the top of the wavetank to pass this signal and block most others. These windows could not be made too small or they would block too much of the energy contained in the bundle of rays.

In order to effectively reduce the multipath, the RF absorber had to be so close to the receive horn that it reduced the effective beamwidth of the horn by

blocking some of the reflected signal. The signal that traveled along the antennas' boresights via reflection from the water surface at the typical water level was partly attenuated, while signals from other water heights were more attenuated by the RF absorber. This increased attenuation took place, because the further the water height varied from the typical wavetank water level the more absorber was between the point of reflection and the receive horn (consequently more loss). A method for removing this absorber effect from the experimental data is discussed in section 5.2.2.

Previously, the strength of the interference was gauged by the size of the peak to trough swing in the interference. Because the absorber window caused the return power versus water level curve (during a drain test) to be u-shaped (see Figure 22), the level of the interference was redefined. With this new definition, the interference level in the return power was measured as the deviation from the u-shape.

The introduction of the absorber windows had an immediate effect. They maintained the interference at a level less than 0.1 volt peak to trough (less then a 0.64 dB power variation). With much trial and error, the absorber configuration shown in Figure 23 was found to be the most successful. As can be seen in Figure 23, absorber was glued to the base of the platform to remove reflections from the platform. Absorber was also placed between the receive horn and the lens to further isolate the receiver from the transmitter. This absorber between the lens and receive horn also kept any reflections from the front of the lens from reaching the receive horn. With this absorber configuration the interference was held below 0.10 dB in the return power (see Figure 22). The reduction in interference could also be seen in the marked improvement in the return phase (see Figure 24 and compare to Figure 20).

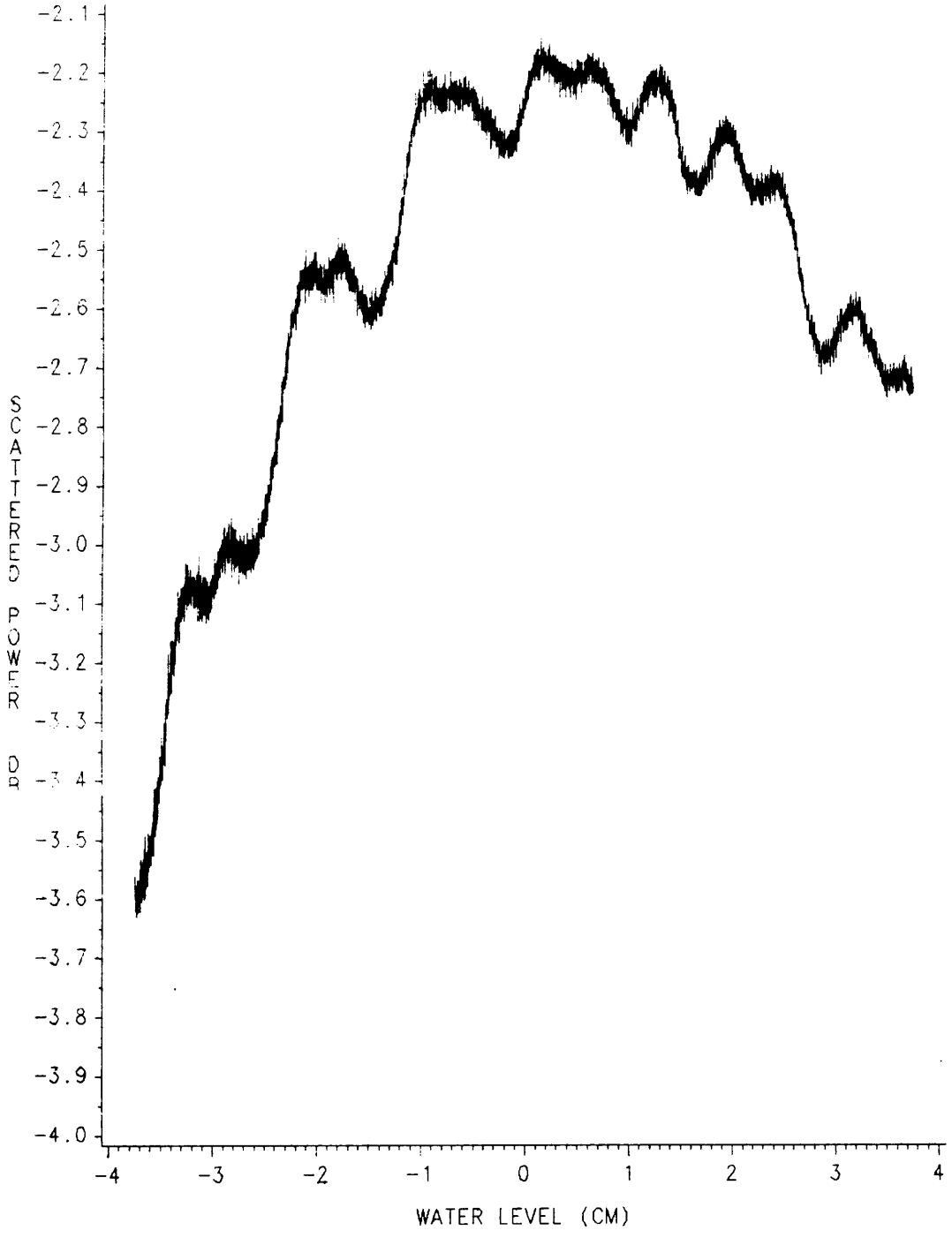

Figure 22. Scattered Power during Drain Test R2: Bistatic radar configuration with absorber windows in place

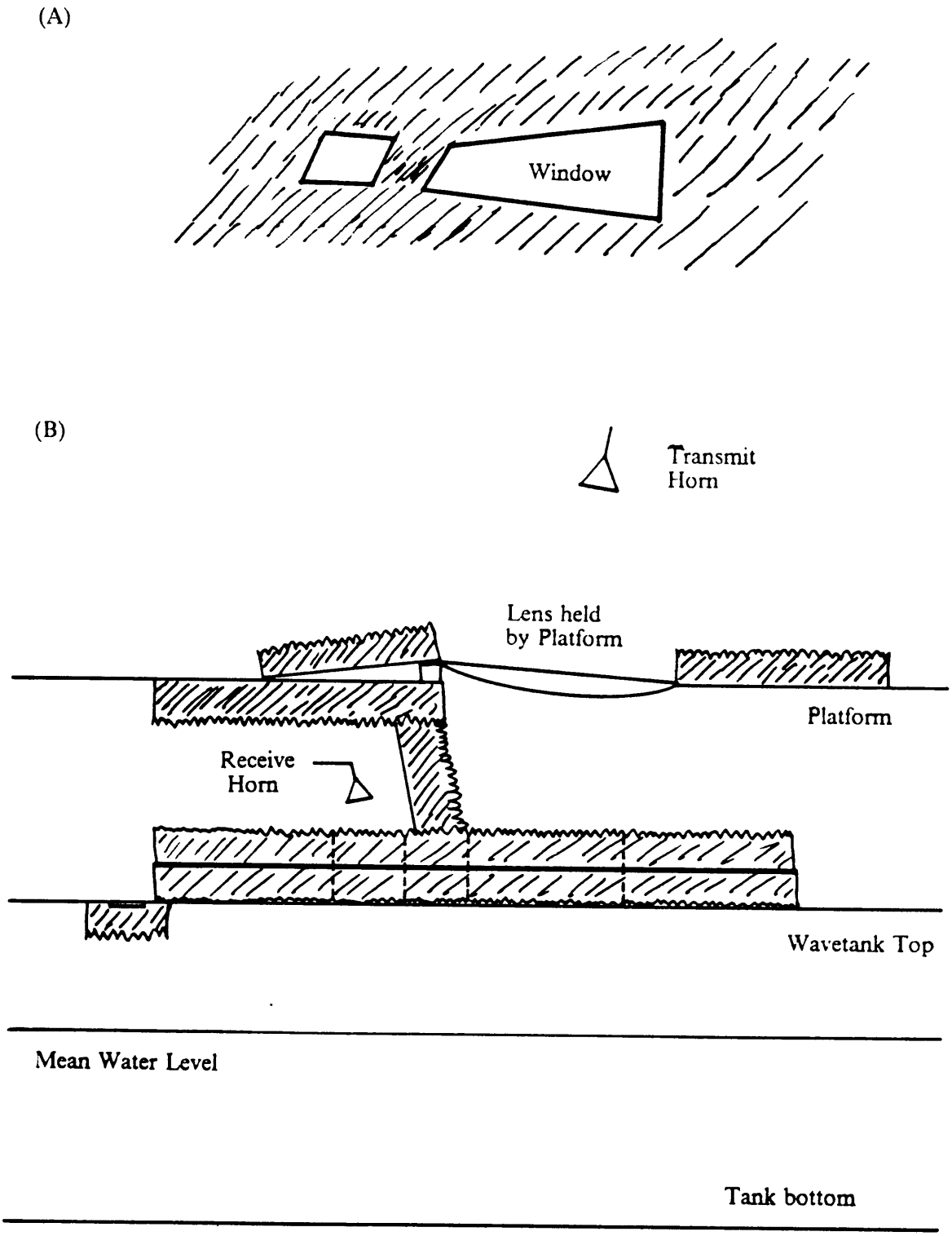

Figure 23. Absorber Window: (A) View of the Wavetank top, (B) Side View

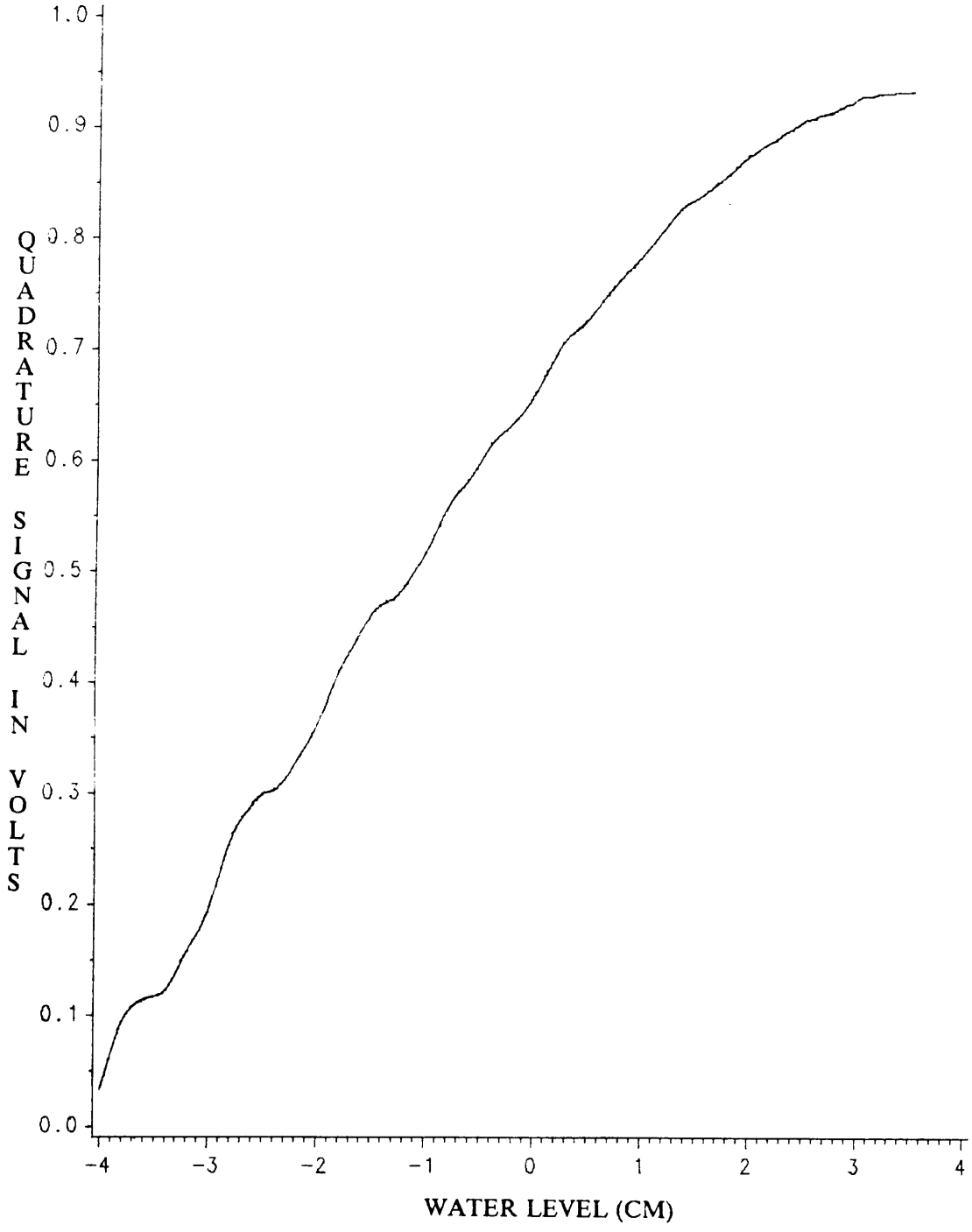

Figure 24. Quadrature output from the Box during Drain Test R2: Bistatic radar configuration with absorber windows in place (deviations in the phase signal correspond to less than a 1 mm error in the water height calculation)

The small oscillations shown in Figure 24 correspond to less than a 1 millimeter error in the water height calculation.

2.4.10 Probe in the Radar Spot

When experiments were first run with the radar system in its original monostatic configuration, the high level of interference made the wave height calculations from the phase information unreliable. For this reason a capacitance probe was suspended through the radar spot to obtain an alternate measurement of the wave height, because its measurements were not influenced by the interference. Even with the reduction in the interference in the phase (with the bistatic set-up and the RF absorber windows) the capacitance probe was still used to measure wave height because it gave continuous height information (see section 3.2).

Since absorber was used to reduce the level of the interference such that accurate data could be collected, it was necessary to check the effect, if any, the probe would have on the level of the interference. This was an important item to check because the probe must be directly in the radar spot in order to give collocated height information.

A probe was placed in the illuminated spot and a drain test run (Drain test R3). The power and phase plots for this drain test are shown in Figures 25 and 26 respectively. The level of interference was found to be slightly greater than the tests run without the probe (see Drain test R2), but it remained less than 0.13 dB in the return power (Figure 25). When experiments are run it was necessary to power the probe so that height measurements could be taken. With the probe powered (Drain test R4), the interference was seen to be slightly greater, but still less than 0.14 dB

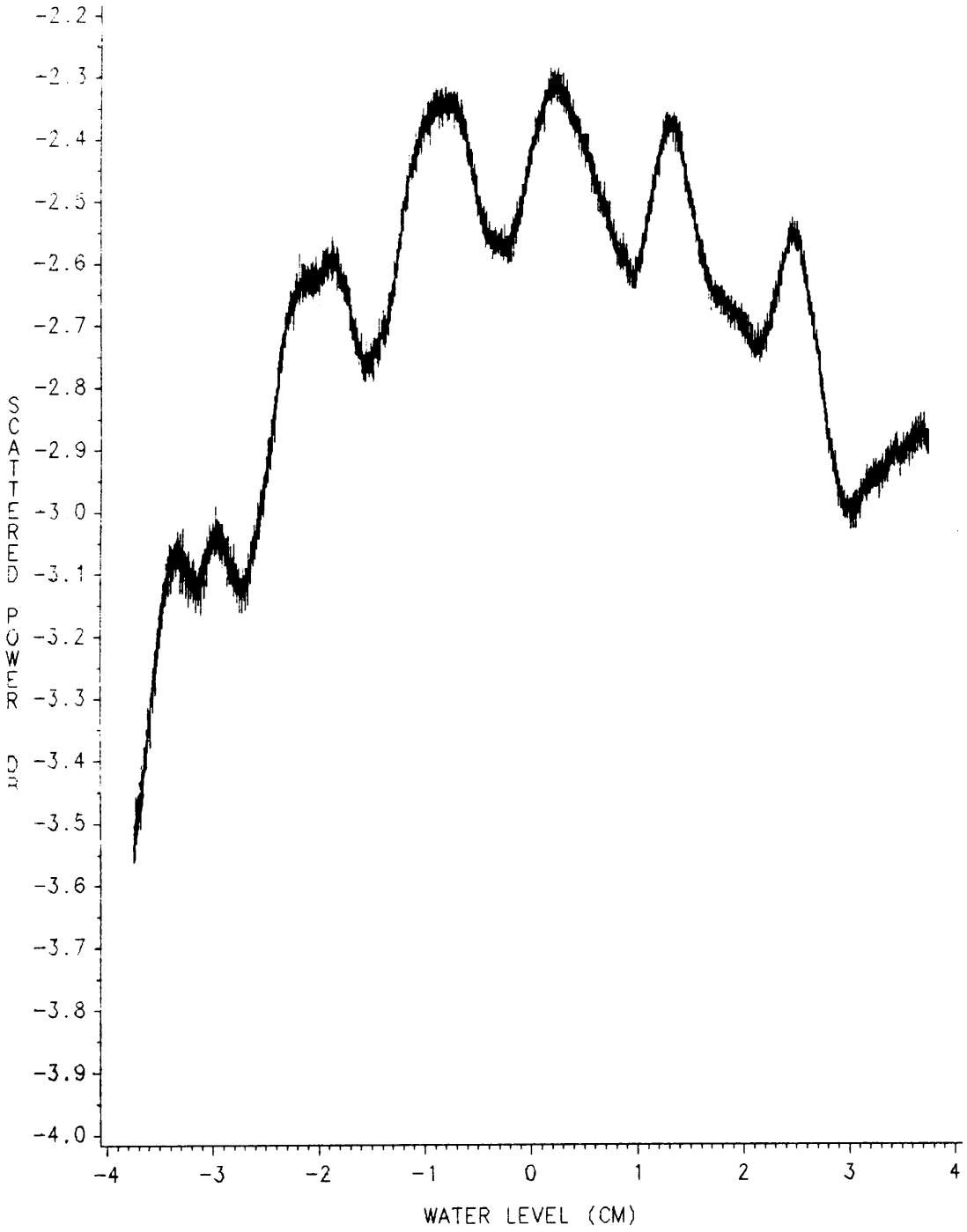

Figure 25. Scattered Power during Drain Test R3: Bistatic radar configuration with absorber windows in place, and a capacitance probe in the radar spot

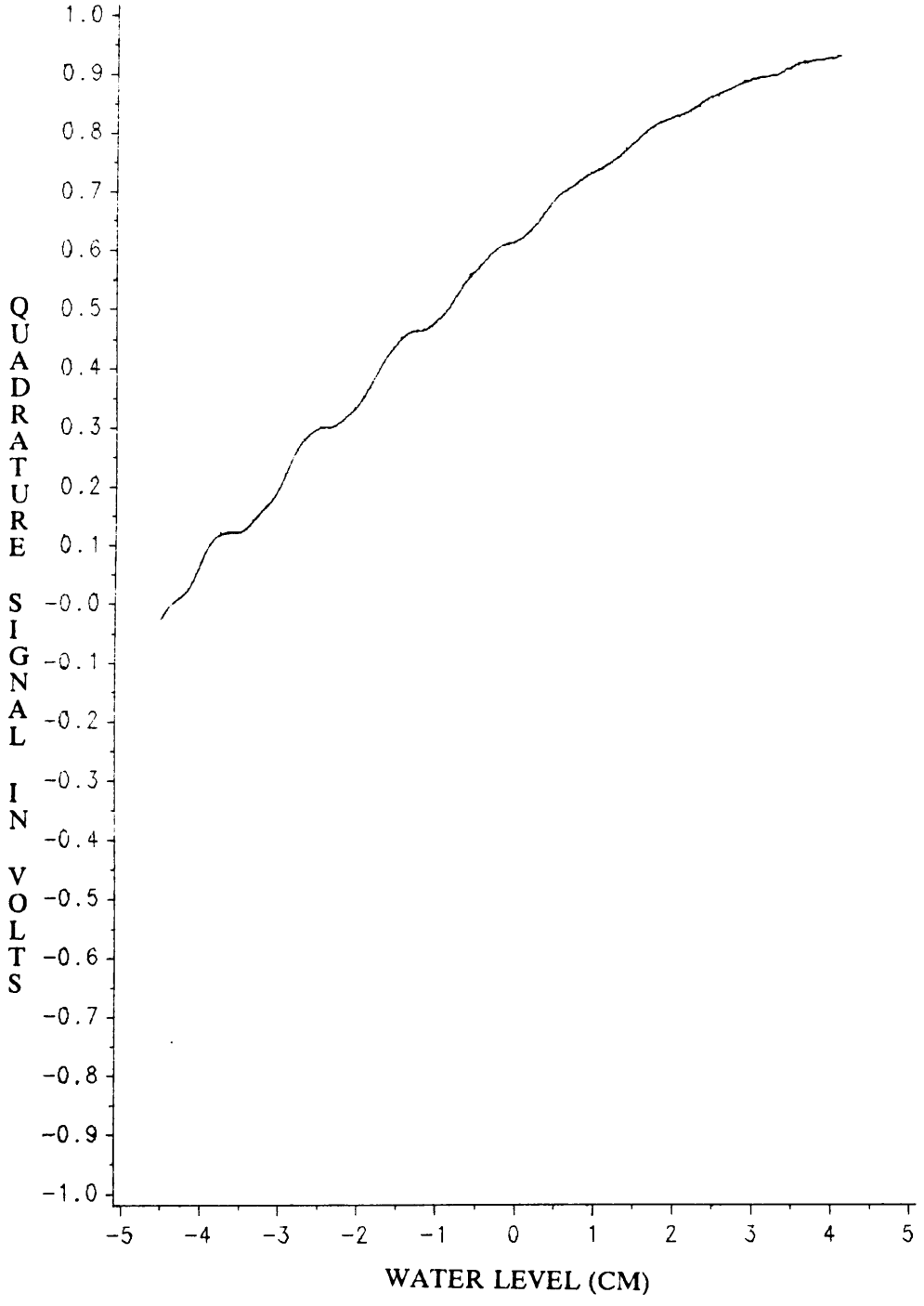

Figure 26. Quadrature output from the Box during Drain Test R3: Bistatic radar configuration with absorber windows in place, and a capacitance probe in the radar spot (deviations in the phase correspond to less than a 1 mm error in the water height calculation)

in the return power (see Figure 27). Like in Drain Test R2, the error in the phase signal for Drain Tests R3 and R4 was very small, and it would result in less than a 1 millimeter error in the water height calculation.

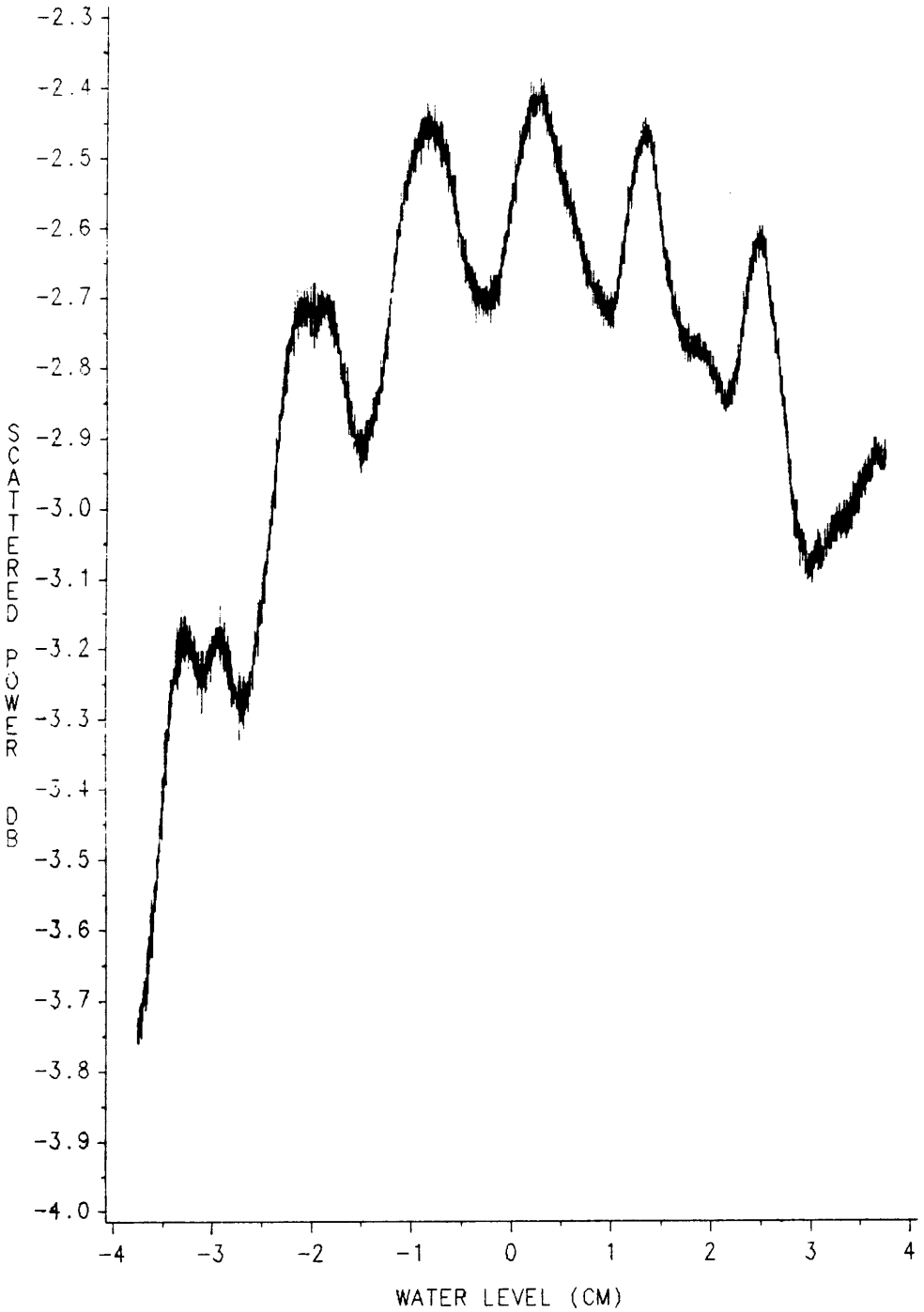

Figure 27. Scattered Power during Drain Test R4: Bistatic radar configuration with absorber windows in place, and a powered capacitance probe in the radar spot

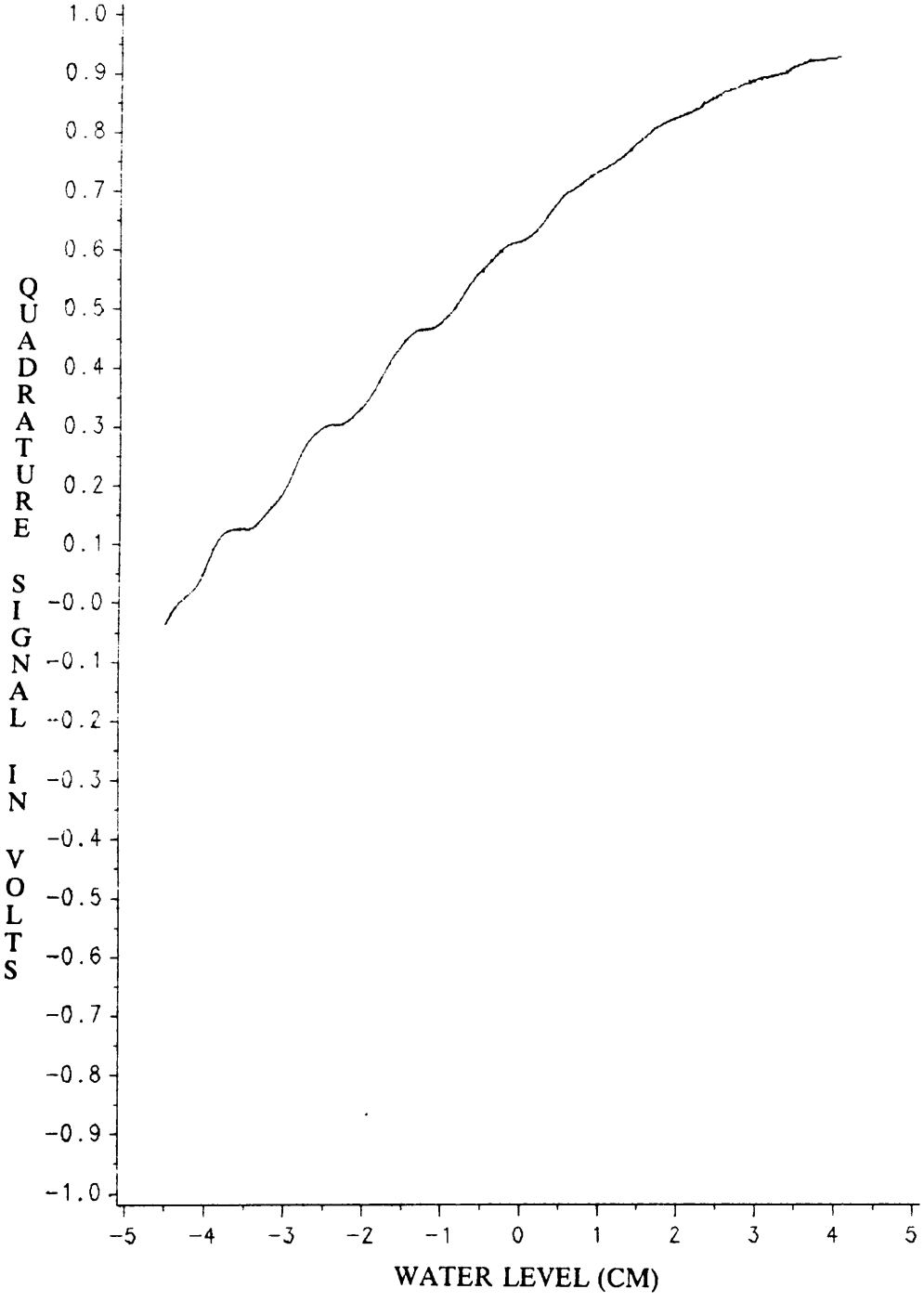

Figure 28. Quadrature output from the Box during Drain Test R4: Bistatic radar configuration with absorber windows in place, and a powered capacitance probe in the radar spot (deviations in the phase signal correspond to less than a 1 mm error in the water height calculation)

Chapter 3

FINAL SYSTEM

3.1 DESCRIPTION

The experiments discussed in the previous sections led to the development of a useful radar configuration. The radar was set up in a bistatic configuration with both the transmit and receive horns pointed 10 degrees off nadir. As can be seen in Figure 23, RF absorber was used to reduce multipath reflections.

The system operated at a suppressed carrier frequency of 13.62 GHz with sidebands 240 MHz above and below the carrier. Figures 29 and 30 show the microwave hardware used to transmit and receive. After detection the signal was fed into the Box for processing. The Box converted the output from the detector into voltage levels from which the backscattered power and wave height could be calculated. The Box was unchanged from the description given in section 1.1.2.

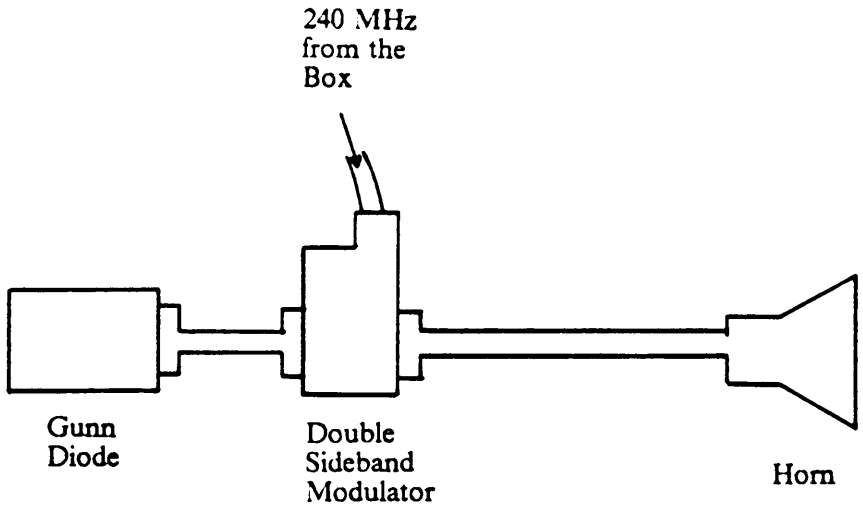

Figure 29. Final Transmit Set-up

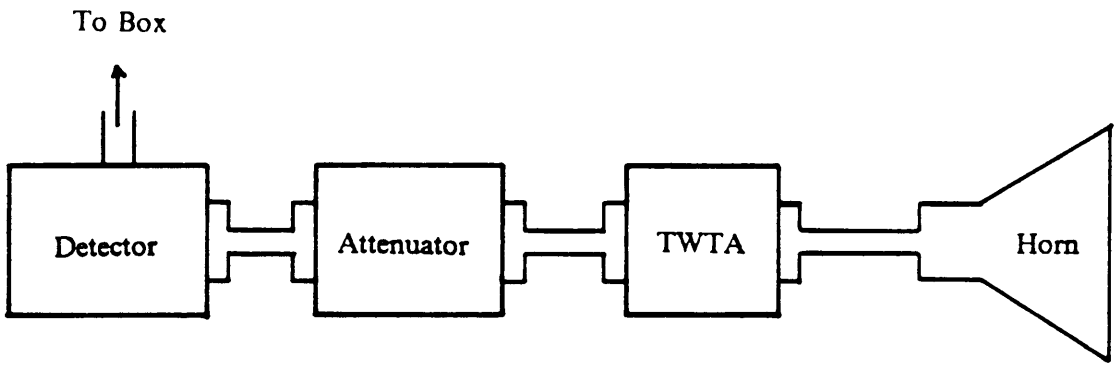

Figure 30. Final Receive Set-up

3.2 PROBE

The capacitance probe was used to measure the height of the water. The radar system generated the phase information, which could be used to calculate the water height, but the probe measurement was used because it gave continuous height measurements. The phase measurement system became unreliable when the signal strength dropped beneath the threshold necessary to drive the phase comparators.

When using the phase information to generate wave height information, a thresholding scheme would be necessary and this thresholding scheme would result in gaps in the height data corresponding to when the power was below the threshold. Also, bistatic operation introduced a small error into the height calculation, because the direction of the change in height was no longer parallel to the direction of the signal propagation. A method for compensating for this error is discussed in section 5.2.3.

The height measurement probe was a capacitance probe that was suspended so that it ran perpendicular to the water surface and through the center of the radar spot. According to Huang [5], the probes have an accuracy of ± 1 percent. The probe self-zeros to mean water level by canceling the capacitance of the probe connecting cable.

3.3 DYNAMIC RANGE

The relationship between the voltage out of the Box and the backscattered power level was nonlinear. This nonlinearity gave an increased power resolution over a small voltage change. When the backscattered power was plotted versus the voltage out of the box, the slope of the curve was approximately 6.38 dB/volt. The difference between the maximum power voltage ($\simeq$4.2 volts) and the minimum power voltage ($\simeq$1.1 volts, system noise level) was about 20 dB.

3.4 REDUCTION IN INTERFERENCE

The amplitude of the interference in the power return was reduced from about 1.0 dB to 0.14 dB or less (when the capacitance probe was receiving power) and 0.13 dB when the probe was not receiving power.

Chapter 4

THEORETICAL WORK

4.1 LENS RADAR SYSTEM LINK EQUATION

Before the interference could be modeled for the monostatic radar system, it was necessary to derive a link equation for the focused radar system. To derive the link equation, the lens was treated as an aperture of area A and gain G.

$$G = \frac{4\pi A}{\lambda^2} \tag{4.1}$$

The antenna efficiency factor η was left out of the gain equation. Also, it was assumed that with the lens focusing all the power illuminating the lens aperture was radiated toward the target. Figure 31 shows the horn and lens placement. Initially, it was assumed that there was no spillover loss.

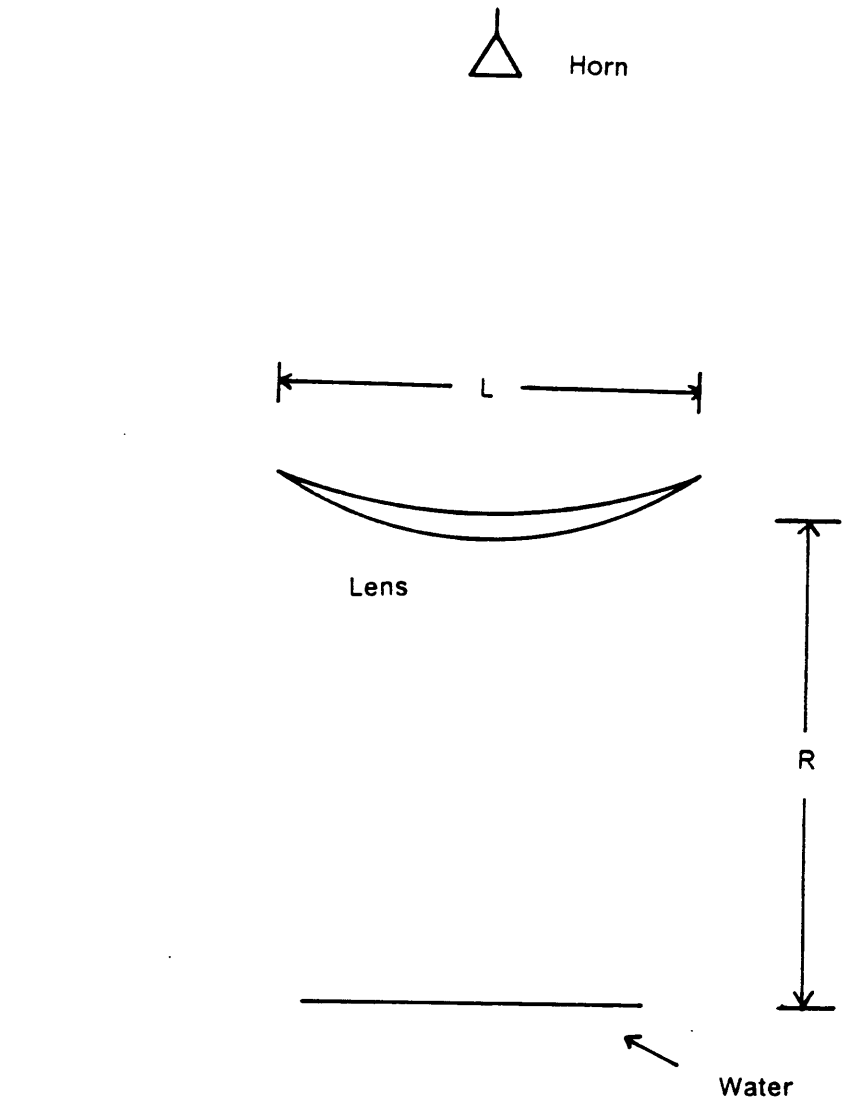

L = lens diameter

R = range to the water

Figure 31. Horn and Lens Placement

The derivation is started with a simple form of the radar equation.

$$P_{rec} = \frac{P_a G A \sigma}{(4\pi)^2 R^4} \tag{4.2}$$

Where P_a is the power illuminating the lens aperture and P_{rec} is the power received by the radar. The radar cross section, σ, is

$$\sigma = \sigma^\circ \delta_r \delta_{az} \sin \psi \tag{4.3}$$

where δ_r = range resolution length,

δ_{az} = azimuth resolution length,

ψ = grazing angle,

R = range from the lens aperture to the water surface, and

σ° = radar cross section per unit area of the water.

For the monostatic radar system, $\psi = 90°$ and $\delta_r = \delta_{az}$. Using ideas borrowed from the description of a focused synthetic aperture radar [6], δ_{az} can be written as

$$\delta_{az} = \frac{R\lambda}{2L} \tag{4.4}$$

Substituting equations (4.1), (4.3), and (4.4) into equation (4.2) results in:

$$P_{rec} = \frac{P_a A^2 \sigma^\circ}{16\pi L^2 R^2} \tag{4.5}$$

Inserting the area of the lens,

$$A = \pi\left(\frac{L}{2}\right)^2 \tag{4.6}$$

leads to

$$P_{rec} = \frac{P_a \pi \sigma^o L^2}{256R^2} \tag{4.7}$$

This final expression does not include losses due to spillover, lens reflections, horn mismatch, etc., but these losses can be easily included if necessary. Note that, with the lens in the system, the power return is proportional to R^2 rather than R^4. This difference clearly shows why the focused system had a much stronger signal strength than the unfocused system.

4.2 MODEL OF THE INTERFERENCE

It was suggested that even though the 3 dB coupler supplied the specified amount of isolation (30 dB), the leakage signal was still strong enough to be the cause of the interference [7]. Miller [8] stated that reflections from the back of the lens could be the cause of the interference seen in the lens radar system. Both of these possibilities were included in a model of the signal return seen by the radar.

The radar signal was traced through the system with lens reflections and leakage included (see Figure 32). Spillover loss was neglected. It was assumed that the power that reaches the detector (port 3) was a combination of the water reflected signal (P_r), leakage through the coupler (P_l), and lens reflections (P_{LN}). The detector voltage (V_D) depends on these power values.

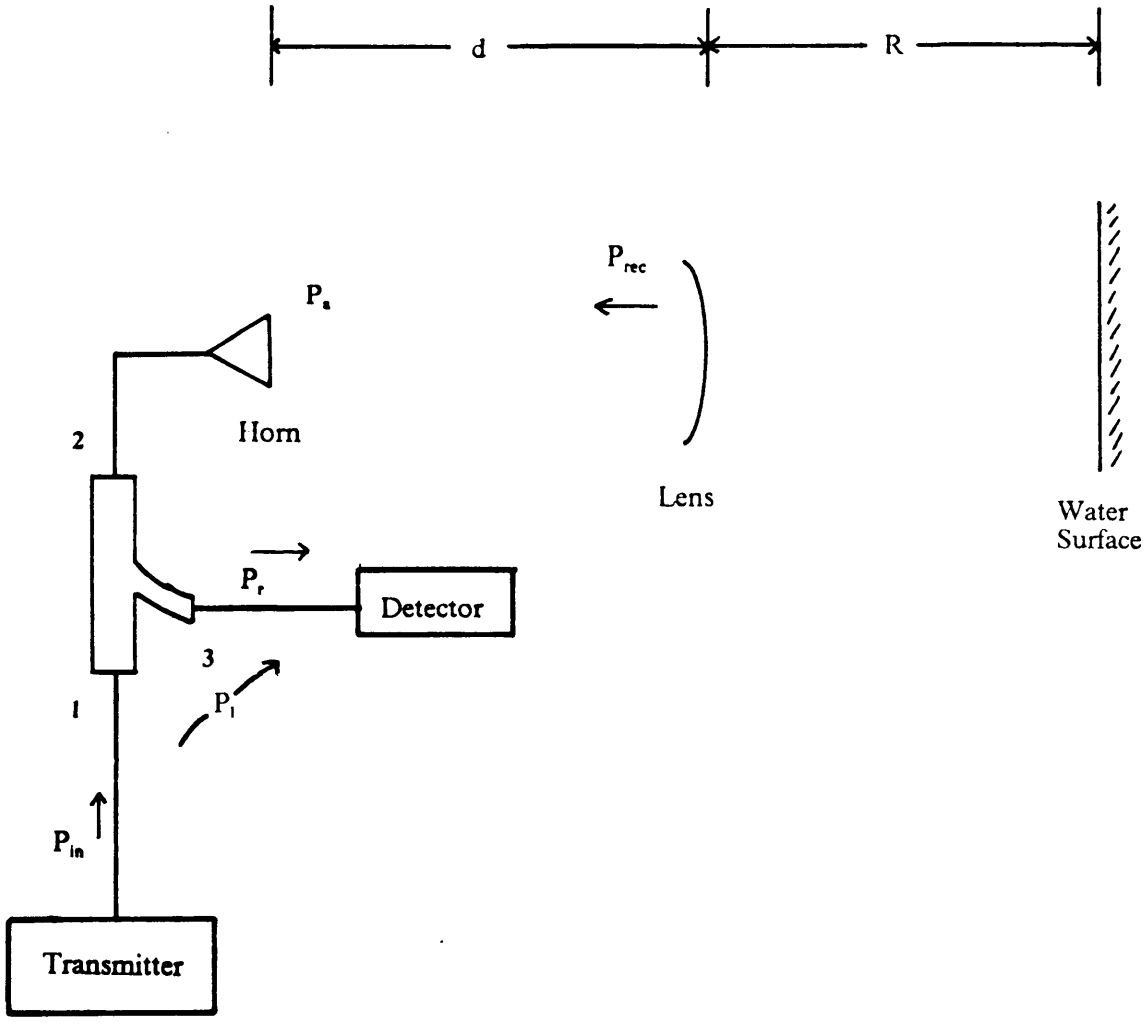

Figure 32. Power Levels in the System

The power at the detector due only to leakage of the transmitted signal through the coupler could be expressed as

$$P_l = \alpha_c P_{in} \tag{4.8}$$

where $\alpha_c = 10^{-3}$ (30 dB), and

P_{in} = power at port 1 due to the transmitter.

The leakage voltage at the detector (V_l) is given by

$$V_l = \sqrt{P_l}\cos(\omega t - \psi_1) \tag{4.9}$$

where ψ_1 is a constant phase change determined by the distance between port 1 and the detector. The power illuminating the lens aperture, P_a, is given by

$$P_a = P_{in}(1 - |\Gamma_t|^2)G_h(0°)(1 - |\Gamma_{LN}|^2) \tag{4.10}$$

where Γ_t = the reflection coefficient into port 1,

Γ_{LN} = the reflection coefficient of the lens, and

$G_h(0°)$ = the horn gain along the boresight, and

spillover loss is neglected.

This expression for P_a assumes that the antenna pattern over the angular extent of the lens is flat and equal to the boresight gain (G(over the lens) = $G_h(0°)$). The power, reflected from the water, at the detector (P_r) is

$$P_r = P_{rec}(1 - |\Gamma_r|^2) \tag{4.11}$$

where Γ_r is the reflection coefficient into the detector. Using equations (4.7), (4.10), and (4.11):

$$P_r = P_{in}(1 - |\Gamma_t|^2)(1 - |\Gamma_r|^2)G_h(0°)\frac{\pi\sigma^o L^2}{256R^2}(1 - |\Gamma_{LN}|^2) \tag{4.12}$$

To make the above substitutions to get P_r it is assumed that the focused system acts ideally (all of the return power is focused into the horn by the lens, therefore P_{rec} is the power entering port 2). The water reflected voltage at the detector (V_r) is

$$V_r = \sqrt{P_r}\cos(\omega t - \psi_2 - 2kd - 2kR) \tag{4.13}$$

where d is the distance from the horn to the lens and ψ_2 is a constant phase change due to the internal radar path length. Let $2kd + 2kR = 2kR'$, and equation (4.13) becomes

$$V_r = \sqrt{P_r}\cos(\omega t - \psi_2 - 2kR') \tag{4.14}$$

The power reflected from the lens, at the detector, (P_{LN}) is

$$P_{LN} = P_{in}(1 - |\Gamma_r|^2)(1 - |\Gamma_t|^2)G_h(0°)|\Gamma_{LN}|^2\frac{A_h\eta}{4\pi d^2} \tag{4.15}$$

where A_h is the horn aperture area, and η is the horn aperture efficiency.

The lens reflected voltage at the detector (V_{LN}) is

$$V_{LN} = \sqrt{P_{LN}}\cos(\omega t - \beta - \psi_2) \tag{4.16}$$

where $\beta = 2kd = (\text{constant})$.

The lens radar system transmits a double sideband suppressed carrier signal. Assume that the sideband frequencies are ω_1 and ω_2, and that the carrier frequency is ω_3. Also assume that

1) the carrier is suppressed such that its power return is negligible (using the spectrum analyzer this could be seen to be true), and
2) $P_{in}(\omega_1) = P_{in}(\omega_2) = P_{in}$ (the sidebands are evenly balanced).

Using voltage equations developed earlier, the voltages at the sideband frequencies can be written as follows

The water reflected voltages at the detector;

$$\begin{aligned} V_1 &= B_1 \cos(\omega_1 t + \phi_1), \quad \phi_1 = -\psi'_2 - 2k_1 R' \\ V_2 &= B_2 \cos(\omega_2 t + \phi_2), \quad \phi_2 = -\psi''_2 - 2k_2 R' \end{aligned} \tag{4.17}$$

The lens reflected voltages at the detector;

$$\begin{aligned} V_4 &= B_4 \cos(\omega_1 + \phi_4), \quad \phi_4 = -\beta_1 - \psi'_2 = (\text{constant}) \\ V_5 &= B_5 \cos(\omega_2 + \phi_5), \quad \phi_5 = -\beta_2 - \psi''_2 = (\text{constant}) \end{aligned} \tag{4.18}$$

The leakage voltages at the detector;

$$\begin{aligned} V_7 &= B_7 \cos(\omega_1 t + \phi_7), \quad \phi_7 = -\psi'_1 = (\text{constant}) \\ V_8 &= b_8 \cos(\omega_2 t + \phi_8), \quad \phi_8 = -\psi''_1 = (\text{constant}) \end{aligned} \tag{4.19}$$

where:

$$B_1 = B_2 = \sqrt{P_r} \tag{4.20}$$

$$B_4 = B_5 = \sqrt{P_{LN}} = \frac{8R|\Gamma_{LN}|\sqrt{P_r}\,A_h\eta}{\pi L d\sqrt{\sigma^\circ(1-|\Gamma_{LN}|^2)}} \tag{4.21}$$

$$B_7 = B_8 = \sqrt{P_l} = \frac{16R\sqrt{\alpha_c}\sqrt{P_r}}{L\sqrt{G_h(1-|\Gamma_t|^2)(1-|\Gamma_r|^2)\pi\sigma^\circ(1-|\Gamma_{LN}|^2)}} \tag{4.22}$$

Detecting as a square law device (V_D = detector voltage) gives

$$V_D = (V_1 + V_2 + V_4 + V_5 + V_7 + V_8)^2 \tag{4.23}$$

Substituting equations (4.17), (4.18), and (4.19) into equation (4.23) leads to :

$$\begin{aligned} V_D = \frac{1}{2}[B_1^2 + B_2^2 + B_4^2 + B_5^2 + B_7^2 + B_8^2] \\ + B_1B_2\cos(\Delta\omega t + \phi_1 - \phi_2) + B_1B_4\cos(\phi_1 - \phi_4) \\ + B_1B_5\cos(\Delta\omega t + \phi_1 - \phi_5) + B_1B_7\cos(\omega_1 - \omega_7) \\ + B_1B_8\cos(\Delta\omega t + \phi_1 - \phi_8) + B_2B_4\cos(\Delta\omega t + \phi_4 - \phi_2) \\ + B_2B_5\cos(\phi_5 - \phi_2) + B_2B_7\cos(\Delta\omega t + \phi_7 - \phi_2) \\ + B_2B_8\cos(\phi_8 - \phi_2) + B_4B_5\cos(\Delta\omega t + \phi_4 - \phi_5) \\ + B_4B_7\cos(\phi_4 - \phi_7) + B_4B_8\cos(\Delta\omega t + \phi_4 - \phi_8) \\ + B_5B_7\cos(\Delta\omega t + \phi_7 - \phi_5) + B_5B_8\cos(\phi_5 - \phi_8) \\ + B_7B_8\cos(\Delta\omega t + \phi_7 - \phi_8) + (\text{HFT}) \end{aligned} \tag{4.24}$$

where: $\Delta\omega t = (\omega_2 - \omega_1)t$

(HFT) = terms that vary as $2\omega_1$, $2\omega_2$, and $(\omega_1 + \omega_2)$

4.2.1 Phase model

After a low pass filter was used to remove the HFT from the detector output V_D, the quadrature signal Q_D was extracted by using the $\Delta\omega$ reference:

$$\begin{aligned} Q_D = {} & B_1B_2 \sin(\phi_1 - \phi_2) \\ & + B_1B_5 \sin(\phi_1 - \phi_5) \\ & + B_1B_8 \sin(\phi_1 - \phi_8) \\ & + B_2B_4 \sin(\phi_4 - \phi_2) \\ & + B_2B_7 \sin(\phi_7 - \phi_2) \\ & + B_4B_5 \sin(\phi_4 - \phi_5) \\ & + B_4B_8 \sin(\phi_4 - \phi_8) \\ & + B_5B_7 \sin(\phi_5 - \phi_7) \\ & + B_7B_8 \sin(\phi_7 - \phi_8) \end{aligned} \tag{4.25}$$

Substituting for the nonconstant ϕ's:

$$\begin{aligned} Q_D = {} & B_1B_2 \sin(-2\Delta kR' - \psi'_2 + \psi''_2) \\ & + B_1B_5 \sin(-2k_1R' - \psi'_2 - \phi_5) \\ & + B_1B_8 \sin(-2k_1R' - \psi'_2 - \phi_8) \\ & + B_2B_4 \sin(2k_2R' + \psi''_2 + \phi_4) \\ & + B_2B_7 \sin(2k_2R' + \psi''_2 + \phi_7) \\ & + B_4B_5 \sin(\phi_4 - \phi_5) \\ & + B_4B_8 \sin(\phi_4 - \phi_8) \\ & + B_5B_7 \sin(\phi_5 - \phi_7) \\ & + B_7B_8 \sin(\phi_7 - \phi_8) \end{aligned} \tag{4.26}$$

Substitute equations (1.19), (1.20), and (1.21) into (1.25):

$$
\begin{aligned}
Q_D = {} & P_r \sin(-2\Delta kR' - \psi'_2 + \psi''_2) \\
& + \sqrt{P_r}\sqrt{P_{LN}}\,[\sin(-2k_1R' - \psi'_2 - \phi_5) + \sin(2k_2R' + \psi''_2 - \beta_1 - \psi'_2)] \\
& + P_{LN}\sin(\phi_4 - \phi_5) \\
& + \sqrt{P_r}\sqrt{P_I}\,[\sin(-2k_1R' - \psi'_2 - \phi_8) + \sin(2k_2R' + \psi''_2 + \phi_7)] \\
& + P_I \sin(\phi_7 - \phi_8) \\
& + \sqrt{P_{LN}}\sqrt{P_I}\,[\sin(\phi_4 - \phi_8) + \sin(\phi_5 - \phi_7)]
\end{aligned}
\tag{4.27}
$$

In the above expression, line 1 is the desired signal (with a constant phase shift that can be removed by zero setting the phase at the mean water level) , lines 2 and 3 are due to lens reflections, lines 4 and 5 are due to coupler leakage, and the last line is due to a combination of lens reflections and coupler leakage. Notice that the third, fifth, and last terms are constant terms. These constant terms act as a dc offset to the desired sinusoidal phase waveform. Zero setting the phase at the mean range level will remove this interference from the signal. The second and fourth term are a manifestation of the interference. Either term accurately describes the noticed cyclic interference (that corresponds to the radar wavelength) observed with the monostatic system.

Because the signals are limited before they pass into the phase detectors, it is not possible to make an accurate numerical comparison between the theoretical interference levels (lens reflection term and the leakage term) and the measured interference levels. This comparison will be possible with the derivation of the power return, because no limiting is done. It seems likely that the limiting process will accentuate the effect of the interference, because the limiting probably reduces the desired signal strength such that it is more on the order of the strength of the interference signal (i.e. the desired signal is stronger than the interference signal). Also it is quite possible that the interference signal is too weak to be limited.

4.2.2 Power model

The power return V_p is found by extracting the dc terms from the detector output (V_D).

$$\begin{aligned} V_D = \frac{1}{2}[B_1^2 + B_2^2 + B_4^2 + B_5^2 + B_7^2 + B_8^2] \\ + B_1B_4\cos(\phi_1 - \phi_4) + B_4B_7\cos(\phi_4 - \phi_7) \\ + B_2B_5\cos(\phi_5 - \phi_2) + B_2B_8\cos(\phi_8 - \phi_2) \\ + B_5B_8\cos(\phi_5 - \phi_8) + B_1B_7\cos(\phi_1 - \phi_7) \end{aligned} \tag{4.28}$$

Substituting equations (4.20), (4.21), and (4.22) into equation (4.28) results in:

$$\begin{aligned} V_P = \frac{1}{2}[2P_r + 2P_{LN} + 2P_I] \\ + \sqrt{P_r}\sqrt{P_{LN}}[\cos(\phi_1 - \phi_4) + + \cos(-\phi_2 + \phi_5)] \\ + \sqrt{P_r}\sqrt{P_I}[\cos(\phi_1 - \phi_7) + \cos(-\phi_2 + \phi_8)] \\ + \sqrt{P_{LN}}\sqrt{P_I}[\cos(\phi_4 - \phi_7) + \cos(\phi_5 - \phi_8)] \end{aligned} \tag{4.29}$$

Rewriting and substituting in for the ϕ's

$$\begin{aligned} V_P = P_r + P_{LN} + P_I \\ + \sqrt{P_r}\sqrt{P_{LN}}[\cos(-2k_1R' + \beta_1) + \cos(2k_2R' - \beta_2)] \\ + \sqrt{P_r}\sqrt{P_I}[\cos(-2k_1R' - \psi'_2 + \psi'_1) + \cos(2k_2R' + \psi''_2 - \psi''_1)] \\ + \sqrt{P_{LN}}\sqrt{P_I}\,\beta_3 \end{aligned} \tag{4.30}$$

Where $\beta_3 = \cos(-\beta_1 - \psi_2' + \psi_1') + \cos(-\beta_2 - \psi_2'' + \psi_1'') = \text{(constant)}$

4.3 COMPARISON OF THEORETICAL MODEL TO EXPERIMENTAL DATA

It can be seen from the models for the return power and phase (equations (4.30) and (4.27)) that both coupler leakage and lens reflections could introduce the type of interference that the monostatic system experienced. The fact that the lens could be removed from the system and the interference remained, implied that coupler leakage was a cause of interference. The potential problem due to lens reflections was noted in the original system design [1]. It is easily seen that the back of the lens is capable of reflecting Γ_{LN}^2 of the incident energy directly back into the horn.

To remove the lens reflections, the back surface of the lens was coated with an impedance matching material (in this case a soft wood had the proper characteristics). The impedance matching was designed to be effective at 36 GHz. With the effect of the lens reflections removed, equations (4.27) and (4.30) can be rewritten as:

$$\begin{aligned} Q_D = {} & P_r \sin(-2\Delta kR' - \psi'_2 + \psi''_2) \\ & + \sqrt{P_r}\sqrt{P_l}\,[\sin(-2k_1R' - \psi'_2 - \phi_8) + \sin(2k_2R' + \psi''_2 + \phi_7)] \\ & + P_l \sin(\phi_7 - \phi_8) \end{aligned} \tag{4.31}$$

$$\begin{aligned} V_p = {} & P_r + P_l \\ & + \sqrt{P_r}\sqrt{P_l}\,[\cos(-2k_1R' - \psi'_2 + \psi'_1) + \cos(2k_2R' + \psi''_2 - \psi''_1)] \end{aligned} \tag{4.32}$$

Using data collected during drain tests run at 36 GHz, it was determined how closely the above theoretical models of the interference agree with the levels of interference observed in the system. As explained before, this comparison was made with the return power data and the return power model rather than the return phase data and phase model, because the phase extraction employs a limiting process. In order to facilitate this comparison, equation (4.32) was written in a different form. First it was noted that k_1 and k_2 could be expressed as

$$\begin{aligned} k_1 &= k - \delta k \\ k_2 &= k + \delta k \end{aligned} \tag{4.33}$$

where $$\delta k = \frac{k_2 - k_1}{2}$$

Also the psi's could be rewritten. ψ_2' is a function of k_1 and γ, a pathlength internal to the radar.

$$\psi_2' = k_1\gamma = (k - \delta k)\gamma \tag{4.34}$$

ψ_1' is a function of k_1 and α, a pathlength internal to the radar.

$$\psi_1' = k_1\alpha = (k - \delta k)\alpha \tag{4.35}$$

ψ_2'' and ψ_1'' are functions of k_2 and pathlengths internal to the radar.

$$\psi_2'' = k_2\gamma = (k + \delta k)\gamma \tag{4.36}$$

$$\psi_1'' = k_2\alpha = (k + \delta k)\alpha \tag{4.37}$$

Using equations (4.33), (4.34), (4.35), (4.36), and (4.37) equation (4.32) was rewritten as

$$V_P = P_r + P_I + \sqrt{P_r}\sqrt{P_I}\cos\left[\left(1-\frac{\delta k}{k}\right)(2R' + \gamma - \alpha)k\right] + \sqrt{P_r}\sqrt{P_I}\cos\left[\left(1+\frac{\delta k}{k}\right)(2R' + \gamma - \alpha)k\right] \tag{4.38}$$

Using the following identity,

$$\cos x + \cos y = 2\cos\left(\frac{x+y}{2}\right)\cos\left(\frac{x-y}{2}\right)$$

equation 4.38 becomes

$$V_P = P_r + P_I + 2\sqrt{P_r}\sqrt{P_I}\cos[\delta k(2R' + \gamma - \alpha)]\cos[(2R' + \gamma - \alpha)k] \tag{4.39}$$

From the two cosine terms in equation (4.39) it was noted that the first cosine term varied very slowly whereas the second cosine term varied much more rapidly ($\delta k = 10.0531\ m^{-1}$, $k = 753.9823\ m^{-1}$) . Both of these effects could be seen when the wavetank was drained; there was the rapidly cycling interference pattern (second cosine term) modulated in amplitude by the first cosine term. Because the first term varied so slowly and the interval (range) of interest was small ($\pm$ 3.5 cm), the first cosine term could be replaced by a constant factor. The factor of unity was chosen to replace the first cosine term because it was noted, during a long drain test, that the range interval to be used for experiments was one where the amplitude of the interference was large (peaking).

With this replacement, equation (4.39) was rewritten (the constant phase terms were also replaced by their equivalent psi's as defined in section 4.2) as follows;

$$V_p \simeq P_r + P_l + 2\sqrt{P_r}\sqrt{P_l}\cos(2kR' + \psi_2 - \psi_1) \qquad (4.40)$$

Equation (4.40) shows that the return power is a combination of an average term and a cyclic term. The average return is $P_r + P_l$, (AVG), and the peak amplitude of the cyclic term is $2\sqrt{P_r}\sqrt{P_l}$, (AMP). From experimental data, i.e. Figure 6, both an average return power (AVG_{exp}) and the peak amplitude (AMP_{exp}) of the interference could be determined.

Not enough information was available to calculate AMP and AVG, so they could not be directly compared to AMP_{exp} and AVG_{exp} ,but a relative comparison could be made because AMP/AVG could be calculated. To make this the calculation, the following reasonable numbers were assumed;

$|\Gamma_t| << 1$

$|\Gamma_r| << 1$

$\eta A_h = G\lambda^2/4\pi = 1.7474 \times 10^{-4}$ m^2

α_c = 0.001 (30 dB isolation)

R = 1 m

$G_h(0°)$ = 31.62 (15 dB gain horn)

L = 0.4168 m

$|\Gamma_{LN}|^2 << 1$

$\sigma°$ = 10

Using equations (4.8) and (4.12):

$$\frac{AMP}{AVG} = \frac{\frac{L}{8R}\sqrt{G_h(0°)\pi\sigma^o\alpha_c}}{\frac{G_h(0°)\pi\sigma^o L^2}{256R^2} + \alpha_c} \tag{4.41}$$

Substituting in the above numbers leads to:

$$\frac{AMP}{AVG} = 0.077$$

Using the data from two different drain tests run at 36 GHz (monostatic system), the relative quantity (AMP_{exp}/AVG_{exp}) was calculated.

From Experiment 2 Run # 1 (Figure 6):

$$\frac{AMP_{exp}}{AVG_{exp}} = 0.36$$

From Experiment 2 Run # 2:

$$\frac{AMP_{exp}}{AVG_{exp}} = 0.42$$

These results show nominal agreement between the theoretical model and the experimental data. Including losses in the theoretical calculation (spillover loss, loss due to lens reflections or spot defocusing, or the fact that the lens does not actually focus all of the return signal into the horn) would cause an increase in the value calculated for AMP/AVG and therefore result in better agreement between the theoretical model and experimental results. For example, including the loss due to lens reflections would make AMP/AVG = 0.081, and including both lens reflections

and a spillover loss of 1.6 dB (an approximate upper bound) would make AMP/AVG = 0.111. The loss due to non-ideal system focusing cannot be accurately approximated, but it is known to be a factor since the radar, when set up in the horn configuration shown in Figure 11 (C), saw the moving plate even though the receive horn was not at the lens focus point. Overall, the comparison between AMP/AVG and AMP_{exp}/AVG_{exp} tends to support the idea that the coupler supplied insufficient isolation.

4.4 DISCUSSION OF ERROR

With the present calibration, it was not possible to establish an exact error bound for the experimental data. Only the reduction in the level of the interference could be quantified (see section 3.4). In order to establish an exact error bound, it would be necessary to generate an exact calibration curve.

The present calibration (which was quite sufficient for calculating EM bias results) was only a relative calibration. It was known that a change of 1 volt corresponds to a 6.38 dB change in power, but an exact value for the power could not be calculated from the voltage value. An absolute calibration could be generated by measuring the power level after the attenuator (see Figure 30) and relating that power level to the voltage level out of the Box.

The return power was histogramed versus water height. Therefore, if it was known how much interference was introduced at each individual water height then the error in the histogram could be removed by multiplying by a correction factor. In Figure 33 (A) the dashed curve, $(P_{rec})_{sum}$, is a sketch of a return power

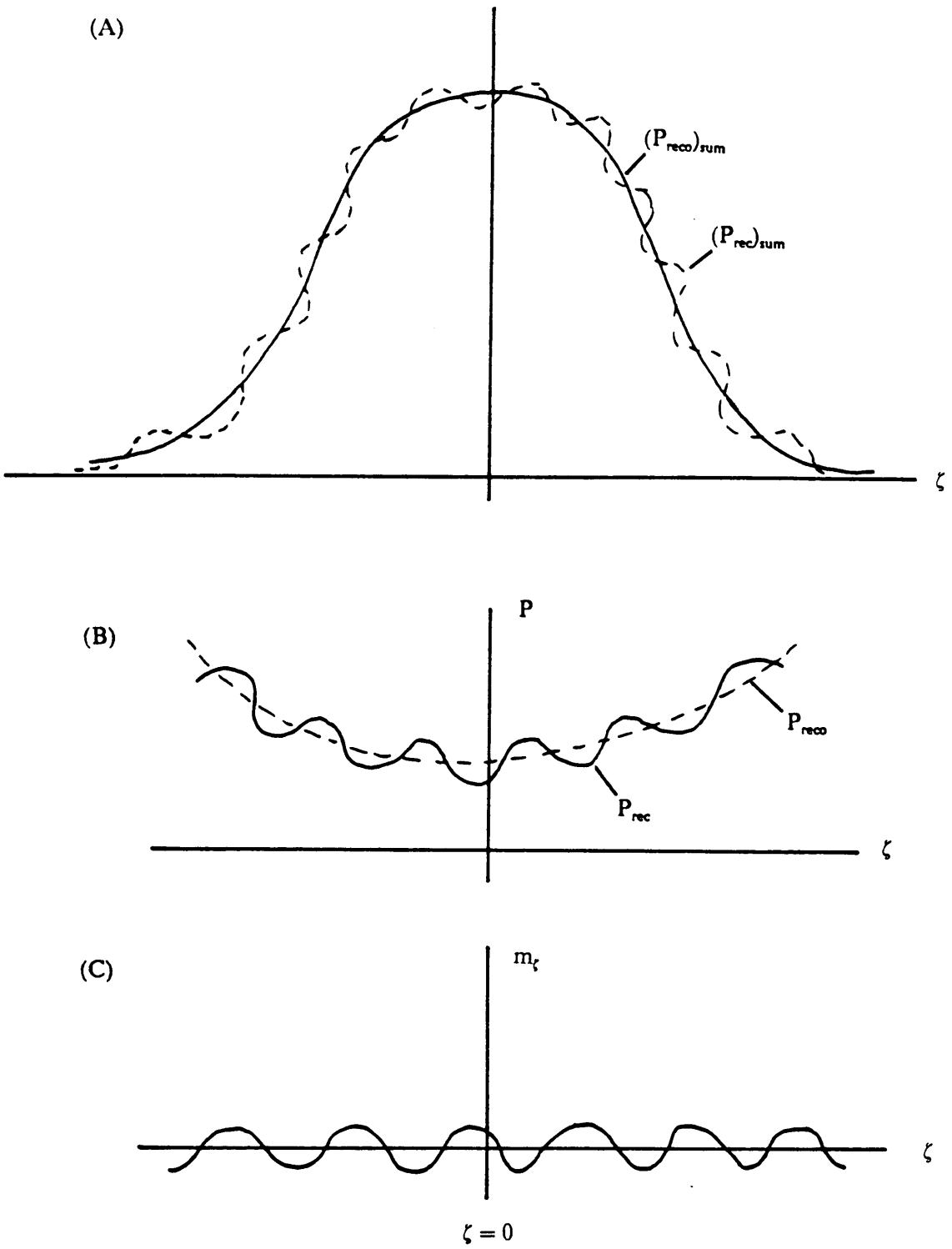

Figure 33. Error Analysis

histogram that contained the interference (the effect of the interference was exaggerated in order to be clearly seen), and if the effect of the interference was removed from the data the return power histogram would look like $(P_{reco})_{sum}$ (the solid line).

The error at individual water heights could not be discerned directly from the power histograms , because the shape of the interference-free histogram was unknown, but it could be measured from drain test data. Figure 33 (B) shows a sketch of a drain test (the return power was plotted versus the water height, ζ) where the dashed curve, P_{reco}, was what the return power would look like if there was no interference and the solid curve, P_{rec}, was the power return as influenced by multipath. The difference between these two curves $(P_{rec} - P_{reco})$ was the error. A clearer view of the interference could be seen when the effect of the absorber and defocusing was removed from the drain test data (see Figure 33 (C)). With these effects removed, the interference m_ζ can be seen to be a sinusoid, oscillating around a mean return power value.

To get an approximate error bound, m_ζ was treated as a sinusoid with a constant amplitude (equal to the maximum excursion from the mean power return);

$$m_\zeta = C_1 \sin(2k\zeta + \phi_1) \tag{4.42}$$

where C_1 = the maximum excursion from the expected return power,

ζ = the water height,

k = radar wavenumber, and

ϕ_1 = constant phase term.

Thus,

$$(P_{rec})_{sum} = (P_{rec0})_{sum}(1 + m_{\zeta}) \tag{4.43}$$

Solving for $(P_{rec0})_{sum}$:

$$(P_{rec0})_{sum} = \frac{(P_{rec})_{sum}}{1 + m_{\zeta}} \tag{4.44}$$

Because C_1 was always small, m_{ζ} was small, and this led to:

$$(P_{rec0})_{sum} \simeq (P_{rec})_{sum}(1 - m_{\zeta}) \tag{4.45}$$

and this implied that the error was m_{ζ}. Therefore the largest the error could be was C_1, the maximum excursion from the expected return power. This error bound was in terms of the absolute error (absolute error = measured value - the corresponding error free value). A more useful gauge of error was the relative error, which is the absolute error divided by the error free value.

It should be noted that the error will be further reduced below the above stated amount, because the calibration used to remove the effects of the absorber (which depends on water height) also contains the effects of the interference (which depends on water height).

Chapter 5

RESULTS AND DISCUSSION

5.1 RESULTS

5.1.1 Effect of the reduction in interference on experimental data

The effects of reducing the interference could clearly be seen when a comparison was made between histogramed data collected with the new bistatic configuration and data collected with the original monostatic system. Processed data from the original monostatic system is shown in Figures 34 through 39. The wave conditions for these tests were as follows:

Figure 34 wind, no paddlewave

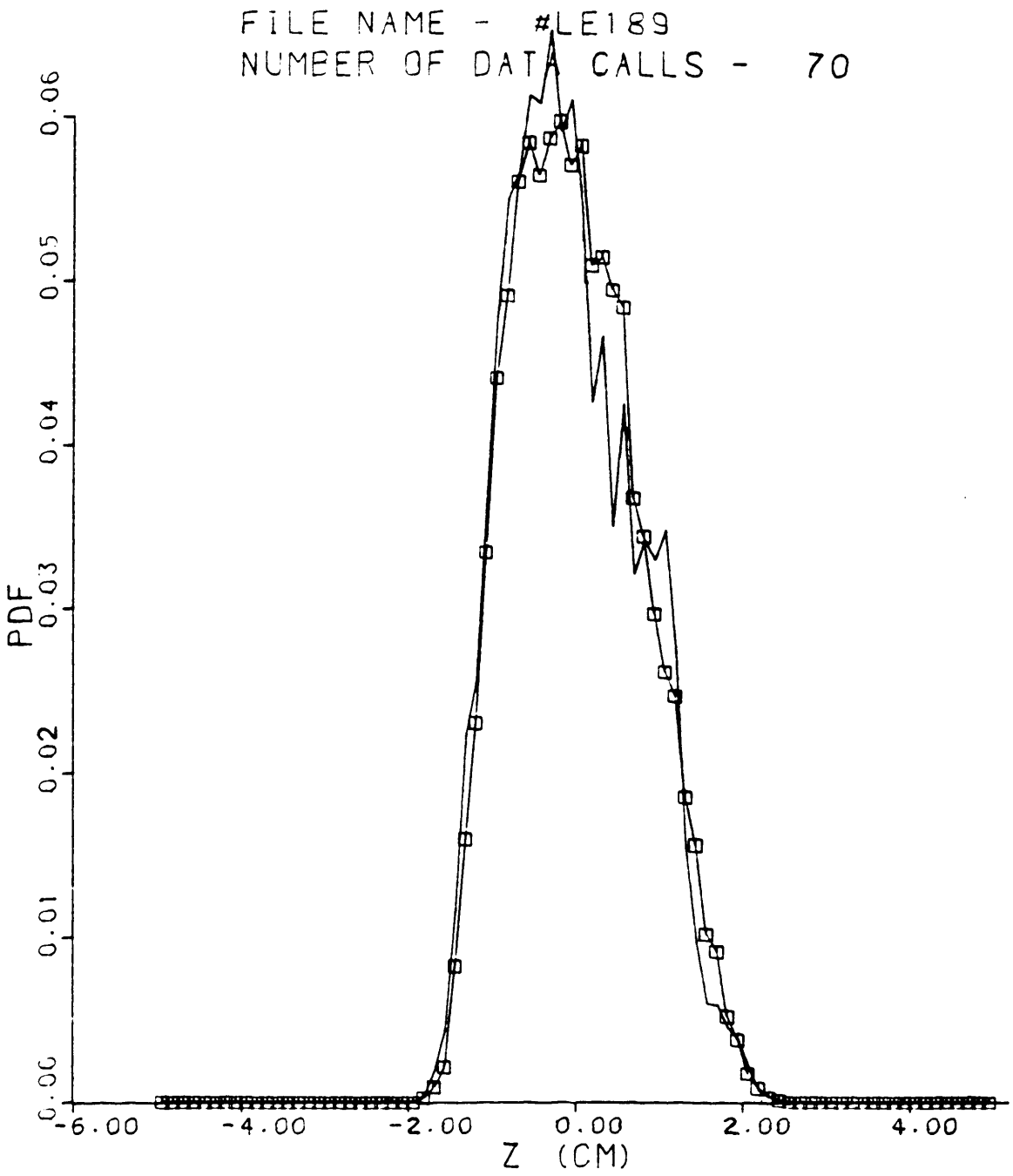

Figure 34. Scattered power (——) and probe measured wave height (-●-●-) histogramed vs displacement from mean water level (File #LE189): 36 GHz monostatic radar configuration with wind generated waves

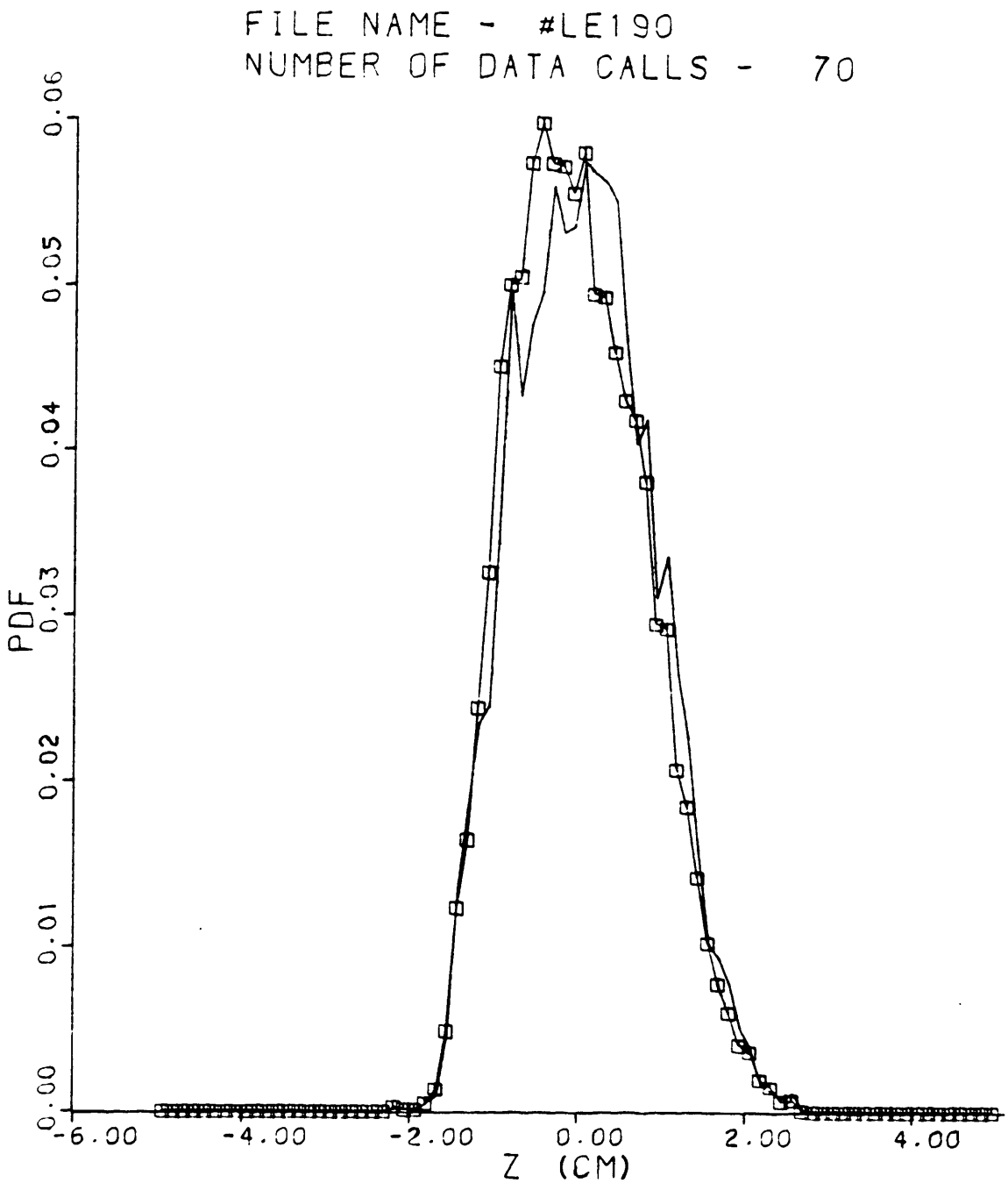

Figure 35. Scattered power (——) and probe measured wave height (-⊟-⊟-) histogramed vs displacement from mean water level (File #LE190): 36 GHz monostatic radar configuration with wind generated waves

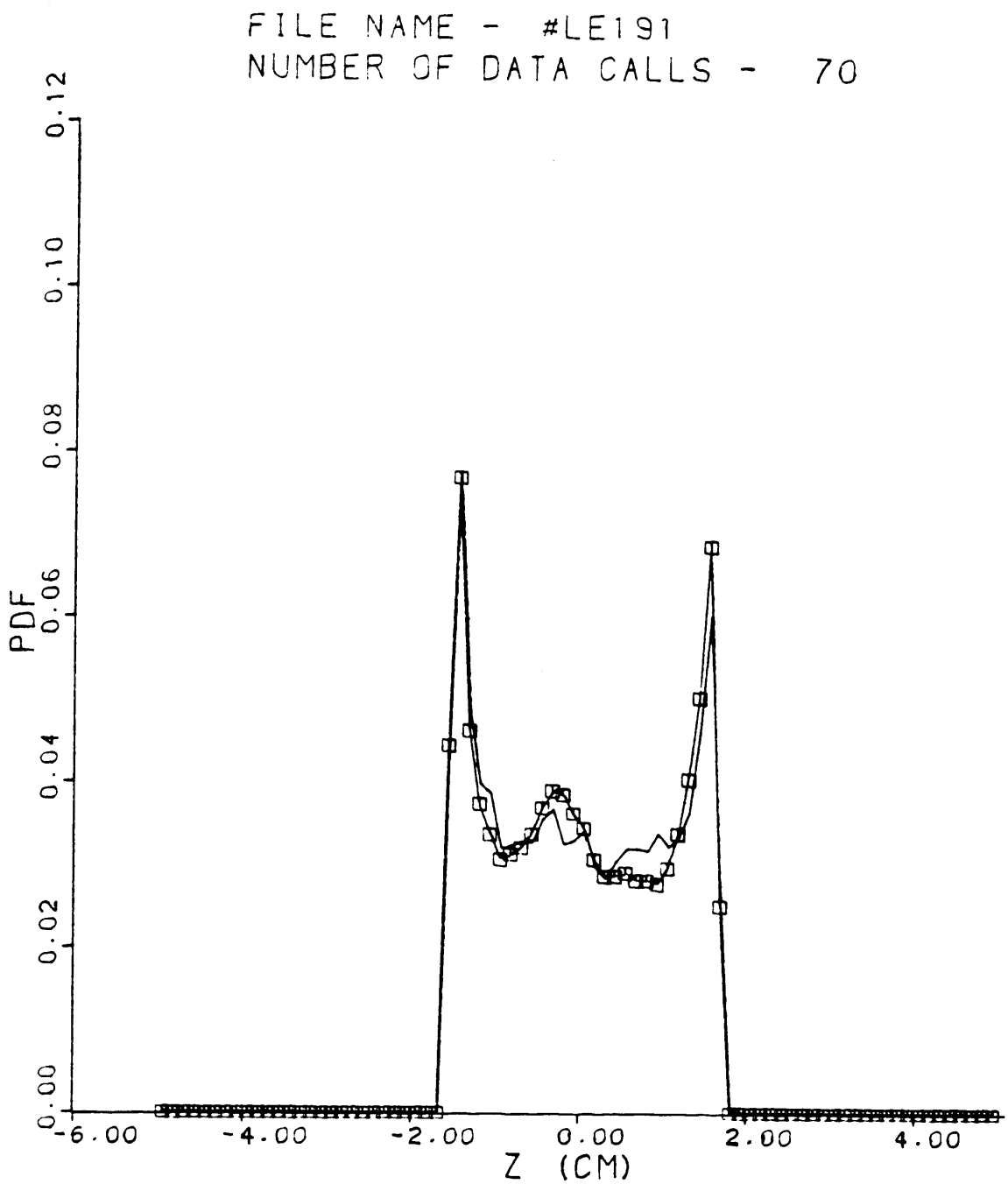

Figure 36. Scattered power (——) and probe measured wave height (-●-●-) histogramed vs displacement from mean water level (File #LE191): 36 GHz monostatic radar configuration with paddle generated waves

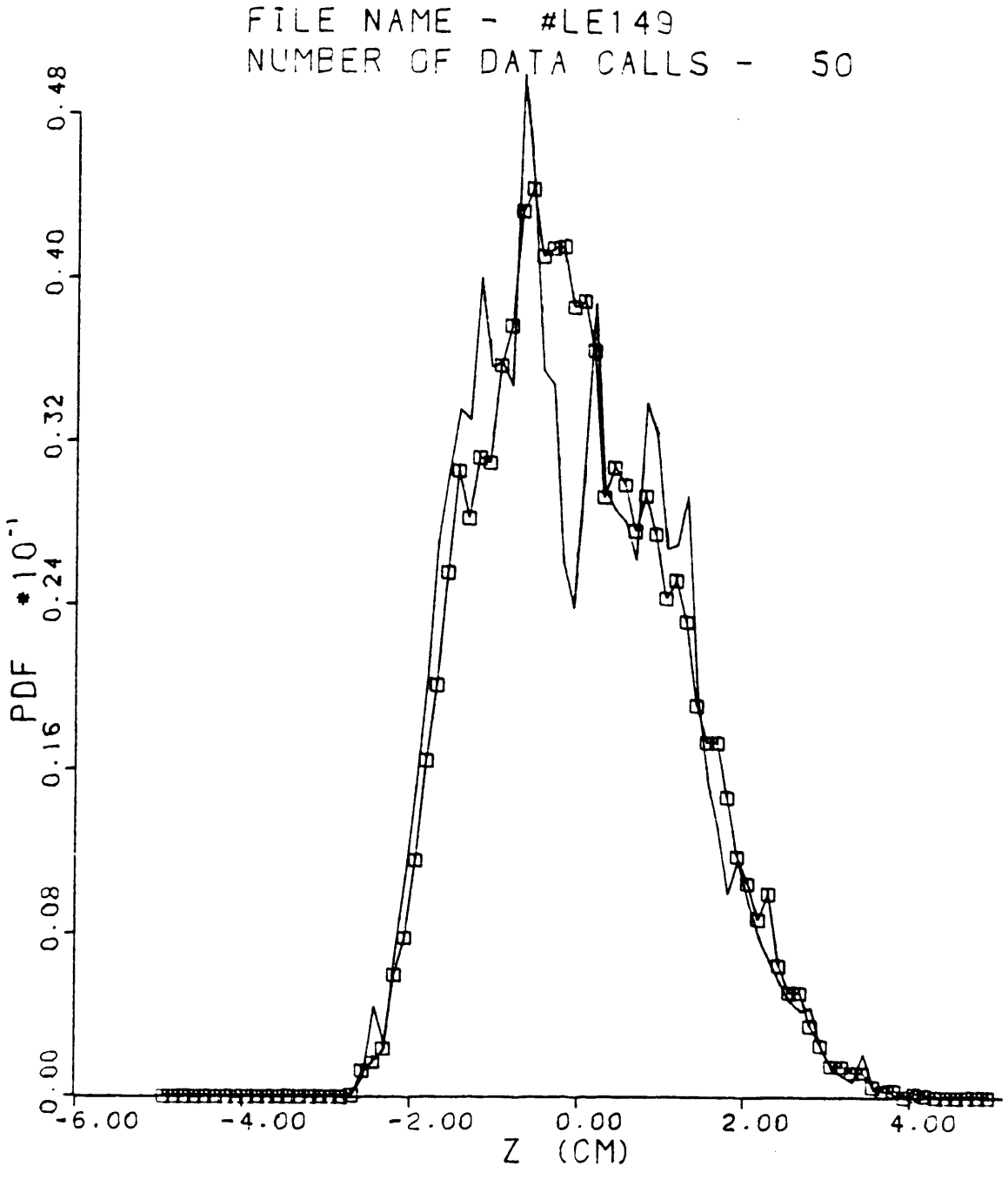

Figure 37. Scattered power (——) and probe measured wave height (-■-■-) histogramed vs displacement from mean water level (File #LE149): 13.5 GHz monostatic radar configuration with wind generated waves

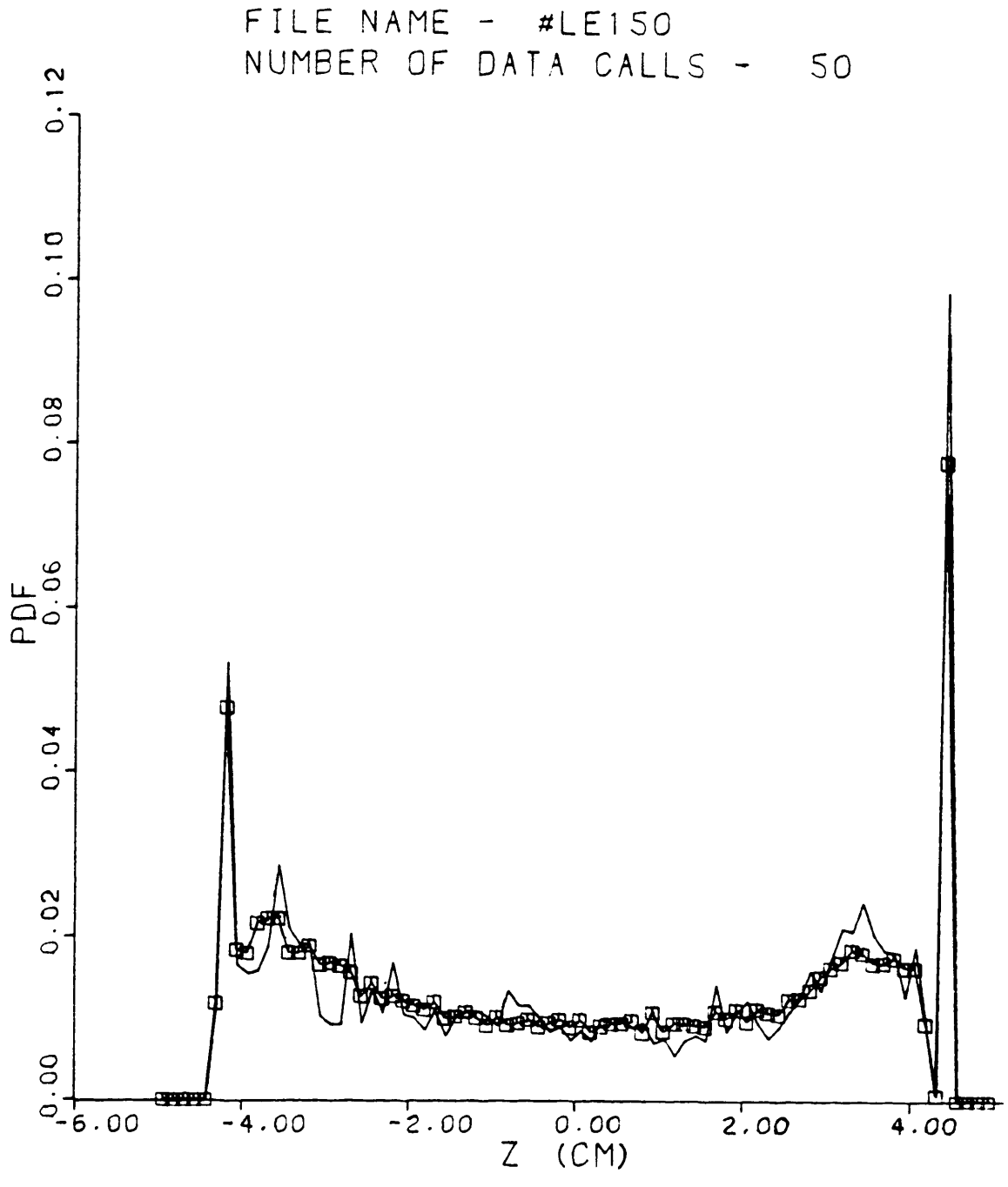

Figure 38. Scattered power (——) and probe measured wave height (-■-■-) histogramed vs displacement from mean water level (File #LE150): 13.5 GHz monostatic radar configuration with wind and paddle generated waves

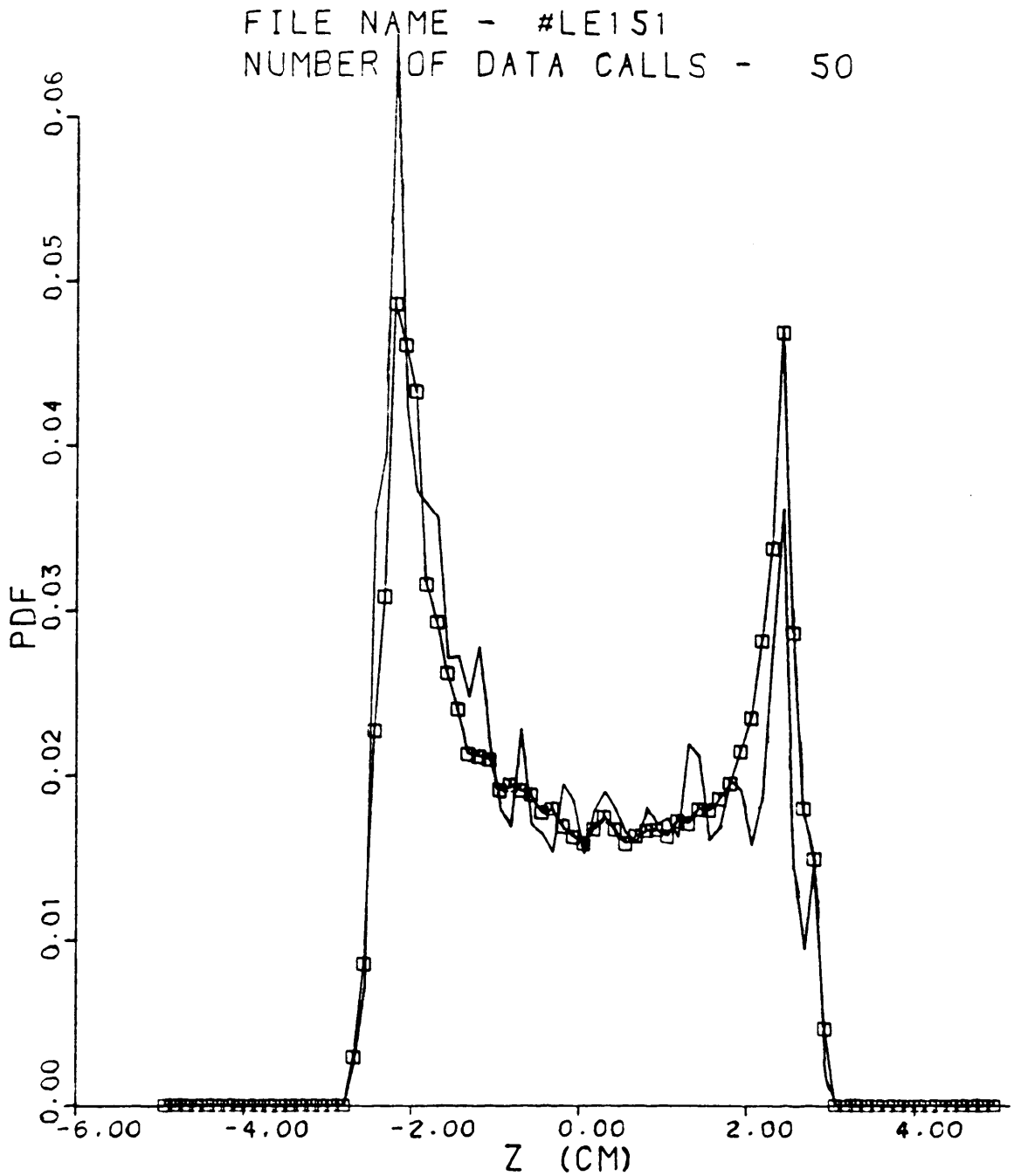

Figure 39. Scattered power (——) and probe measured wave height (-⊟-) histogramed vs displacement from mean water level (File #LE151): 13.5 GHz monostatic radar configuration with paddle generated waves

Figure 35 wind, no paddlewave

Figure 36 no wind, 1.25 Hz paddlewave

Figure 37 wind, no paddlewave

Figure 38 wind, 1.0 Hz paddlewave

Figure 39 no wind, 1.0 Hz paddlewave

Wind was generated by moving air through the wavetank with a suction fan, and waves were generated with a servo-controlled paddle at one end of the wavetank. The line with no symbol is the radar return power conditional probability density function (pdf), and the line with the square symbol is the probe height pdf. As can be seen in all of these figures (especially Figure 37), the radar return power pdf is rather jagged. These jagged oscillations were thought to be caused by the interference. The theoretical model shows this belief to be reasonable, and also the jagged quality was not present in the data collected with the bistatic configuration (which has much reduced interference).

Some samples of histogram data from the bistatic system are shown in Figures 40 through 45. The wave conditions for these tests were as follows:

Figure 40 no wind, 4.0 volt 1.25 Hz paddlewave

Figure 41 no wind, 3.5 volt 2.25 Hz paddlewave

Figure 42 wind, no paddlewave

Figure 43 wind, no paddlewave

Figure 44 wind, 1.0 volt 1.25 Hz paddlewave

Figure 45 wind, 1.5 volt 1.60 Hz paddlewave

The return power pdf's can be seen to be smoothly changing.

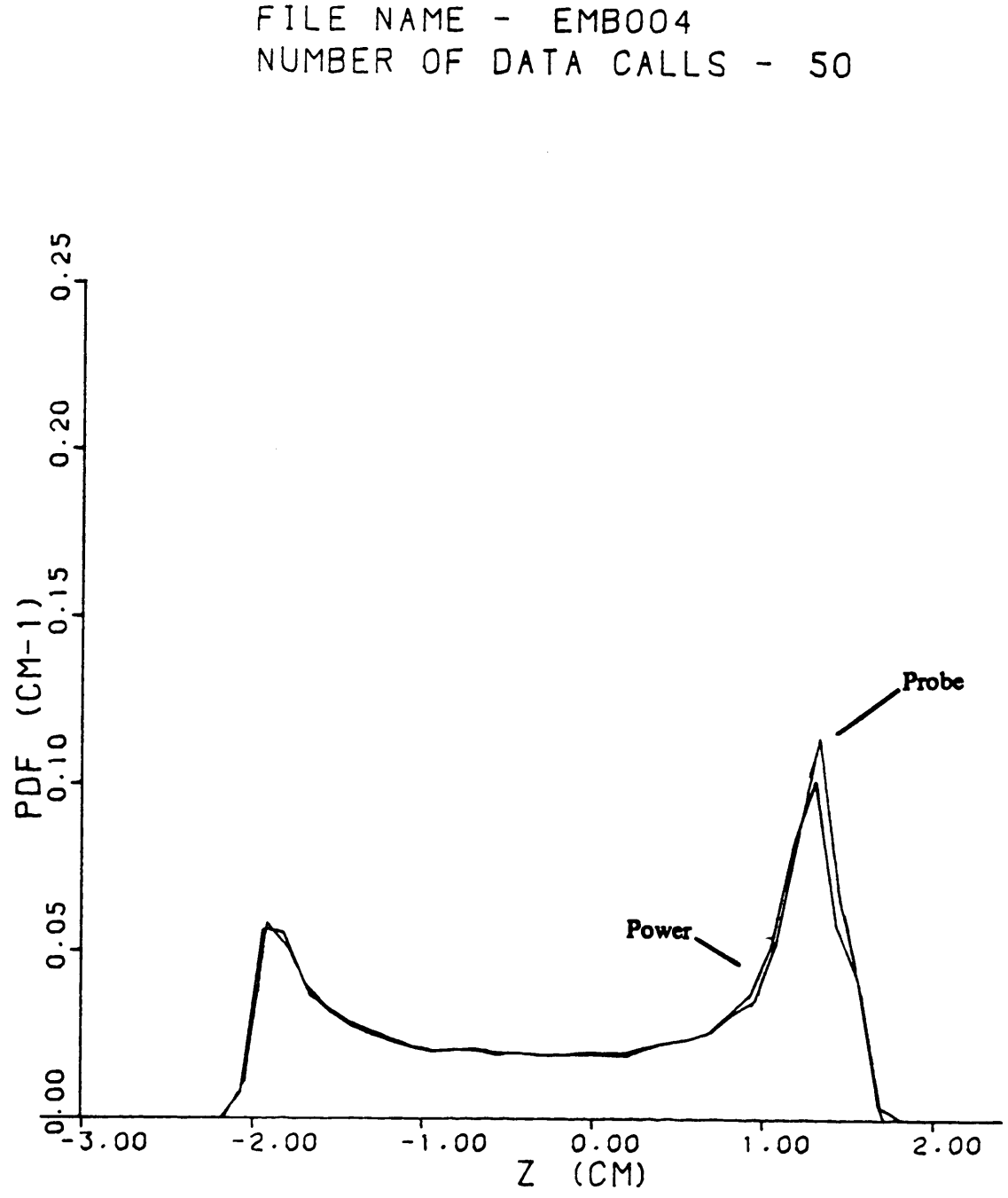

Figure 40. Scattered power and probe measured wave height histogramed vs displacement from mean water level (File EMB004): 13.5 GHz bistatic radar configuration with paddle generated waves

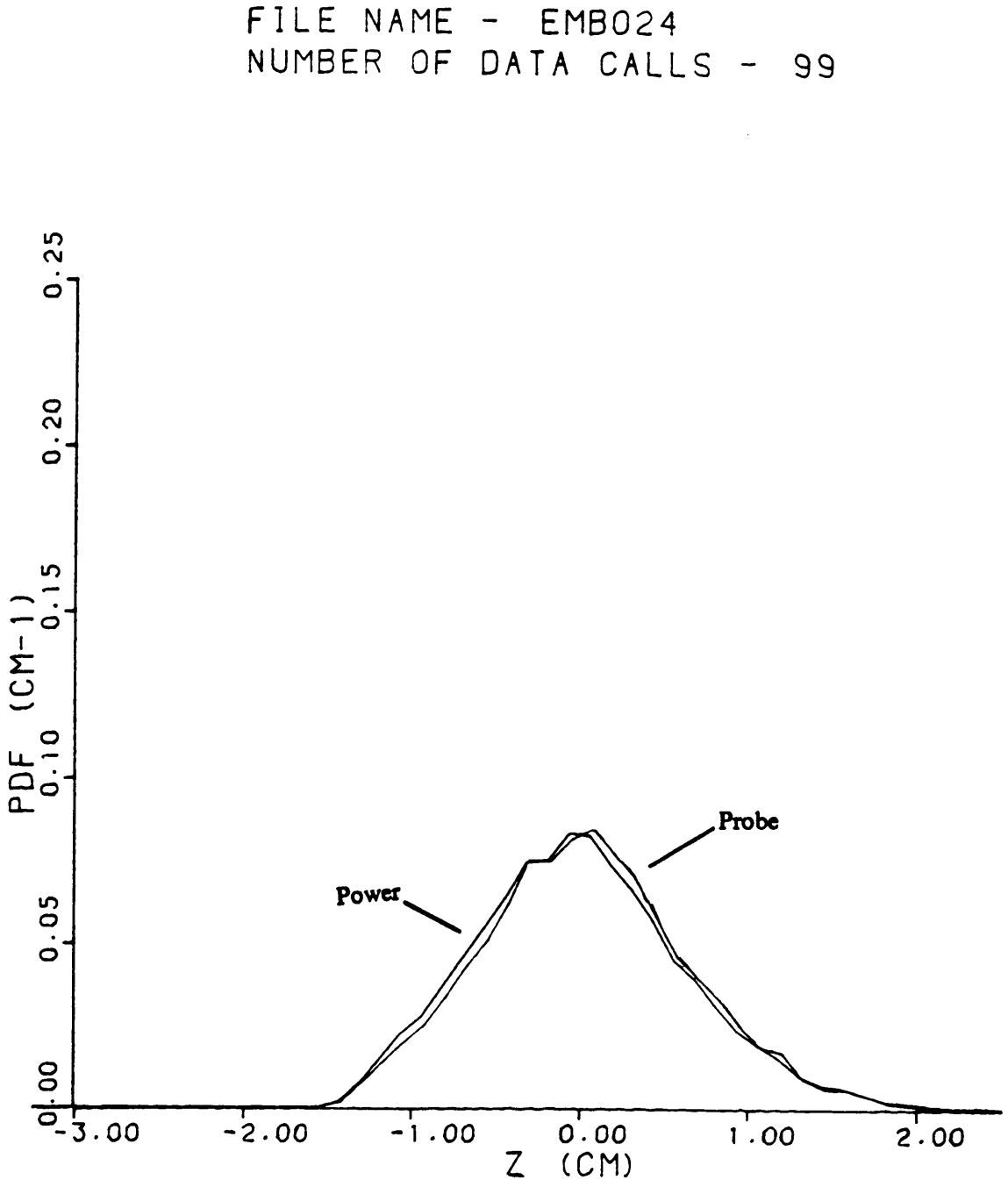

Figure 41. Scattered power and probe measured wave height histogramed vs displacement from mean water level (File EMB024): 13.5 GHz bistatic radar configuration with paddle generated waves

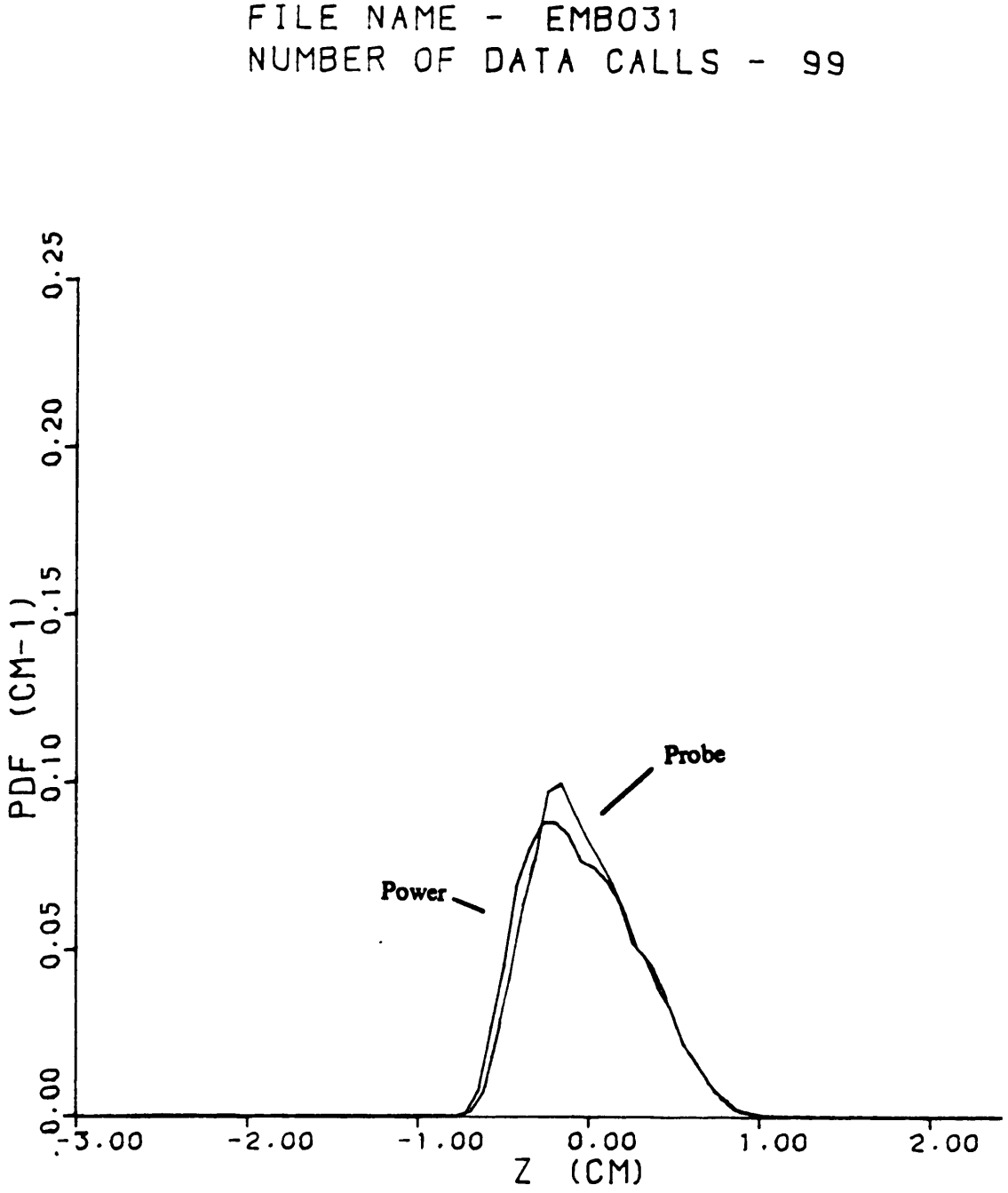

Figure 42. Scattered power and probe measured wave height histogramed vs displacement from mean water level (File EMB031): 13.5 GHz bistatic radar configuration with wind generated waves

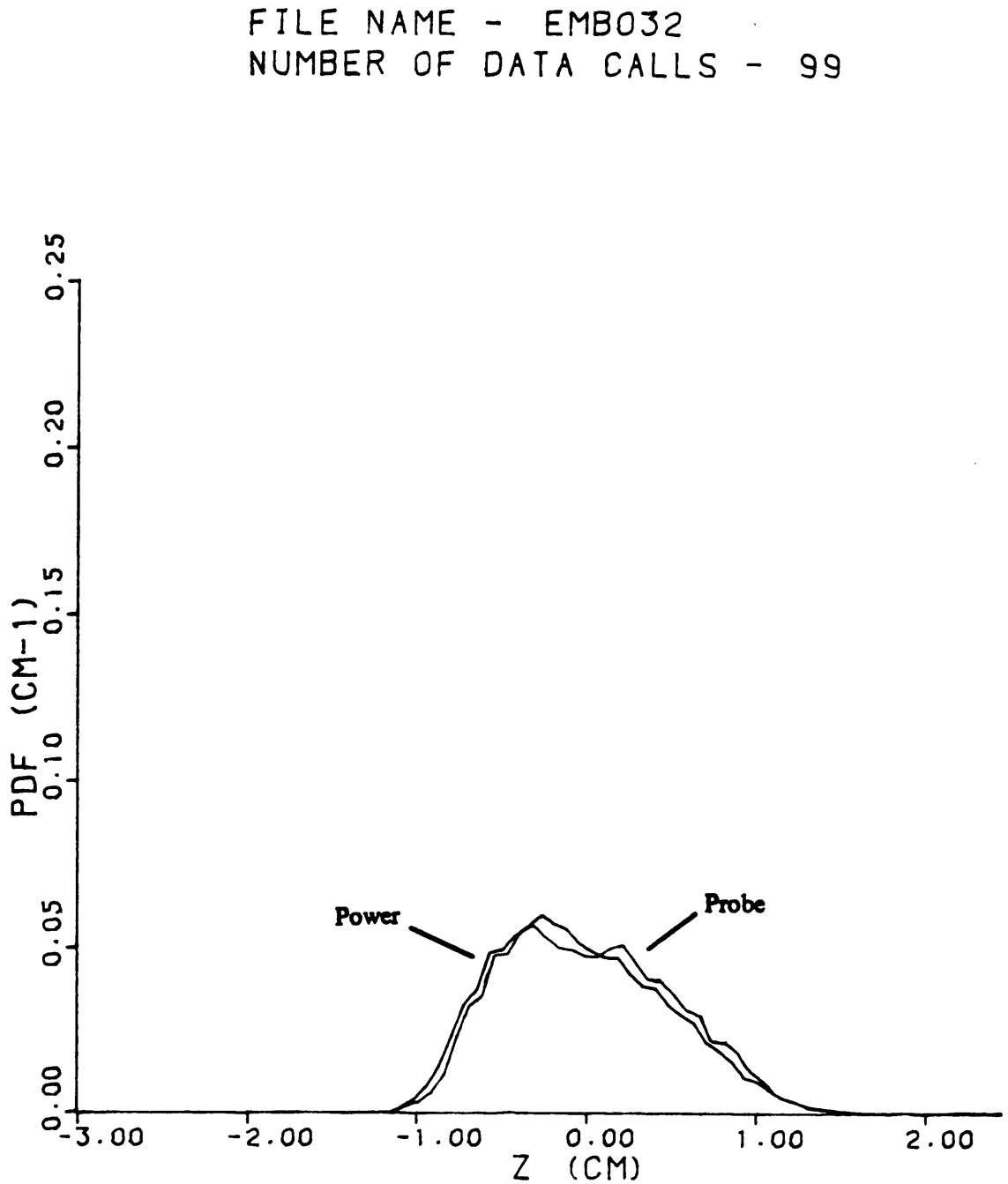

Figure 43. Scattered power and probe measured wave height histogramed vs displacement from mean water level (File EMB032): 13.5 GHz bistatic radar configuration with wind generated waves

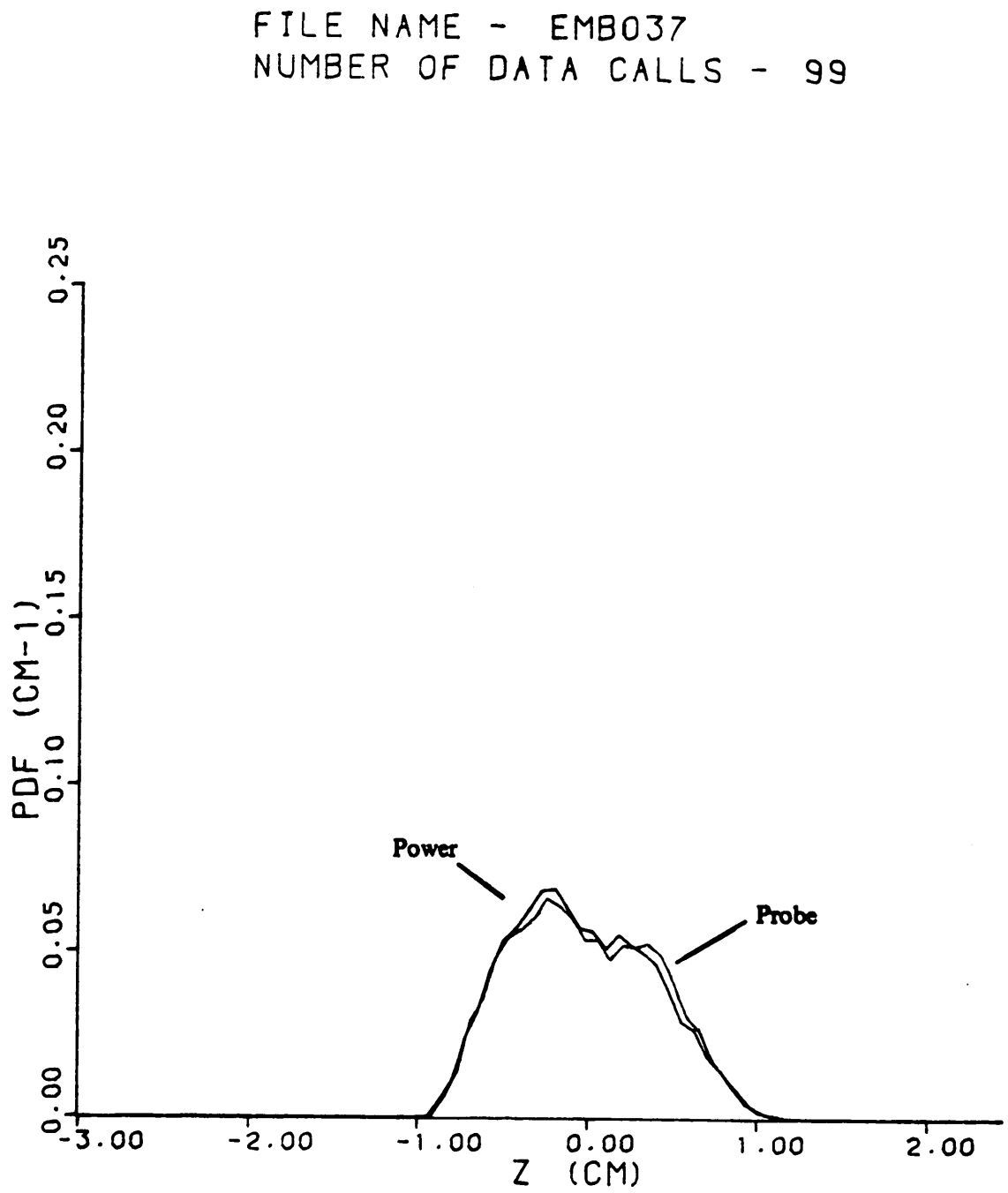

Figure 44. Scattered power and probe measured wave height histogramed vs displacement from mean water level (File EMB037): 13.5 GHz bistatic radar configuration with wind and paddle generated waves

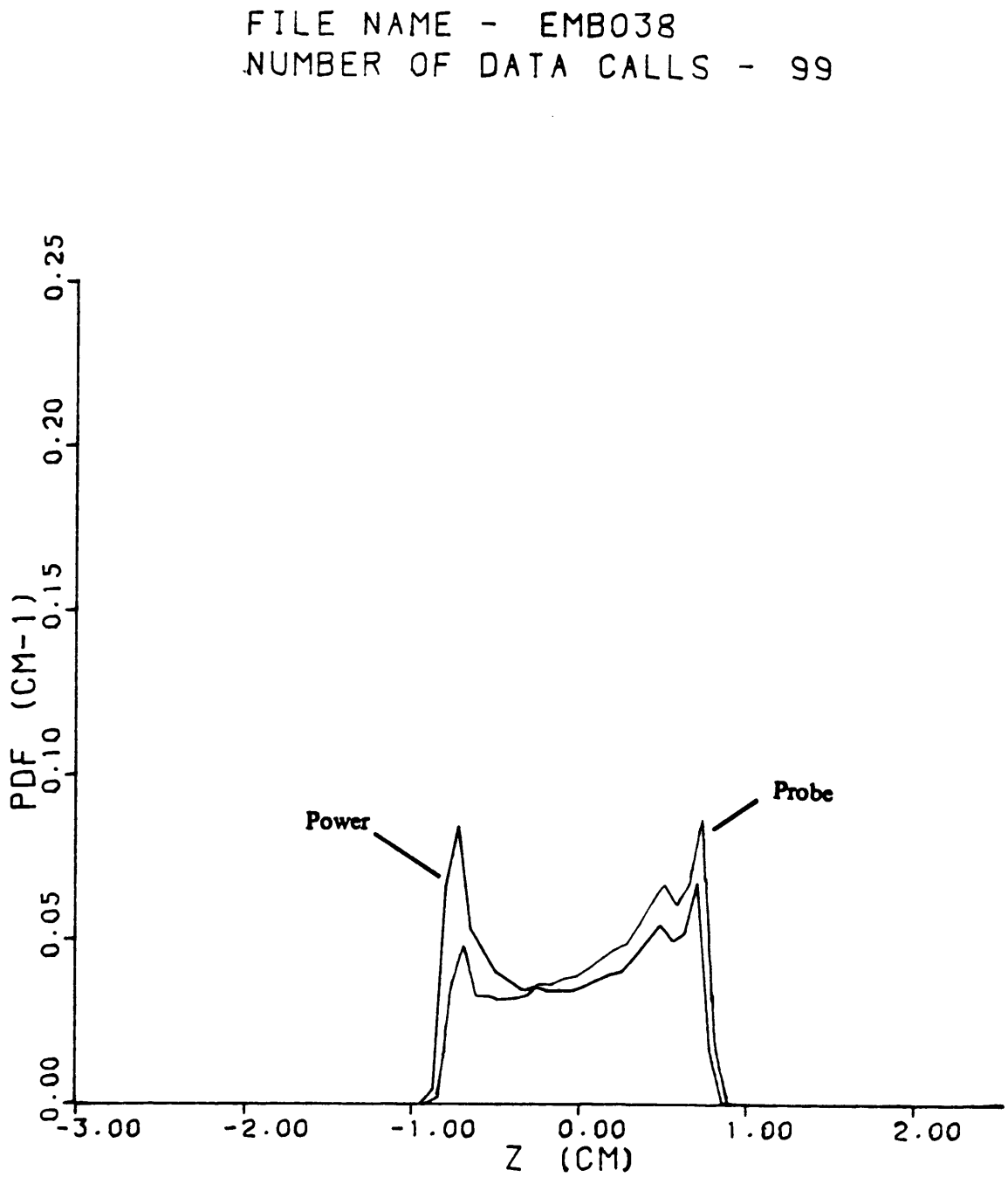

Figure 45. Scattered power and probe measured wave height histogramed vs displacement from mean water level (File EMB038): 13.5 GHz bistatic radar configuration with wind and paddle generated waves

Although these histograms show that the interference did not corrupt the data, they still need to have the effect of the absorber window removed. Removing the RF absorber effect can be done in software when the data is processed (see section 5.2.2), and it will raise the values near the edges (away from 0 cm water height) of the power distribution.

5.1.2 Effect of error on EM bias calculations

It was difficult to quantify the error present in the EM bias calculations, but the influencing factors will be discussed. The method used to calculate EM bias consists of finding the difference between the mean of the wave height pdf (generated using probe measurements) and the mean of the radar return power conditional pdf. These means could be influenced by errors in the height and power measurements.

Using the results from Drain Test R4, the maximum relative error in the return power at any height, in the range of interest (± 3.5 cm), could be seen to be 0.69 percent. This value put the error in the return power on the same order as the error in the probe measurement of the height (± 1 percent). The maximum relative error in the return power was found by dividing the maximum deviation from the expected return power by the minimum return power in the ± 3.5 centimeter range of interest; this calculation gave an upper bound on the error. Typically the error was less than this value. As mentioned previously, using a look-up table to remove the absorber effect would have the bonus of reducing the error to an even lower level.

The height error and power error would have different effects on the EM bias calculation. The error introduced by the probe would be fairly random and therefore have little or no effect on the calculation of the pdf means. On the other

hand, the error in the return power was not random, it was dependent on the water height. For this reason, it was important to reduce the power error as much as possible to minimize it's effect on the mean calculation.

The error in the return power has already been reduced by going to a bistatic configuration, using absorber to block multipath interference, and using the look-up table to remove the absorber effect. If it was desired to reduce the effect of the interference further, it could be done by taking advantage of the characteristic manner in which the interference manifests itself. The interference can be seen to be sinusoidal in shape. If the mean water level was chosen such that the interference was at a peak or a trough, the effect of the interference on the mean calculation would under go some self canceling because of symmetry. Similarly, the effect of the interference would be increased if the mean water level was chosen to correspond to a null in the interference.

5.2 *DISCUSSION*

5.2.1 Methods for further reducing the interference

There are several possible methods for reducing the interference to an even lower level. These methods will be discussed, so that they could be implemented in the future if they are deemed to be worthwhile.

Experiments have shown that strategic placement of RF absorber will reduce the level of multipath interference. For example, covering a small part of the platform (that holds the lens) with absorber did reduce the level of the interference by removing any reflections from that section of the platform. As there is plenty of RF absorber still available for use, it might be worthwhile to cover the rest of the platform base with absorber to remove other possible reflections. This would require little effort and could be done with available materials.

Another part of the system around which RF absorber could be placed is the stand holding the receive horn. At present, there is RF absorber between the horn and the metal crosspiece which supports the horn, but there is no absorber on the rest of the stand (the wooden uprights). Placing absorber on these parts poses little or no difficulty and would remove another possible source of reflection.

A more difficult place from which to remove multipath reflections is inside the wavetank (where most reflections probably occur). Experiments have shown that multipath reflections occur off the glass walls of the wavetank. These reflections were confirmed by placing RF absorber on the walls of the wavetank in the proximity to the radar spot and noting that the level of interference was drastically reduced. However and as explained earlier, affixing RF absorber inside of the wavetank was not a feasible solution. This limitation was why the absorber window was built as an alternate solution.

If the ceiling and walls of the wavetank could be made nonreflective, the multipath problem would be greatly reduced and the absorber window on top of the wavetank might not be necessary. The Wallops Wind Wavetank Facility does have available a thin sheet of material that, when attached to a metal surface, the material/metal surface will no longer reflect signals at a frequency around 13.5 GHz. This material is thin enough (less than 1/4 inch) that when affixed to a metal plate and

bolted to the side of the wavetank, the effects on air flow through the tank would be minimal. It would only be necessary to cover the tank ceiling and walls in the part of the wavetank that the radar operates. The coated plate would be attached to the tank ceiling and walls and would extend down to a level above the expected maximum wave height. This material/metal surface would only completely cancel reflections that were at normal incidence, but it could be expected to partially cancel reflections at other incidences. Because this solution to the multipath problem would take time and effort to implement, as long as the radar system is working in a satisfactory manner, perhaps it should only be considered as a possible future option if the system is ever dismantled and then reassembled.

5.2.2 Removal of the absorber window effect

As mentioned previously, not only did the absorber window block multipath signals, but it also blocked part of the desired signal. The blocking of the desired signal introduced a variation into the strength of the return signal that depended on the water height. This variation was introduced because the amount of signal blocked by the absorber depended on the location of the point of reflection. A simple way to describe the effect was to note that, at close to mean water level, the most signal got through the absorber windows and, as the water level moved away from this maximum point, more and more of the reflected signal was blocked by the RF absorber.

This absorber effect could clearly be seen in the trend the return power shows in Figure 27. It is necessary to remove this effect because the algorithm being used to calculate EM bias from the data assumes that the return power depends only

on the characteristics of the water surface, not on the range to the water or absorber induced attenuation. The easiest way to remove the absorber effect is by running a drain test over the range of interest and generating a software look-up table which holds the proper factor for each measured water height. Using the look-up table and probe height information, the power data can be processed. The look-up table approach will also help remove some of the remaining interference effects, because the effects of the interference are included in the drain test data.

A look-up table was generated (see section 5.2.4) using the data from Drain Test R4 (Figure 27), assuming that the range from + 3 centimeters to - 3 centimeters was divided up into 80 range intervals (bins). It is recommended that a more careful drain test be run and a new look-up table generated because, in most of the drain test experiments, the change in water level was approximated by assuming a constant drain rate. This approximation could be made because it did not influence the study made to reduce the interference. From drain tests, it can be seen that the drain rate is not constant; it increases. Therefore, when the drain test is run to generate the look-up table, the water level should be noted at various times during the test (the more times the more accurate) in order that the look-up table be derived more accurately.

5.2.3 Correction to phase/range calculation

Even though the probe data was what was being used to calculate the water height, the option still existed to use the phase information to calculate water height. To use the phase information, a correction term would have to be added to

the height calculation algorithm, because the change in two-way path length was no longer equal to the change in the water height (as it was in the monostatic system).

In the monostatic system the water height h was found from:

$$h = -\frac{\sin^{-1}(Q)}{2\Delta k} \tag{5.1}$$

where Q was the output from the quadrature phase channel. To correct for the 10° off nadir bistatic angle, a sin(80°) term must be included in the denominator. Also because the amplitude of the the quadrature phase channel was about 0.95 rather that 1.0, the Q must be divided by 0.95 . These changes led to the new expression for h:

$$h = -\frac{\sin^{-1}(\frac{Q}{0.95})}{2\Delta k(\sin 80°)} \tag{5.2}$$

The above equation is an approximation, but calculations show it to be accurate to within 0.16 percent at h = ±3.5 centimeters and 0.75 percent at h = ±4.0 centimeters (the closer to h = 0 the more accurate).

5.2.4 Look-up table generation

The following look-up table (LPOW BIN) was formed such that the ±3.0 centimeter range of interest was divided up into 80 range increments (bins). Therefore each bin covered a .075 centimeter height change. The program LPOW FORTRAN (listed in Appendix D) was used to convert the voltage data from Drain Test R4 (return power) to a linear scale with the maximum return power normalized to

unity (the data in R4 which corresponded to the drain test was from ≃124.509 seconds to ≃602.406 seconds, 3251 data points).

After the power data were converted to linear power values and normalized, BIN FORTRAN (listed in Appendix D) was used to find the average power values for each of the 80 bins on the ±3.0 centimeter interval (≃183.603 seconds to ≃518.763 seconds, 2280 data points). These average power values were printed out in file LPOW BIN next to their corresponding bin number (bin 1 was at +3.0 cm and bin 80 was at -3.0 cm). The look-up table, LPOW BIN, is given in Appendix E and is to be used to remove the absorber effects from the power data collected when an experiment is run, by dividing the power summations for each bin (experimental data) by the number given in the look-up table corresponding to that bin.

5.3 CONCLUSION

The lens radar system, designed for use in the Wallops wind-wavetank to study the characteristics of electromagnetic bias (EM bias), had been plagued with interference problems since it was originally installed in 1983. The interference was present in both the in-phase and quadrature signals (from which the water height was to be calculated), and the backscattered power. This contamination of the data made it impossible to make the high precision measurements needed for the study of EM bias. For example, there were 2 dB oscillations in the return power due to the interference and the interference oscillations in the phase signals made it impossible to accurately calculate wave height.

After running numerous tests and experiments it was concluded that the interference was primarily caused by inadequate isolation between the transmitter and the receiver. This conclusion was also supported by predictions of a theoretical model of the interference. To overcome this problem the system was operated in a bistatic configuration.

With the system operating bistatically in the wavetank the interference was found to be greatly reduced (less than half of what it had been with the original monostatic system). Further experimentation proved that the remaining interference was caused by multipath signals reaching the receiver. Through strategic placement of radio frequency (RF) absorber much of the multipath interference was removed.

With these changes made to the lens radar system (bistatic operation and use of RF absorber), it can now be used to make the precision measurements for which it was designed. If the system is operated as originally planned with the wave height being calculated from the phase information, the error in the power is less than 0.10 dB and the error in the height calculation is less than 1 millimeter. The system can also be operated with a capacitance probe suspended in the radar spot for the collection of wave height data (accurate to ± 1 percent). With this method of finding the wave height, the error in the power is slightly greater but still less than 0.14 dB. With the system now capable of making precision measurements, meaningful data can be collected for the study of EM bias.

REFERENCES

1. Miller, L. S., "A 35 GHz Instrumentation Radar For Very High Resolution Measurements". Task IV Final Report. Prepared under NASA Contract No. NAS6-3120 for National Aeronautics and Space Administration GSFC/Wallops Flight Facility. July 1983.

2. Norden E. Huang, et al. "The Non-Gaussian Joint Probability Density Function of Slope and Elevation for a Nonlinear Gravity Wave Field". Journal of Geophysical Research, Vol. 89, March 1984.

3. C. L. Parsons and G. Norcross, Private Communications.

4. Choy, L. W., et al. "The Electromagnetic Bias of Altimeter Measurements of Mean Sea Level as Determined by an Airborne 10 GHz Radar". NRL Memorandum Report 5006. January 1983.

5. Norden E. Huang, et. al. "A Non-Gaussian Statistical Model for Surface Elevation of Nonlinear Random Wave Fields". Journal of Geophysical Research, Vol. 88, September 1983.

6. Skolnik, Merrill I., Introduction to Radar Systems. McGraw Hill, 1980.

7. Brown, G. S., Private Communications.

8. Miller, L. S., "A Laboratory Study of Water-Wave Backscattering Using A 13.5 GHz and 36 GHz High Resolution Radar". Task I Final Report. Prepared under NASA Contract No. NAS5-28926 for NASA GSFC/Wallops Flight Facility.

9. Stutzman, Warren L. and Gary Thiele, Antenna Theory and Design. John Wiley and Sons, 1981.

10. Skolnik, Merrill I., Radar Handbook. McGraw Hill, 1980.

11. Parsons, C. L., Communications with L. S. Miller concerning the NASA Wallops lens radar system.

12. Collin, Robert E., Antennas and Radiowave Propagation. Mcgraw Hill, 1985.

13. Beyer, William H., CRC Standard Mathematical Tables 27th Edition. CRC Press, 1984.

14. Hansen, R. C., Microwave Scanning Antennas, Volume 1 Apertures. Academic Press, 1964.

Appendix A

DECREASED RETURN POWER WITH REMOVAL OF THE FOCUSING LENS

In the experiments run on the bench, when the focusing lens was removed from the system, the radar was unable to see the metal plate at a range of 2 meters (measured from the horn). The following calculations support this result. From the development in section 4.1, the power received from a rough surface when the lens was used (P_{rec}) was

$$P_{rec} = \frac{P_a \pi \sigma^o L^2}{256 R^2} \tag{A.1}$$

With the lens removed and the system illuminating a large flat plate the power received (P_{rec}') could be calculated using image theory (see Figure 46) by assuming that the conductivity of the metal plate was infinite and the plate was infinitely large, i.e.

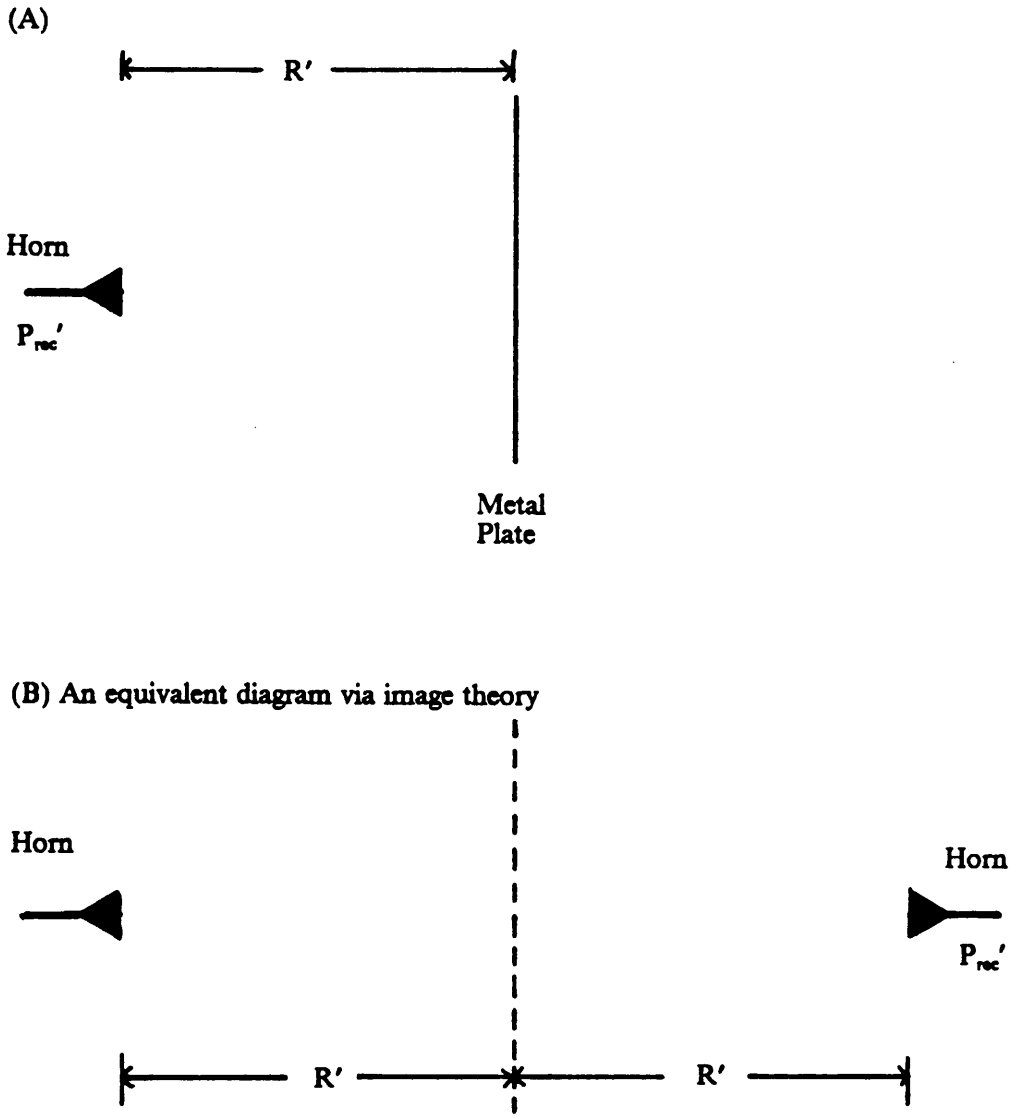

Figure 46. Image Theory

$$P_{rec}' = \frac{P_{in}\lambda^2 G_h^2(0°)}{(4\pi)^2(2R')^2} \tag{A.2}$$

Using

$$G_h(0°) = \frac{4\pi A_h \eta}{\lambda^2} \tag{A.3}$$

and

$$P_a = P_{in} G_h(0°) \tag{A.4}$$

equation (A.2) could be rewritten as

$$P_{rec}' = \frac{P_a A_h \eta}{16\pi(R')^2} \tag{A.5}$$

To determine the approximate value of $\sigma°$ for the metal plate, the expressions for the return power from a rough and smooth metal target were written, and the target was let to go from a rough surface to a smooth metal surface in order to observe what $\sigma°$ should approach when this transition took place. The return power from a rough surface was derived in section 4.1 and was rewritten as equation (A.1). Assuming a ideal focused system and using image theory (see Figure 48 in Appendix C), the return power from a smooth metal plate would be

$$(P_{rec})_{smooth} = P_a \tag{A.6}$$

Letting the surface go from rough to smooth, thus, implies that

$$\sigma° \rightarrow \frac{256R^2}{\pi L^2} \tag{A.7}$$

Using R equals 1 meter and L equals 0.4168 meter, σ° for the metal plate (focused system) was found to be 26.71 dB. To make the comparison of the return power with and without the focusing lens, it was assumed that the metal plate was at the focal point of the lens ($R' = 2R$). Using equations (A.1), (A.7), and (A.8) the ratio of the return power with the focusing lens (P_{rec}) and the return power without the focusing lens (P_{rec}') could be written as follows;

$$\frac{P_{rec}}{P_{rec}'} = \frac{64\pi R^2}{A_h \eta} \tag{A.8}$$

Using the same values as used in section 4.3 this ratio is

$$\frac{P_{rec}}{P_{rec}'} = 60.61 \text{ dB} \tag{A.9}$$

With the radar system's dynamic range (~20 dB), a return signal 60 dB below a signal within the dynamic range of the radar could not be detected because it would be below the noise floor. Even if the metal plate did not have the ideal radar cross section per unit area as derived ($\sigma^{\circ} = 26.71$dB) and only had a cross section per unit area of 0 dB, the radar would still not see the metal plate at a range of 2 meters.

Appendix B

INVESTIGATIONS USING AN OPEN ENDED WAVEGUIDE

B.1 RETURN SIGNAL

When transmitting and receiving with an open ended waveguide and the focusing lens removed (see Figure 47 (A)) the plate reflected signal was very weak. It was not strong enough to drive the phase comparators; therefore, there was no range information available. Even with this lack of range information, the interference was observed in both the phase and power when the plate was moved in range. Using the model of the interference developed in section 4.2 this result was further studied. Even though the limiting process employed in the phase comparison system removed the possibility of doing an exact comparison of the signal strengths, which signal (leakage or return) was dominate could still be calculated.

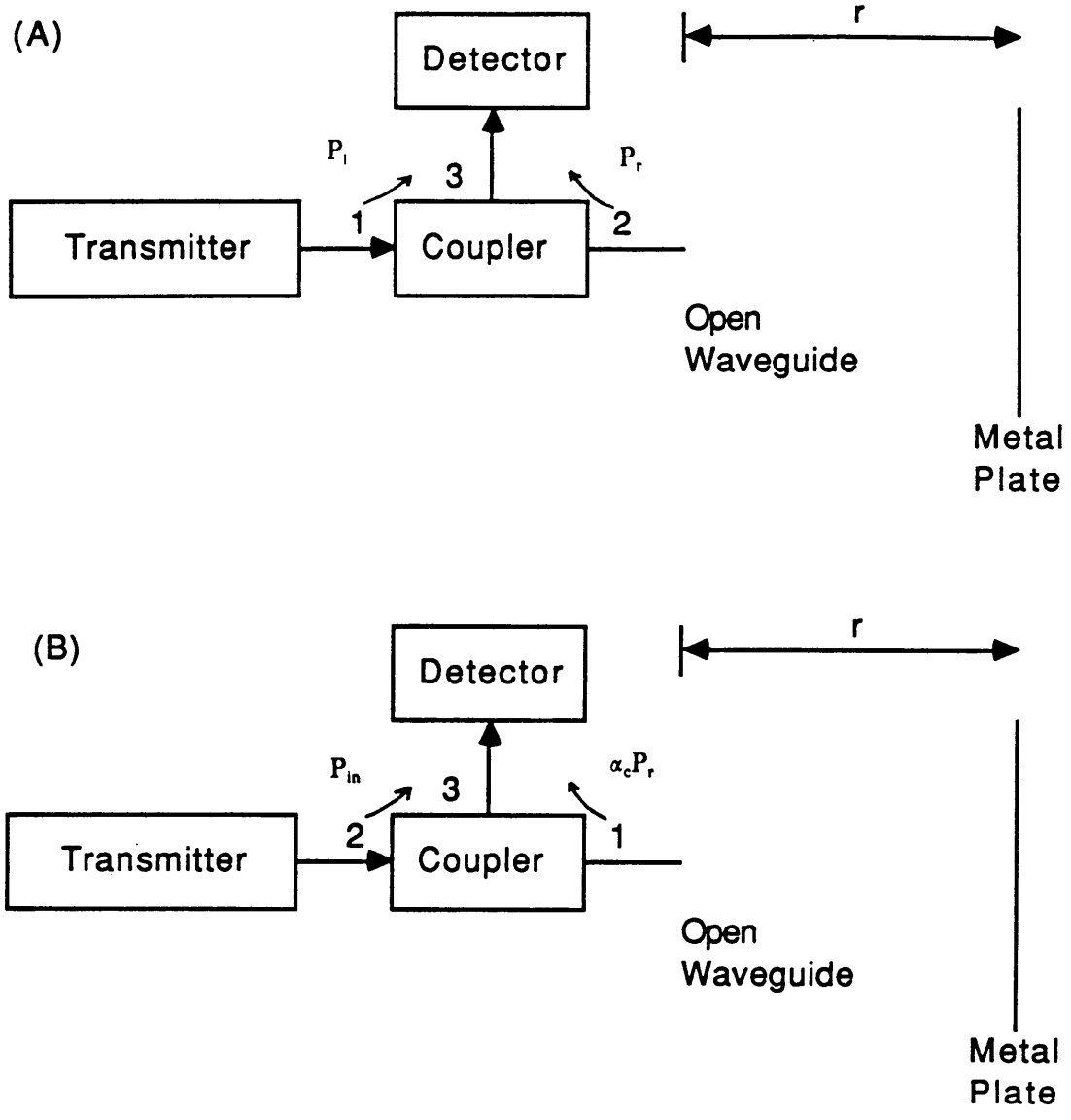

Figure 47. No Horn or Lens

For set-up (A) (return signal) the quadrature signal (Q_D) was known from the development in chapter 4 (equation (4.31) neglecting the constant term).

$$\begin{aligned} Q_D = {} & P_r \sin(-2\Delta kR' - \psi'_2 + \psi''_2) \\ & + \sqrt{P_r}\sqrt{P_l}\,[\sin(-2k_1R' - \psi'_2 - \phi_8) + \sin(2k_2R' + \psi''_2 + \phi_7)] \end{aligned} \tag{B.1}$$

The corresponding in-phase signal (I_D) could also be written.

$$\begin{aligned} I_D = {} & P_r \cos(-2\Delta kR' - \psi'_2 + \psi''_2) \\ & + \sqrt{P_r}\sqrt{P_l}\,[\cos(-2k_1R' - \psi'_2 - \psi_1'') + \cos(2k_2R' + \psi''_2 + \psi_1')] \end{aligned} \tag{B.2}$$

Using the same substitutions, identity, and assumption as in section 4.3 on the second term, equation (B.2) was rewritten.

$$\begin{aligned} I_D = {} & P_r \cos(-2\Delta kR' - \psi'_2 + \psi''_2) \\ & + \sqrt{P_r}\sqrt{P_l}\,\cos[k(2R' + \gamma - \alpha)] \end{aligned} \tag{B.3}$$

Letting COMP be the ratio of the amplitude of the leakage signal ($2\sqrt{P_r}\sqrt{P_l}$) to the amplitude of the return signal (P_r) yielded

$$\text{COMP} = \frac{2\sqrt{P_l}}{\sqrt{P_r}} \tag{B.4}$$

As before the leakage power (P_l) was

$$P_l = \alpha_c P_{in} \tag{B.5}$$

With no lens or horn the return signal power (P_r) was derived using image theory.

$$P_r = \frac{\lambda^2}{4\pi} G_w^2 \frac{P_{in}}{4\pi(2r)^2} \tag{B.6}$$

where G_w was the gain of the rectangular waveguide radiating aperture.

$$G_w \simeq \frac{32ab}{\pi\lambda^2} \tag{B.7}$$

where a and b were the dimensions of the waveguide [9]. Substituting equations (B.5), (B.6), and (B.7) into (B.4) led to

$$COMP = \frac{\sqrt{\alpha_c}\,\pi^2 r\lambda}{2ab} \tag{B.8}$$

where r was the range to the plate. Substituting the following values:

α_c = .001

λ = 0.8333 cm

r = 30 cm

a = 0.71 cm

b = 0.36 cm

led to

$$COMP \simeq 15.26 \tag{B.9}$$

This result showed that the leakage (interference) signal was the dominant signal (more than 15 times greater than the return signal). As the amplitude of the interference was very small (~0.04 V peak to peak), it seemed reasonable that the return signal was to weak to drive the phase comparators.

B.2 TRANSMITTED SIGNAL

Since the interference was not present when the plate was moved in range (Figure 47 (B)), the plate reflected signal that leaked through the coupler must have been to weak to be detected. In set-up (B), the signal being looked at directly was P_{in} and the leakage signal was equal to $\alpha_c P_r$. Letting COMP be the ratio of the leakage signal to the direct signal led to

$$COMP = \frac{\alpha_c P_r}{P_{in}} \tag{B.10}$$

Substituting equations (B.6) and (B.7)

$$COMP \simeq \frac{16\alpha_c a^2 b^2}{\lambda_2 \pi^4 r^2} \tag{B.11}$$

Substituting in values

$$COMP = -77.65\ dB \tag{B.12}$$

This result supports the suggestion that the plate reflected signal leaking through the coupler would be to weak to have any effect.

Appendix C

INTERFERENCE WHEN STUDYING THE TRANSMITTED SIGNAL

Assuming an ideal focused system and using image theory (see Figure 48), the power received (P_r) was the power transmitted (P_a)

$$P_r = P_a \tag{C.1}$$

Comparing the signal strengths seen at the detector (COMP) yielded

$$COMP = \frac{\alpha_c P_r}{P_{in}} \tag{C.2}$$

where P_{in} was the transmitter power reaching the detector directly. Noting that $P_a = G_h(0°)P_{in}$ and using equation (C.1) led to

$$COMP = \alpha_c G_h(0°) \tag{C.3}$$

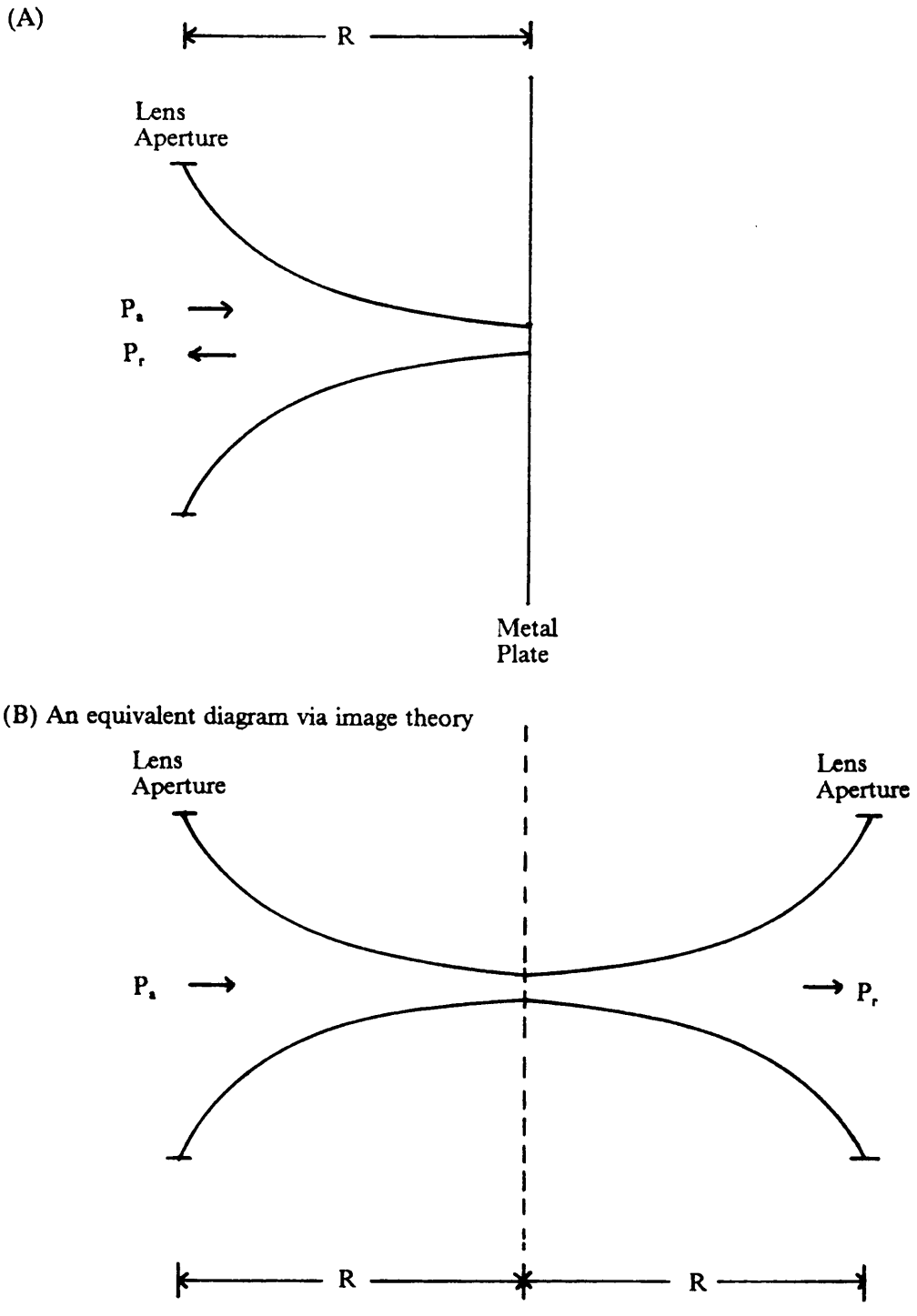

Figure 48. Focused System

Plugging in values resulted in

$$\text{COMP} = -15 \text{ dB}$$

With the plate reflected signal, reaching the detector, only 15 dB down from the direct signal, it was reasonable that the detector saw both signals and thereby the interference was introduced.

Appendix D

PROGRAMS

D.1 LPOW FORTRAN

```
C     THIS PROGRAM READS DRAIN TEST R4PW (IN DECIMAL FORMAT)
C        AND CONVERTS THE POWER VALUES TO LINEAR FORM,
C        WITH THE MAXIMUM POWER RETURN NORMALIZED TO
C        UNITY.
      DOUBLE PRECISION A(3254),B,C,D,E(3254),G,F(3254),O,P
C     IGNORE FIRST 847 POINTS (DO NOT CONTAIN TEST DATA)
      DO 25 J = 1,847,1
         READ (2,*)O,P
 25   CONTINUE
C     INITIALIZE G TO ZERO
      G = 0.0
C     READ DATA
      DO 10 I = 1,3251
         READ(2,*)A(I),B
C         CONVERT TO DB
         C = 27.87-6.38*B
C         CONVERT TO LINEAR
         D = C/10.0
         E(I) = 10**D
C         STORE LARGEST POWER RETURN
         IF (E(I).GT.G)G = E(I)
```

```
 10      CONTINUE
C       WRITE NORMALIZED LINEAR VALUES
       DO 20 J = 1,3251
         F(J) = E(J)/G
C         WRITE TO FILE LPOW DATA
         WRITE(8,*)A(J),F(J)
 20      CONTINUE
         STOP
         END
```

D.2 BIN FORTRAN

```
C     THIS PROGRAM READS DATA FROM FILE LPOW DATA
C        AND CALCULATES THE AVERAGE NORMALIZED POWER
C        VALUES FOR EACH OF THE 80 POWER BINS.
      DOUBLE PRECISION B,D,A,SUM,AVG
C     THE BINS RUN FROM -3CM TO +3CM
C     SKIP TO VALUES OF INTEREST (+3 TO -3CM)
      DO 30 M = 1,403
          READ(7,*)B,D
30    CONTINUE
C     SET-UP TO BEGIN CALCULATIONS
C     2280 POINTS OF INTEREST
C          ODD BINS AVERAGE 29
C          EVEN BINS AVERAGE 28
      DO 20 I = 1,80
          A = FLOAT(I)/2.0 + .1
          L = INT(A)
          N = 29
          IF(L*2 .EQ.I)N = 28
C          INITIALIZE SUM TO ZERO
          SUM = 0.0
C          READ DATA FROM LPOW DATA
          DO 10 J = 1,N
              READ(7,*)B,D
              SUM = SUM + D
10          CONTINUE
C       FIND BIN AVERAGE
        AVG = SUM/FLOAT(N)
C       WRITE BIN VALUES TO FILE LPOW BIN AND SCREEN
        WRITE(8,*)I,AVG
        WRITE(6,*)I,AVG
20      CONTINUE
```

```
STOP
END
```

Appendix E

LPOW BIN

Bin	Average power
1	0.853192636258058593
2	0.860248314893344496
3	0.871443376102109549
4	0.894525829457230554
5	0.914431862252277308
6	0.931916079013764609
7	0.946794681098745788
8	0.943619783246517782
9	0.931698282613098408
10	0.913606894881621071
11	0.903282550094862358
12	0.899473979566610585
13	0.904855769270072996
14	0.909530383509108198
15	0.913489516035383156
16	0.914852361211619364
17	0.915721596433403312
18	0.920814908781965757
19	0.930750969549990495
20	0.944371669024450980
21	0.964145871508824401
22	0.978885354780478639
23	0.980101529759162260
24	0.970643995829430395
25	0.955635499950981127
26	0.937859700728949086
27	0.926806235348645868

28 0.927084816413705062
29 0.930863895693905319
30 0.935944563348745540
31 0.943269870451283091
32 0.953009793980540643
33 0.961295872566978821
34 0.969846742723590477
35 0.979332561212670843
36 0.989634777936864829
37 0.992653712527513832
38 0.989505167686352965
39 0.980197557661074831
40 0.966802230554028308
41 0.951611016362417572
42 0.937455836681168719
43 0.930335556275386291
44 0.929366818654222160
45 0.930539825872431142
46 0.935453483445603029
47 0.944555951139922842
48 0.958756133969078272
49 0.971212969548088167
50 0.978823516589986745
51 0.982681510597295221
52 0.983262228747111638
53 0.978523661451644280
54 0.971344177826326566
55 0.959660919422988132
56 0.942828831144385121
57 0.921529532928182835
58 0.904955765941204471
59 0.895001198357401967
60 0.886883072478233656
61 0.885727432465380951
62 0.893513999800488679
63 0.905694339130771908
64 0.918708733970233685
65 0.926397261099438152
66 0.927116582164712197
67 0.925319294416103749
68 0.925840351846179604
69 0.925225181545126299
70 0.917297333473094945
71 0.903761062508880622
72 0.882070346648131220
73 0.859201635446070991
74 0.841125471021806473
75 0.826085980796497726
76 0.816279136288835208
77 0.815274793628051803
78 0.821007014514160610

79 0.828600160068350133
80 0.830882782800406228

The vita has been removed from the scanned document